Anion-exchange facilitated selective extraction of sulfate and phosphate by overcoming Hofmeister bias

Anamika Gogoi,[a] Dipjyoti Dutta,[a] Beatriz Gil-Hernández,[c] Sandeep Kumar Dey,*[a,b]

[a]*Material Science and Technology Division, CSIR-North East Institute of Science and Technology, Jorhat, Assam 785006, India. Email: sandeep@neist.res.in Phone: +91-7387633550*

[b]*Academy of Scientific and Innovative Research (AcSIR), Ghaziabad, Uttar Pradesh, India.*

[c]*Departmento de Química, Facultad de Ciencias, Sección Química, Universidad de La Laguna, 38206, La Laguna, Tenerife, Spain. Email: beagher@ull.es.*

Contents

1. Materials and experimental methods

All reagents and solvents were obtained from commercial sources and used as received without any further purification. Tris(2-aminoethyl) amine (Tren), 3-nitrophenyl isocyanate, 4-nitrophenyl isocyanate, 4-fluorophenyl isocyanate, 4-nitrophenyl isothiocyanate and all quaternary ammonium (tetraalkylammonium) salts were purchased from Sigma-Aldrich or TCI Chemicals. Solvents (analytical grade) for synthesis and extraction experiments were purchased from Merck (India), and used without further purification. ^{1}H, ^{31}P and ^{19}F NMR spectra were recorded in DMSO-D_6 (99.9% D) on a Bruker FT-500 MHz spectrometer at 298 K and chemical shifts were recorded in parts per million (ppm) on the scale using residual solvent peak as a reference, and ^{13}C-NMR spectra were obtained at 125 MHz instrument. Powder X-ray diffraction analysis was carried out on a Rigaku Ultima-IV diffractometer (Cu-K_α λ = 1.5418 Å).

2. Synthesis and characterization of tris-urea receptors (L_1, L_2 and L_3)

Receptors **L_1-L_3** were synthesized by the reaction of tris(2-aminoethyl)amine with 3-nitrophenylisocyante/4-nitrophenylisocyante/4-fluorophenylisocyanate in a 1:3.1 molar ratio at room temperature (Scheme S1).[1] In a 50 mL flat bottom flask, 146 µL of tris(2-aminoethyl)amine (1 mmol) was dissolved in 10 mL of tetrahydrofuran (THF) and 510 mg of 3-nitrophenylisocyante/4-nitrophenylisocyante (3.1 mmol) was added into the above solution mixture and was allowed to stir at room temperature (25−30 ºC) for about 12 hours. The precipitate formed in the reaction mixture was then filtered and washed with methanol a couple of times (2 x 10 mL) and dried at room temperature. Yield: **L_1** 83%, **L_2** 85%, and **L_3** 80% (percentage yields reported are the average value of three reactions in each case).

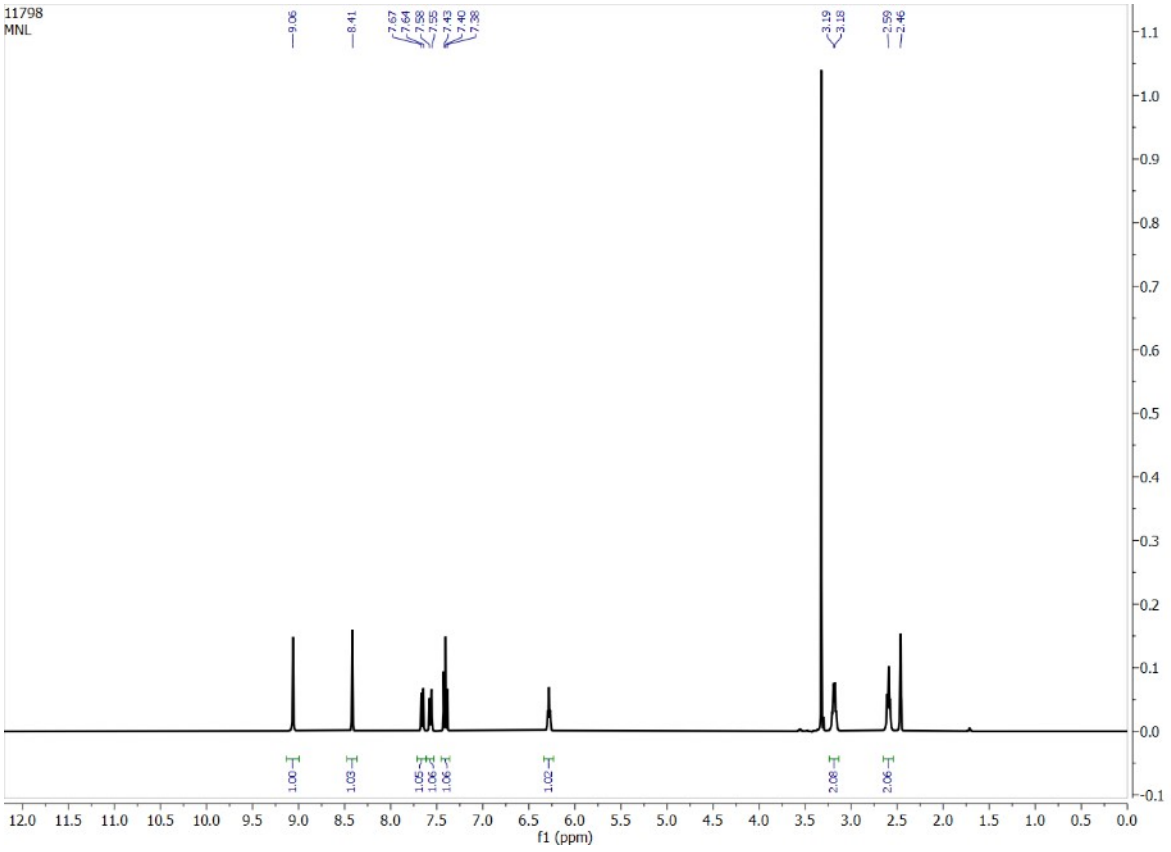

Fig S1. ^{1}H-NMR spectrum of **L_1** in DMSO-D_6.

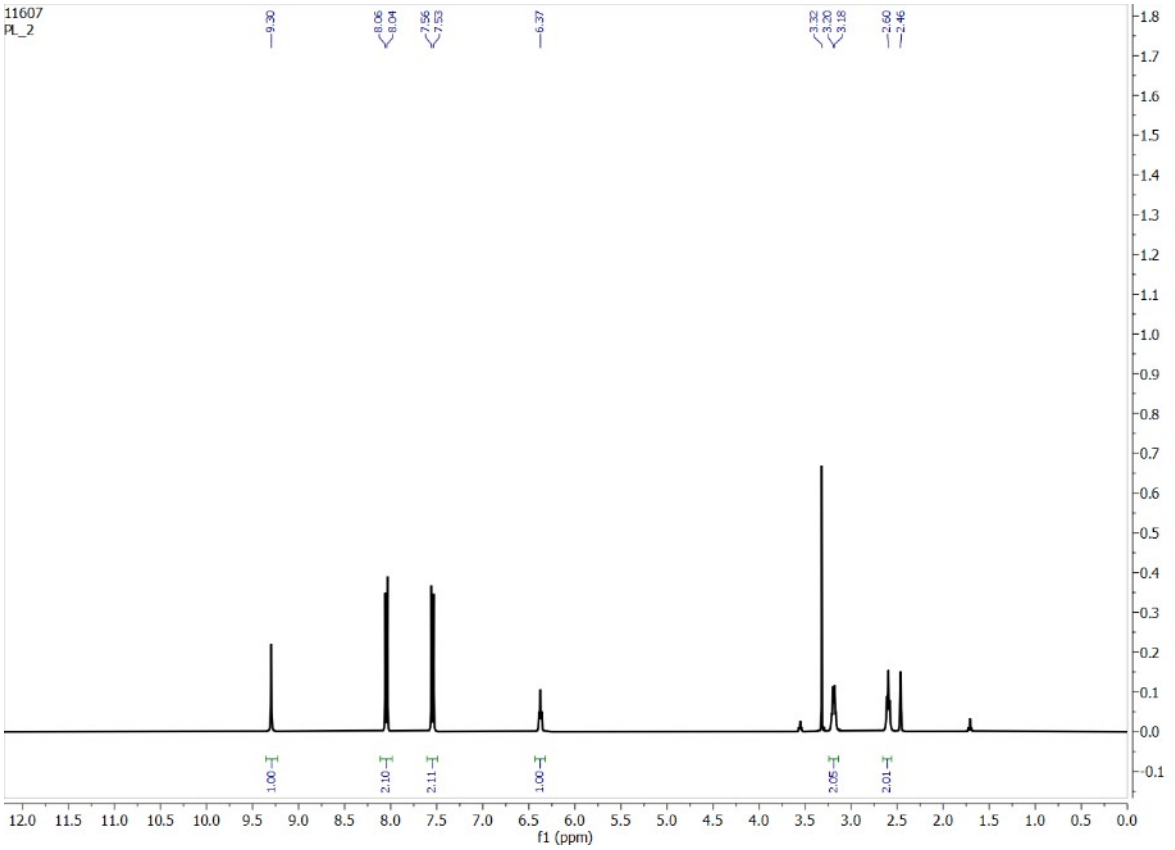

Fig S2. ^{1}H-NMR spectrum of $\mathbf{L_2}$ in DMSO-D_6.

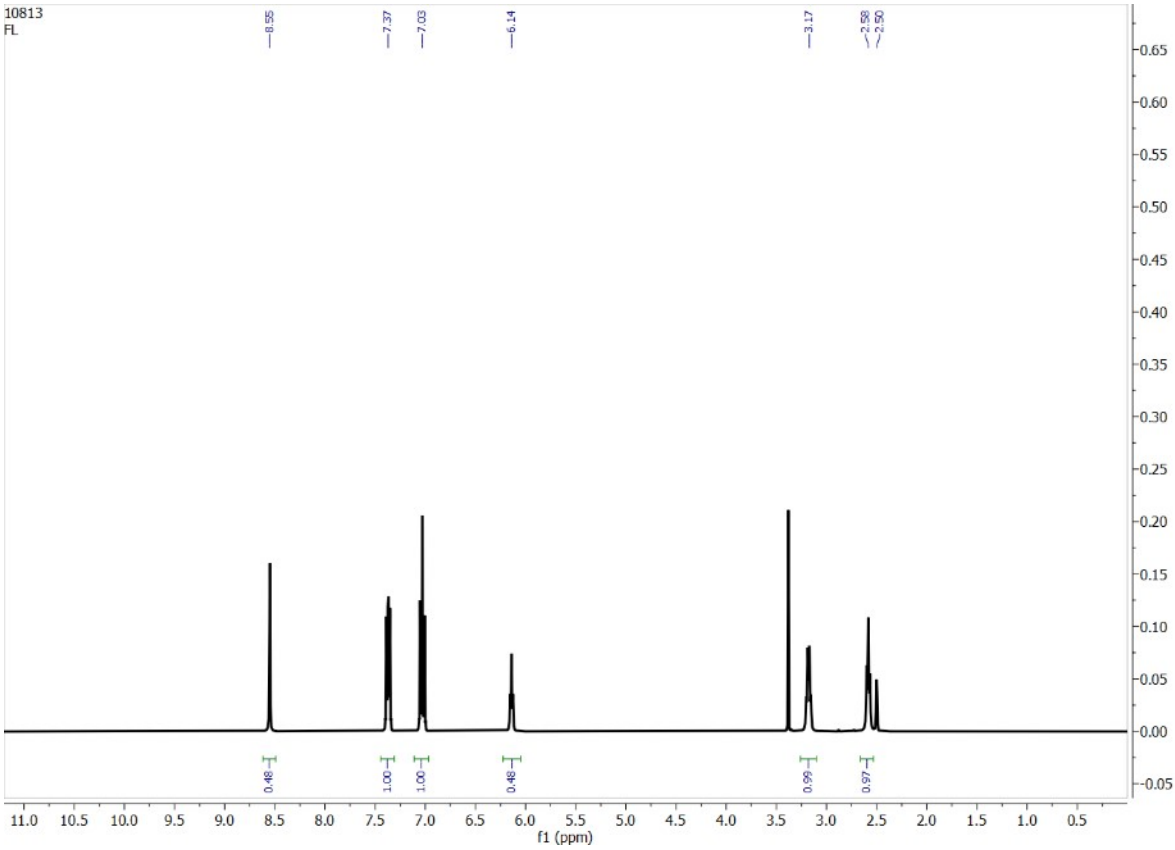

Fig S3. ^{1}H-NMR spectrum of $\mathbf{L_3}$ in DMSO-D_6.

3. Synthesis and characterization of tris-thiourea receptor (L_4)

Receptors **L_3** was synthesized by the reaction of tris(2-aminoethyl)amine with 4-nitrophenylisothiocyante in a 1:3.1 molar ratio at room temperature (Scheme S1).[2] In a 50 mL flat bottom flask, 146 µL of tris(2-aminoethyl)amine (1 mmol) was dissolved in 10 mL of tetrahydrofuran (THF) and 560 mg of 4-nitrophenylisothiocyante (3.1 mmol) was added into the above solution mixture and was allowed to stir at room temperature (25−30 ºC) for about 12 hours. The solvent was evaporated under reduced pressure at 40 ºC to obtain a thick oily compound, which was then treated with 20 mL of methanol to precipitate the final product. The pale-yellow precipitate obtained was then filtered and washed with 20 mL methanol and dried at room temperature. Yield: 82% (percentage yield reported are the average value of three reactions).

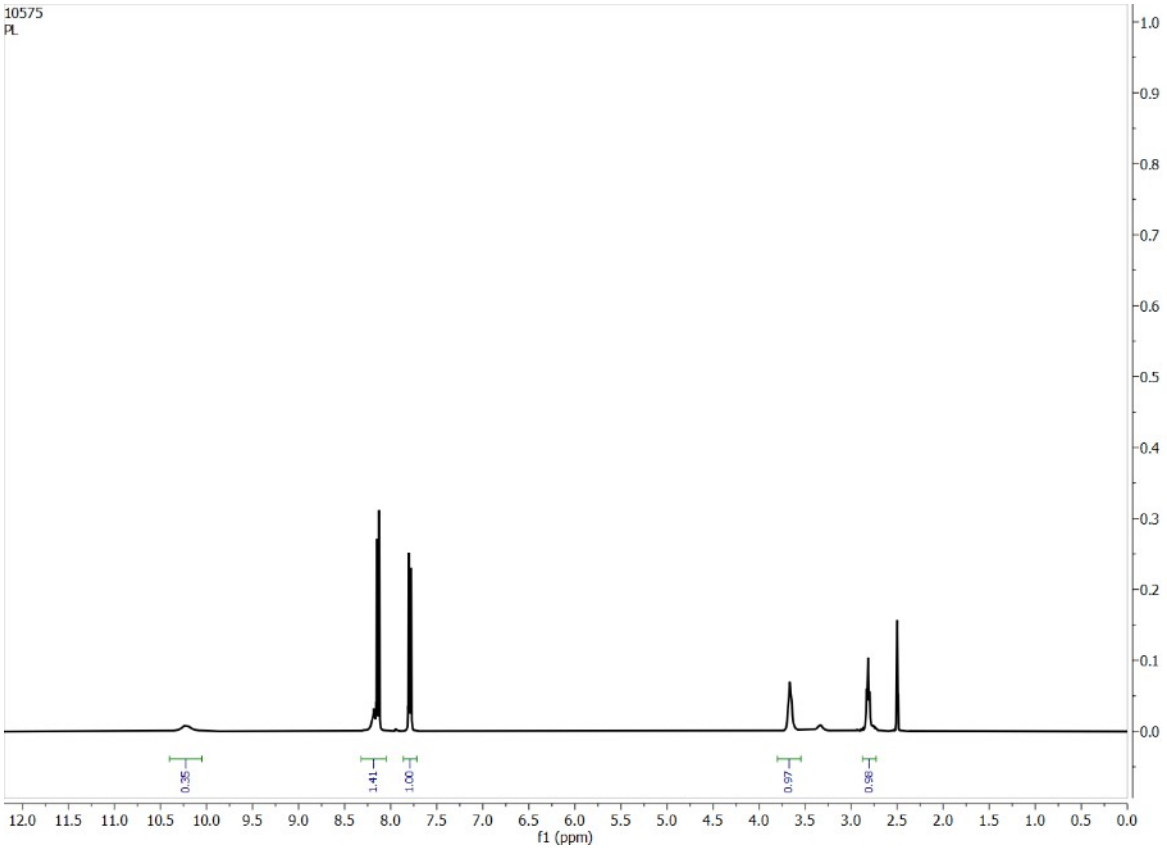

Fig S4. ^{1}H-NMR spectrum of **L_4** in DMSO-D_6.

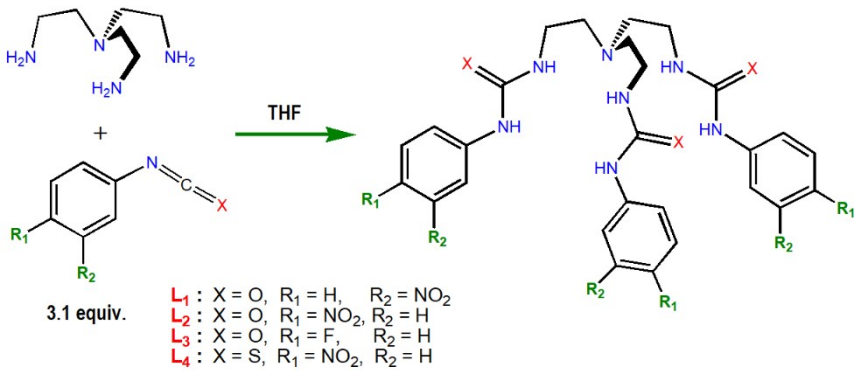

Scheme S1. Synthesis of urea and thiourea-based tripodal receptors.

4. Synthesis of oxoanion complexes of tris-urea receptors (L_1-L_3)

The receptor-oxoanion complexes were obtained by liquid-liquid extraction experiments. In a typical liquid-liquid extraction experiment, **L_1/L_2/L_3**(100 mg) was dissolved in dichloromethane (DCM, 20 mL) in the presence of two equivalents (n-Bu_4N^+)OH^- and an aqueous solution of an oxoanion (one equivalent of Na_2SO_4, Na_2SeO_4, Na_2HPO_4, Na_2HAsO_4 or Na_2CO_3 dissolved in 20 mL of deionized water) was added into the DCM solution. The solution mixture was then stirred at room temperature for about an hour and the separated organic layer was washed with 20 mL of deionized water (10 min. of stirring) in each case. The DCM layer was then isolated again using a separating funnel and treated with anhydrous sodium sulfate in each case. The solution was then filtered and evaporated to dryness at room temperature to obtain yellow crystalline powder of the host-guest complex which was characterized by NMR spectroscopy in DMSO-D_6.

5. Synthesis of oxoanion complexes of tris-thiourea receptors (L_4)

The receptor-oxoanion complexes were obtained by liquid-liquid extraction experiments. In a typical liquid-liquid extraction experiment, **L_4** (100 mg) was dissolved in dichloromethane (DCM, 20 mL) in the presence of three equivalents (n-Bu_4N^+)$CH_3CO_2^-$ and an aqueous solution of an oxoanion (one equivalent of Na_2SO_4, Na_2SeO_4, Na_2HPO_4, Na_2HAsO_4 or Na_2CO_3 dissolved in 20 mL of deionized water) was added into the DCM solution. The solution mixture was then stirred at room temperature for about an hour and the separated organic layer was washed with 20 mL of deionized water (10 min. of stirring) in each case. The DCM layer was then isolated again using a separating funnel and treated with anhydrous sodium sulfate in each case. The solution was then filtered and evaporated to dryness at room temperature to obtain yellow crystalline powder of the host-guest complex which was characterized by NMR spectroscopy in DMSO-D_6.

Competitive liquid-liquid extraction experiments: In a typical competitive liquid-liquid extraction experiment for the selective sulfate extraction, **L_1/L_2** (100 mg) was dissolved in dichloromethane (DCM, 20 mL) in the presence of two equivalents (n-Bu_4N^+)OH^- and an aqueous solution mixture of sulfate and one or more competing anions (Na^+ salts dissolved in 20 mL of deionized water) was added into the DCM solution. The solution mixture was then stirred at room temperature for about an hour and the DCM layer was isolated using a separating funnel and treated with anhydrous sodium sulfate in each case. The solution was then filtered and evaporated to dryness at room temperature to obtain yellow crystalline powder of the receptor-sulfate complex which was characterized by NMR spectroscopy in DMSO-D_6. The yield of the isolated complex was calculated with respect to the receptor. Similar experiments have also been performed with receptors **L_3** and **L_4** for sulfate and phosphate extractions, respectively.

6. Anion complexes of L_1: Characterization by NMR spectroscopy

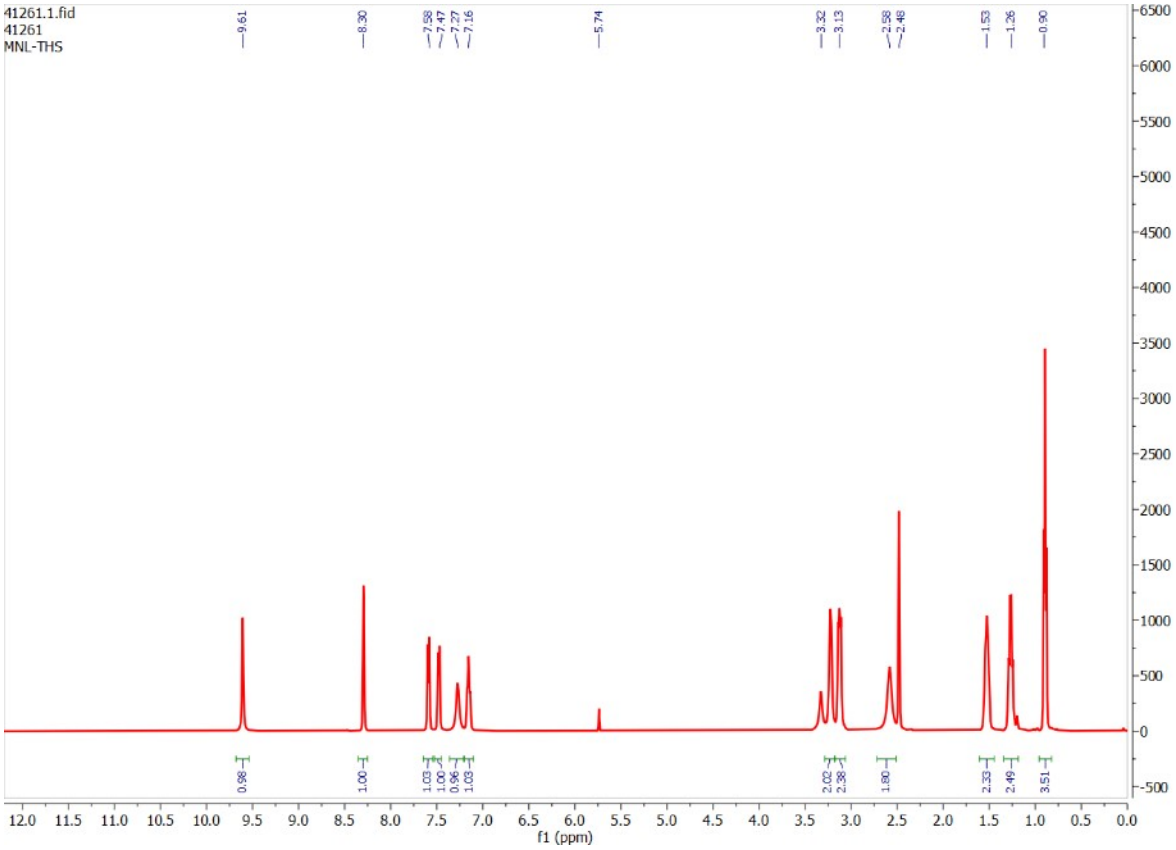

Fig. S5. ^{1}H-NMR spectrum of sulfate complex, [(n-$Bu_4N)_2$(2**L_1**·SO_4)] in DMSO-D_6.

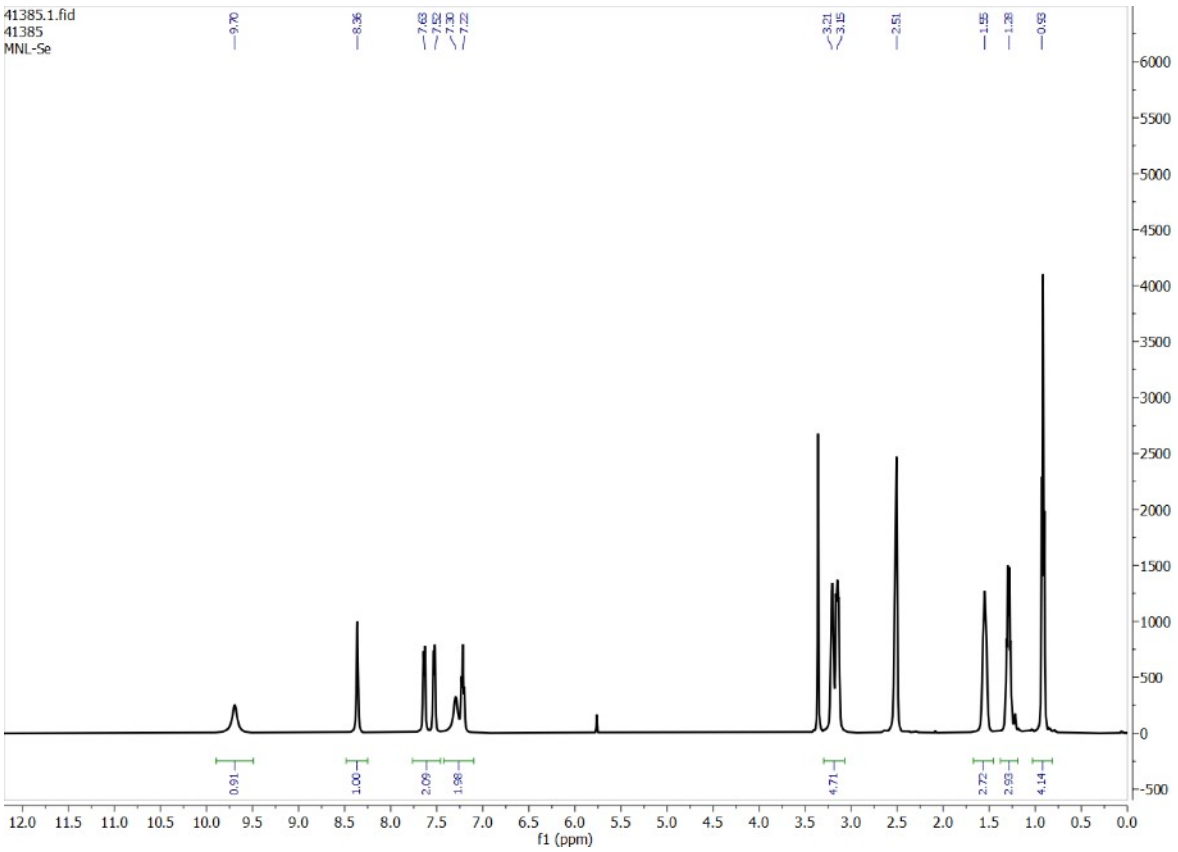

Fig. S6. ^{1}H-NMR spectrum of selenate complex, [(n-Bu_4N)$_2$(2$\mathbf{L_1}$·SeO_4)] in DMSO-D_6.

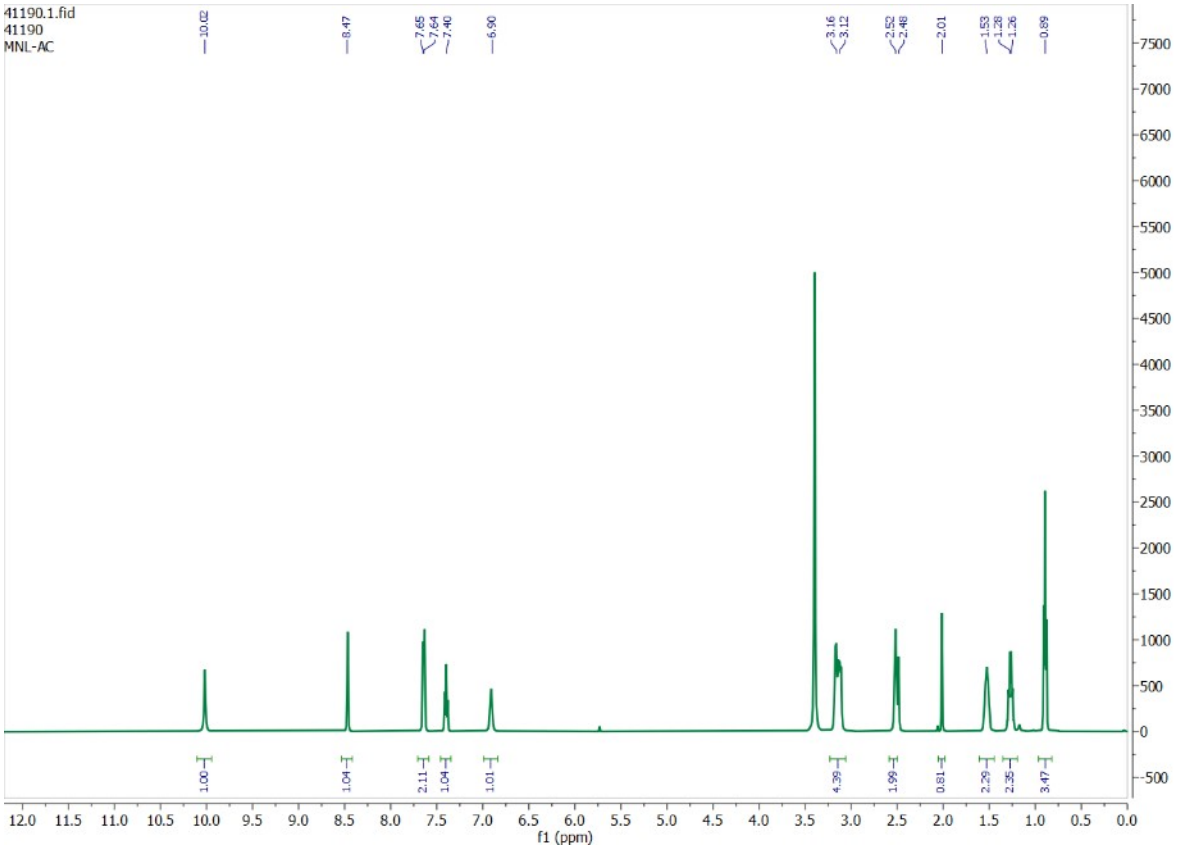

Fig. S7. ^{1}H-NMR spectrum of acetate complex, [(n-Bu_4N)($\mathbf{L_1}$·CH_3CO_2)] in DMSO-D_6.

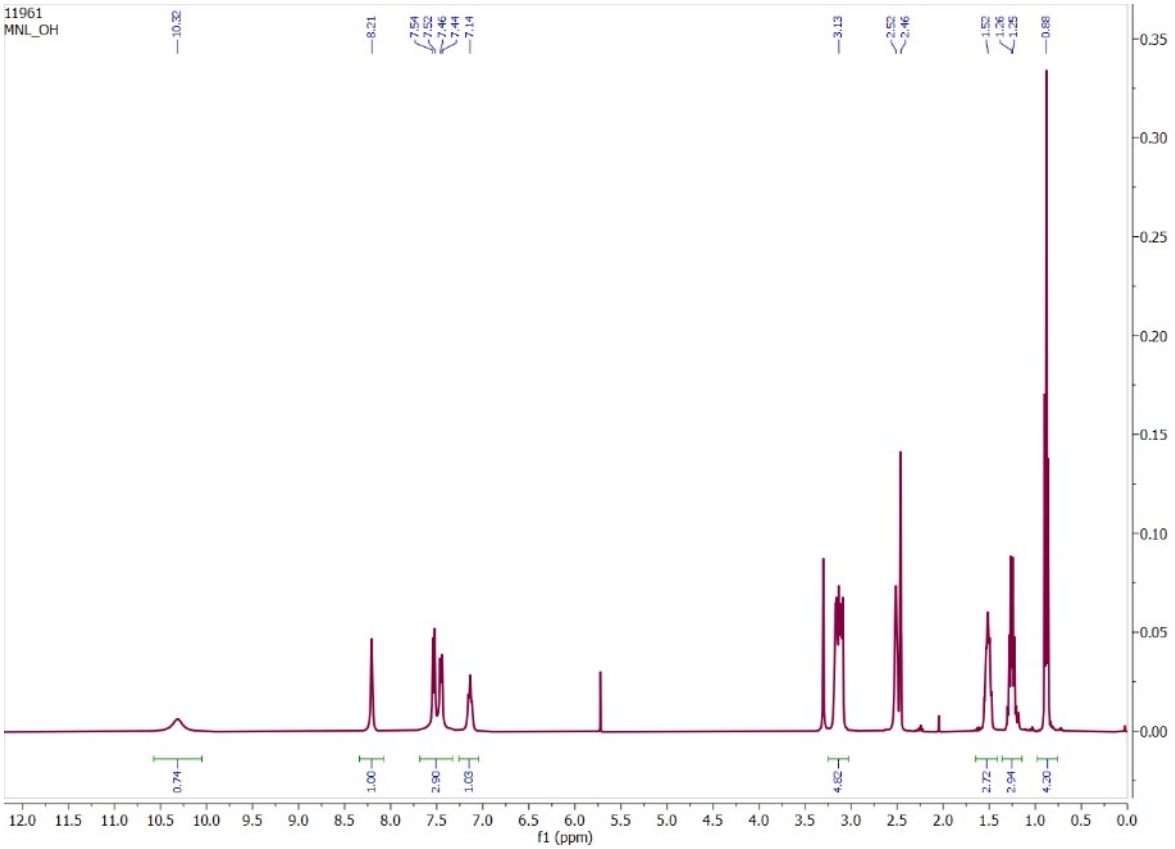

Fig. S8. ^{1}H-NMR spectrum of hydroxide complex, [(n-Bu_4N)(**L_1**·OH)] in DMSO-D_6.

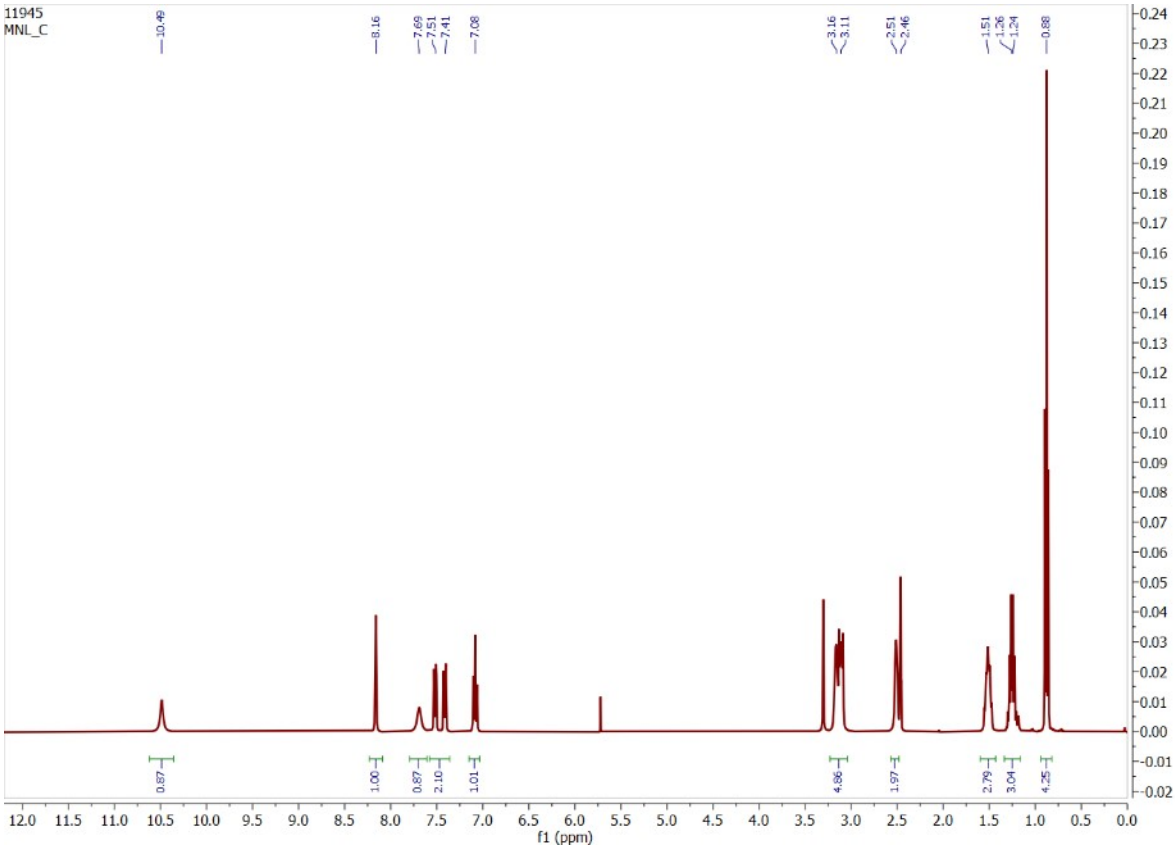

Fig. S9. ^{1}H-NMR spectrum of carbonate complex, [(n-Bu_4N)$_2$(2**L_1**·CO_3)] in DMSO-D_6.

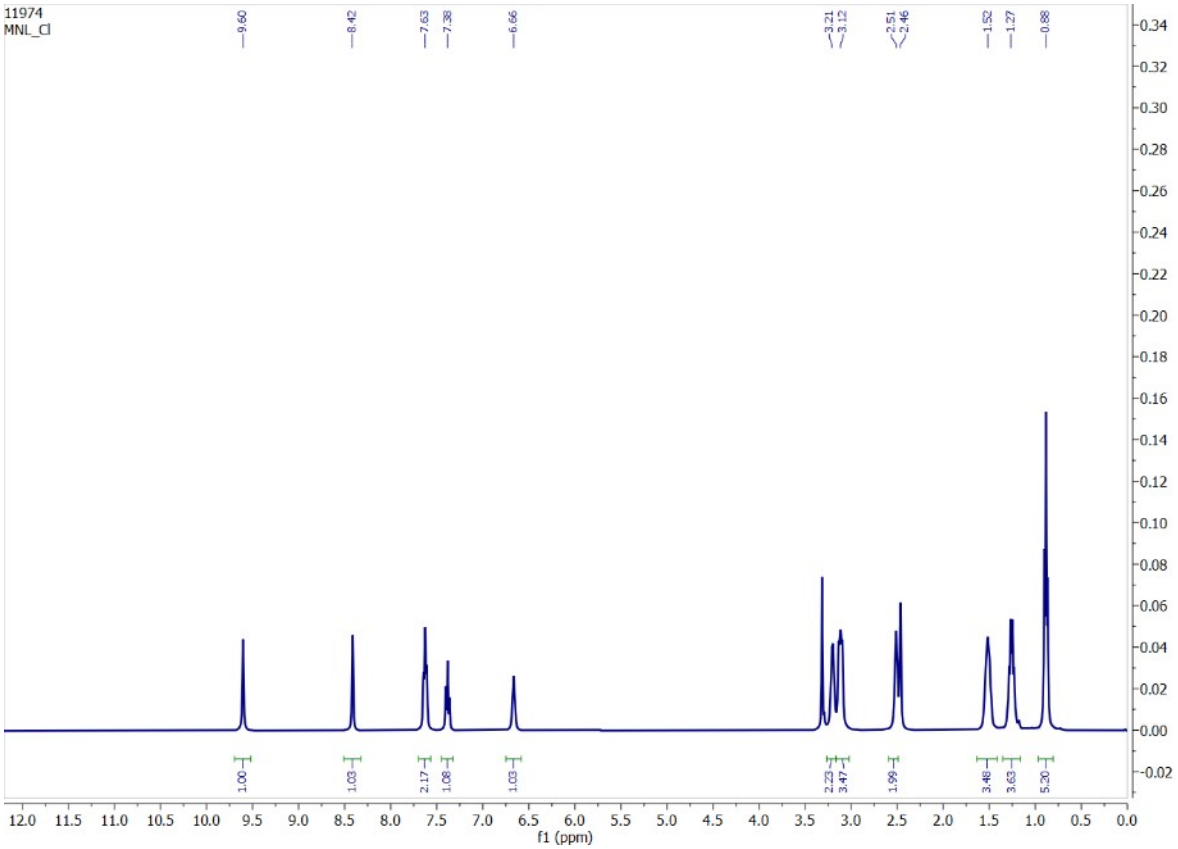

Fig. S10. ^{1}H-NMR spectrum of chloride complex, [(n-Bu_4N)(**L_1**·Cl)] in DMSO-D_6.

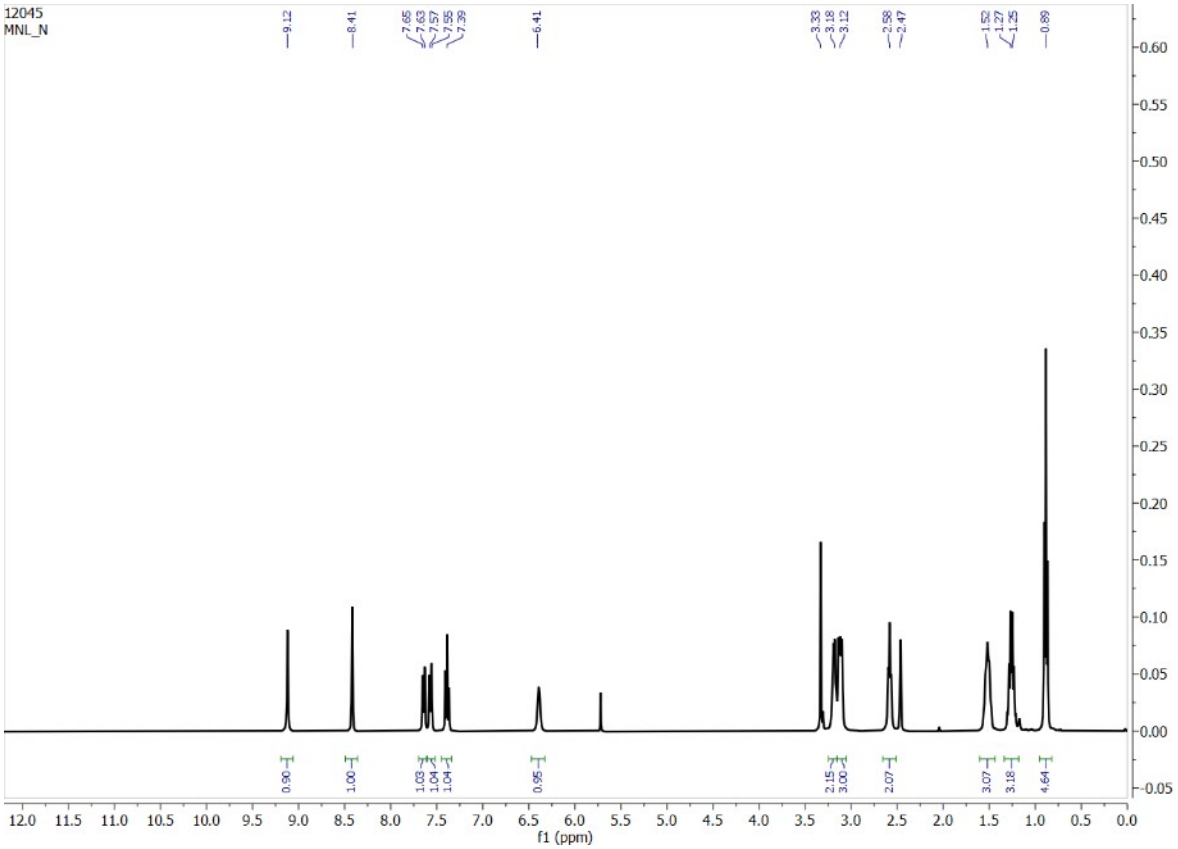

Fig. S11. ^{1}H-NMR spectrum of nitrate complex, [(n-Bu_4N)(**L_1**·NO_3)] in DMSO-D_6.

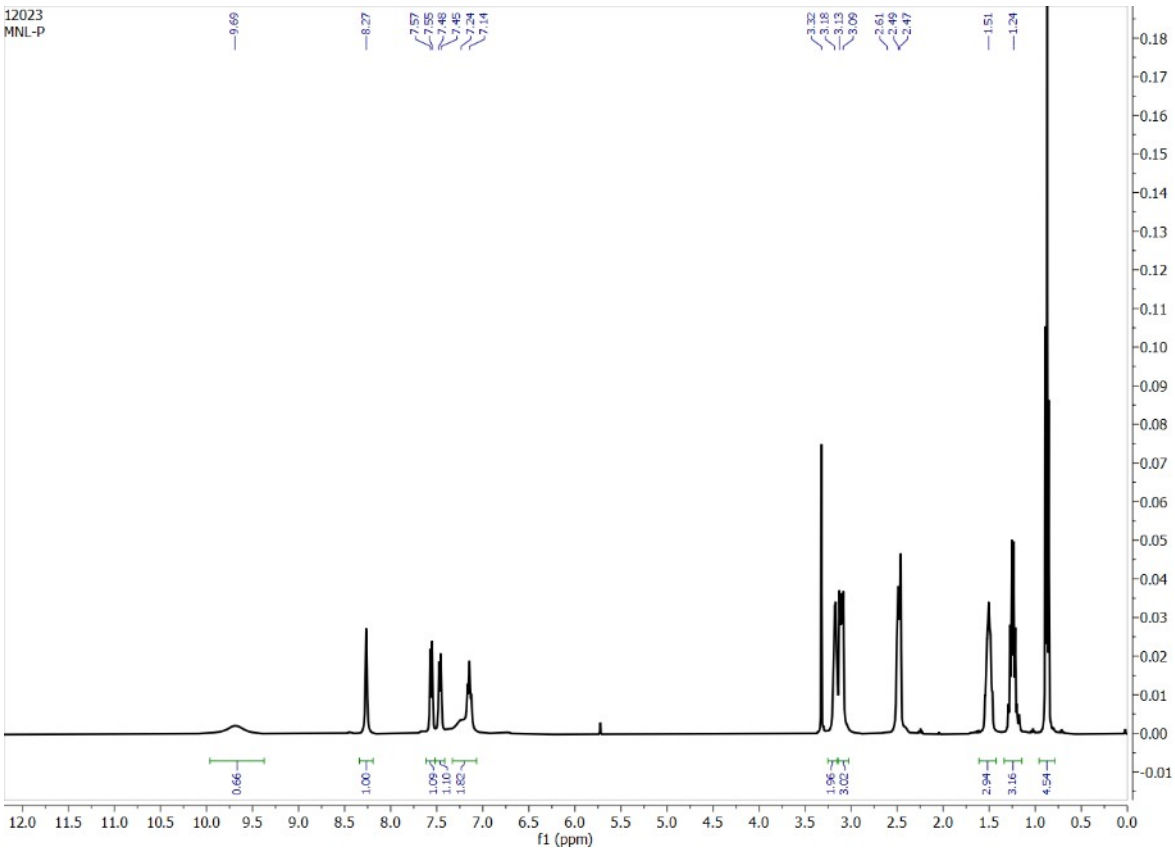

Fig. S12. ^{1}H-NMR spectrum of phosphate complex, mixture of [(n-$Bu_4N)_2$(2$\mathbf{L_1}$·HPO_4)]+[(n-$Bu_4N)_3$(2$\mathbf{L_1}$·PO_4)] in DMSO-D_6.

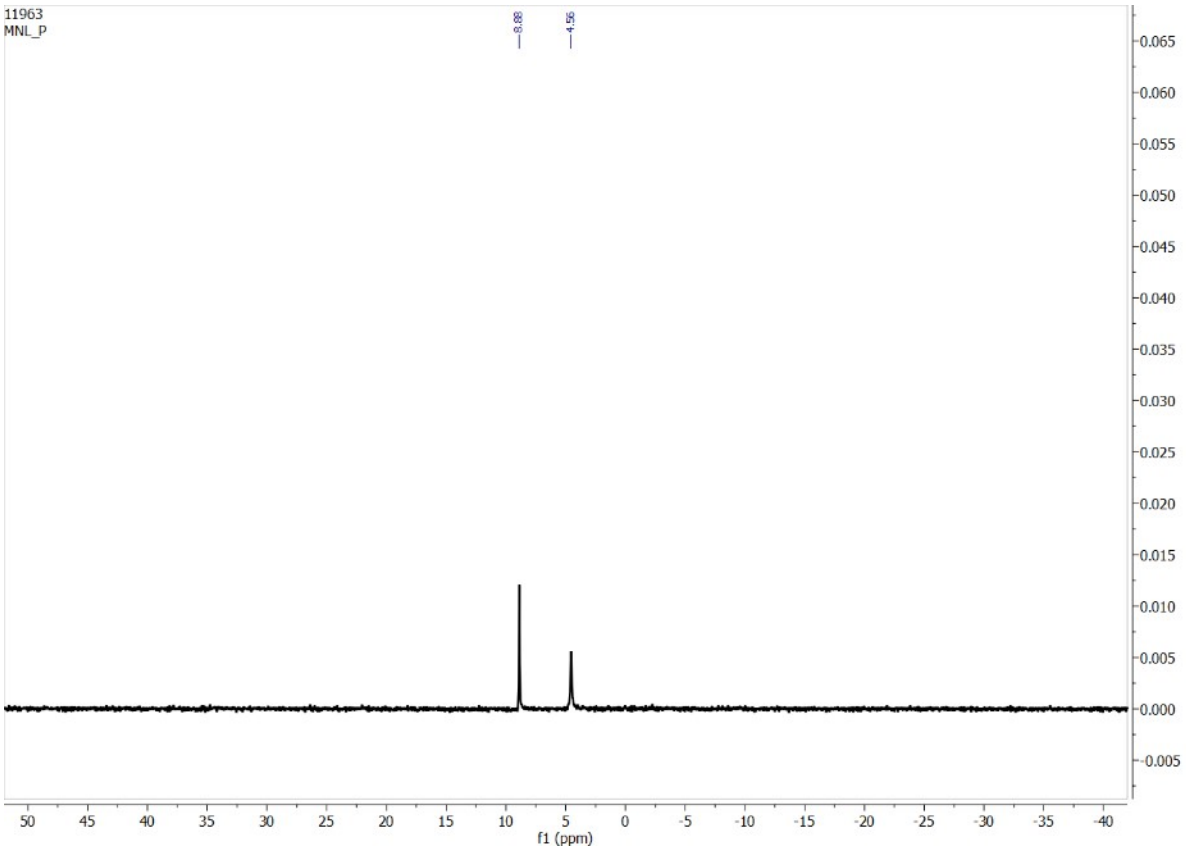

Fig. S13. ^{31}P-NMR spectrum of phosphate complex in DMSO-D_6, showing the presence of two phosphate species i.e., mixture of [(n-$Bu_4N)_2$(2**L_1**·HPO_4)] and [(n-$Bu_4N)_3$(2**L_1**·PO_4)].

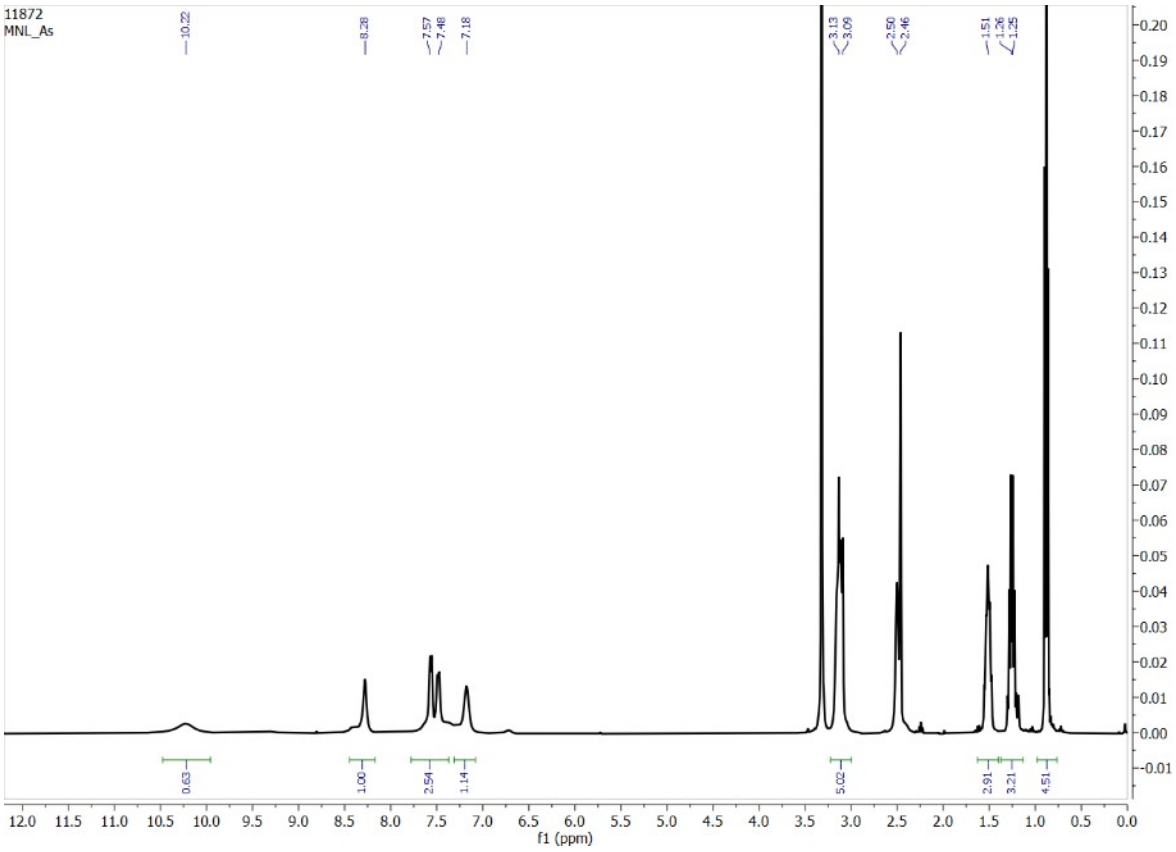

Fig. S14. ^{1}H-NMR spectrum of arsenate complex, [(n-$Bu_4N)_2$(2**L_1**·$HAsO_4$)] in DMSO-D_6.

7. Anion complexes of L_2: Characterization by NMR spectroscopy

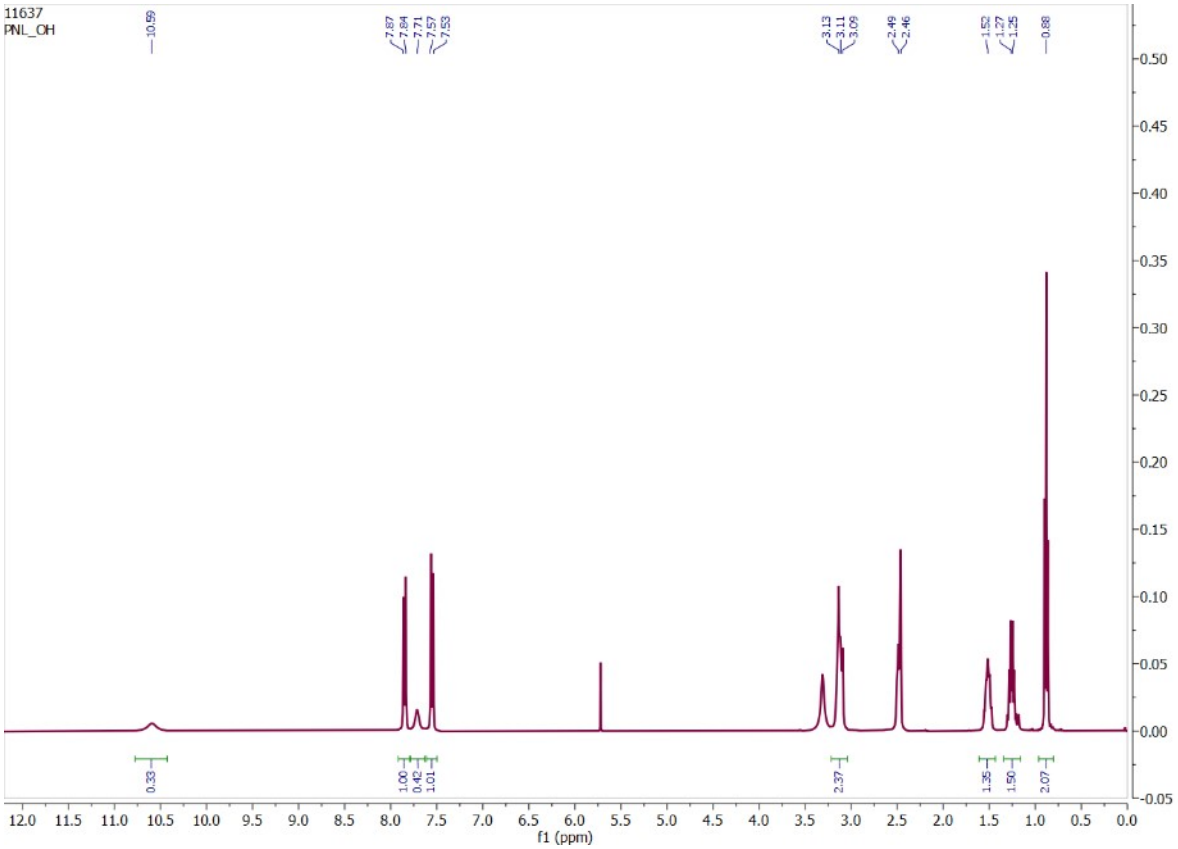

Fig. S15. ^{1}H-NMR spectrum of hydroxide complex, [(n-Bu_4N)(**L_2**·OH)] in DMSO-D_6.

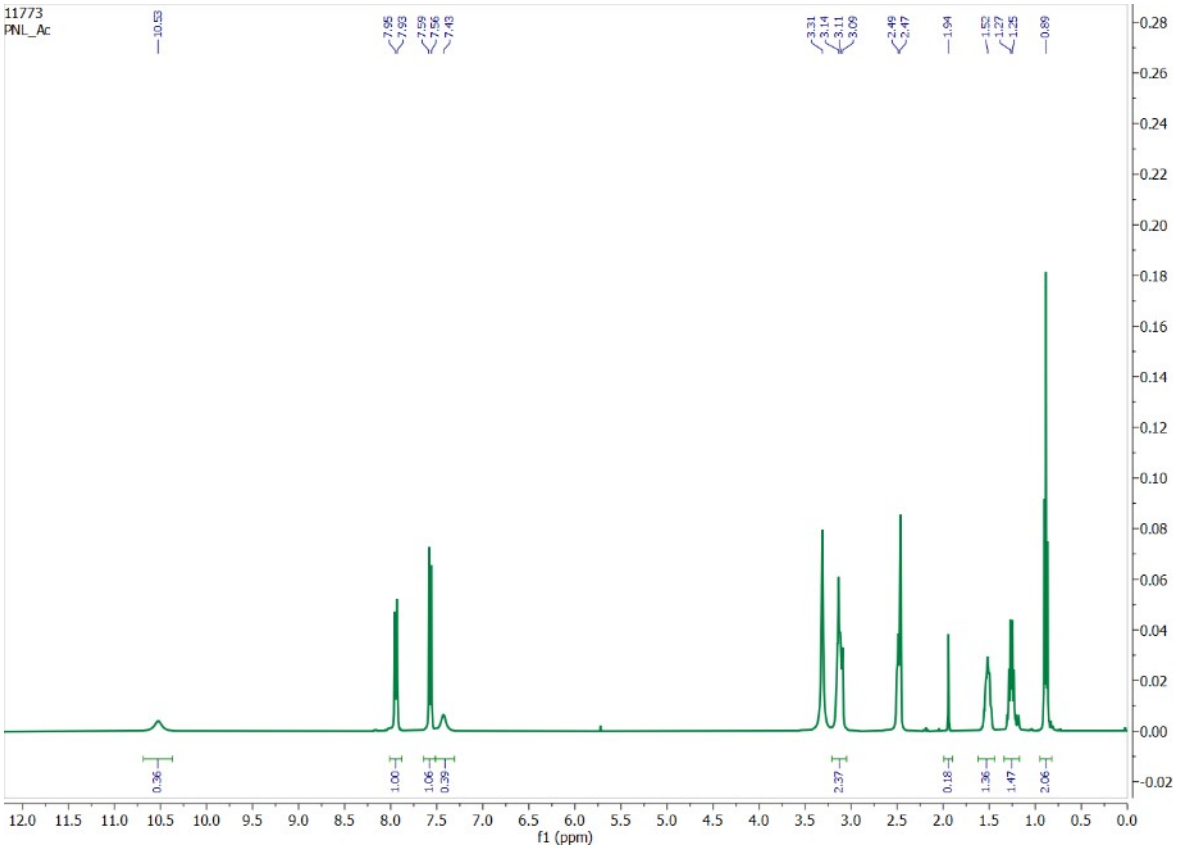

Fig. S16. ^{1}H-NMR spectrum of acetate complex, [(n-Bu_4N)(**L_2**·CH_3CO_2)] in DMSO-D_6.

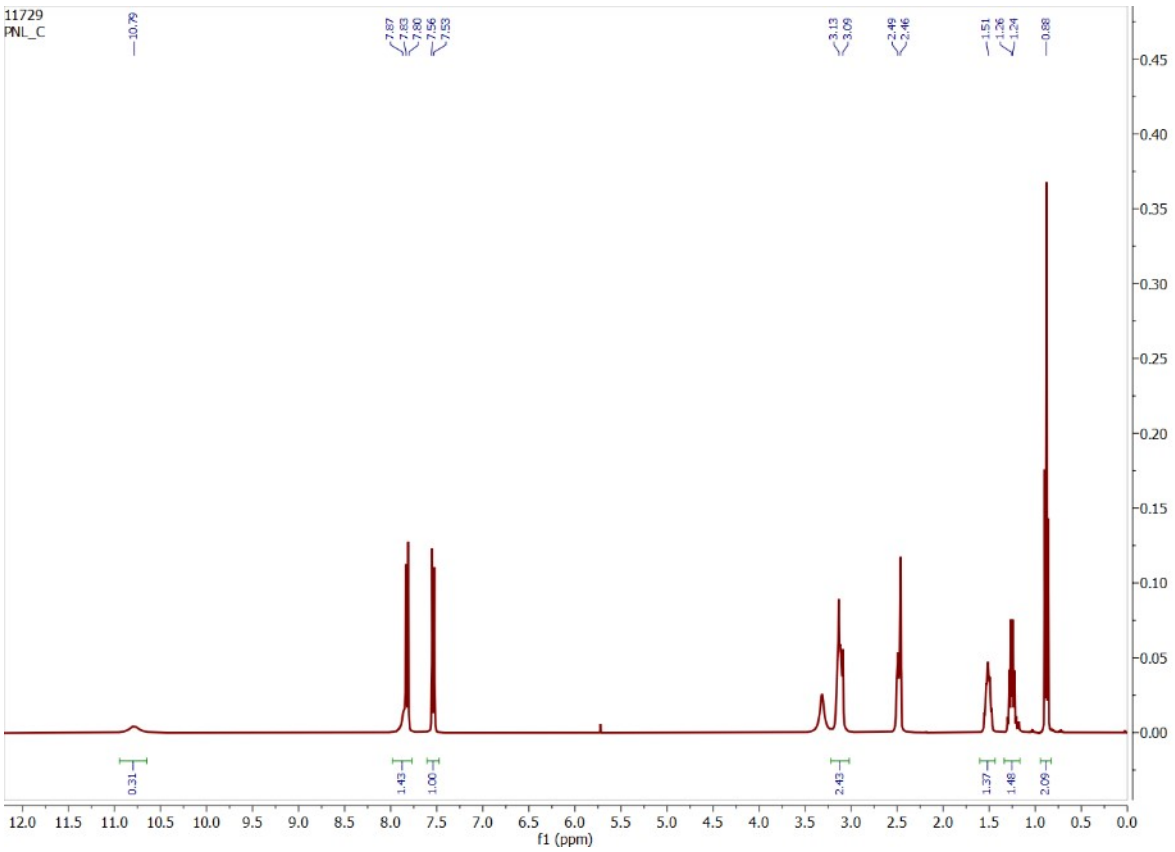

Fig. S17. ^{1}H-NMR spectrum of carbonate complex, [(n-$Bu_4N)_2$(2$\mathbf{L_2}$·CO_3)] in DMSO-D_6.

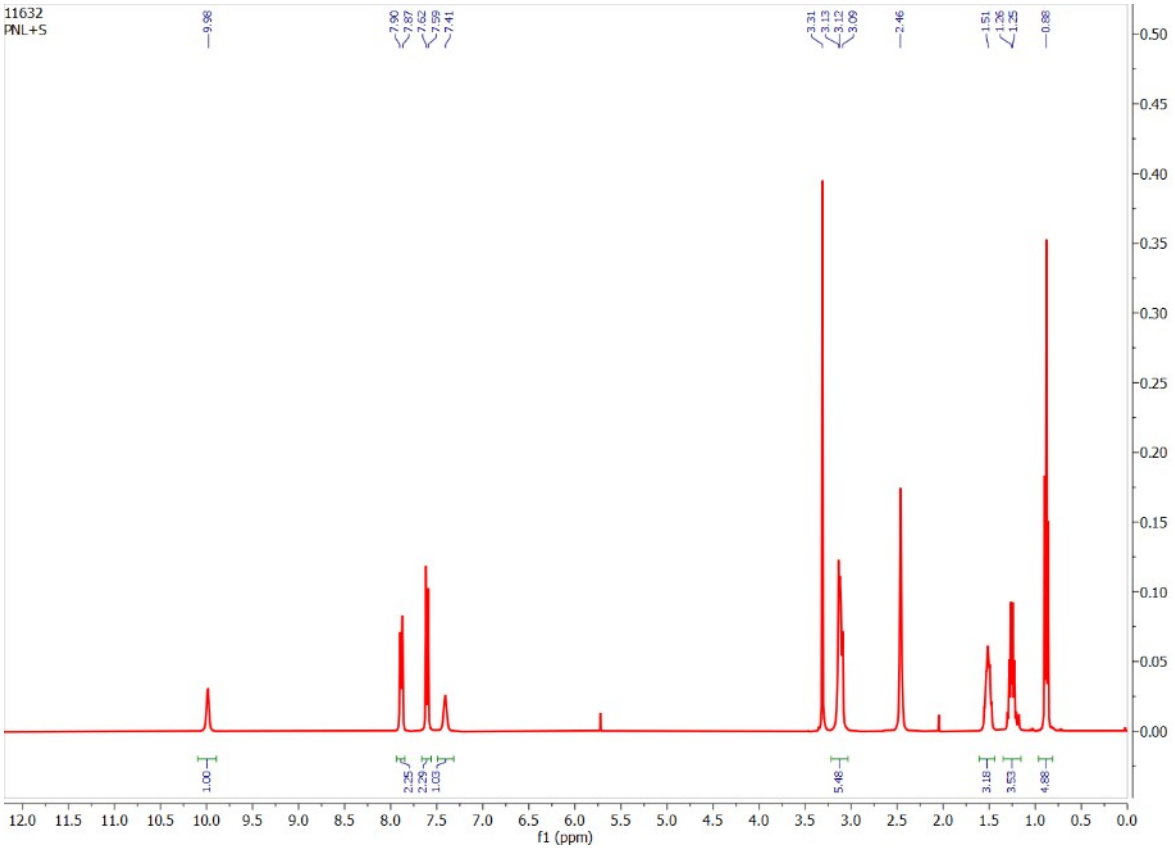

Fig. S18. ^{1}H-NMR spectrum of sulfate complex, [(n-$Bu_4N)_2$(2$\mathbf{L_2}$·SO_4)] in DMSO-D_6.

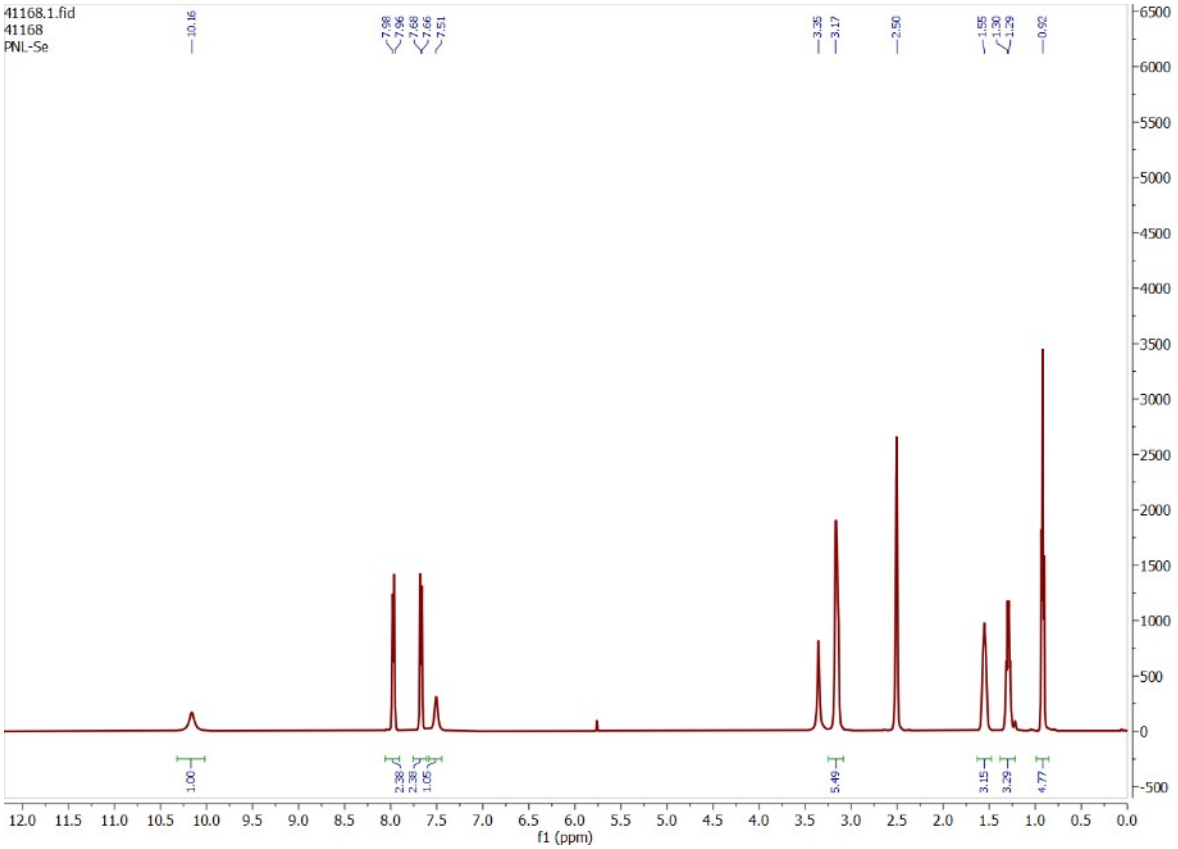

Fig. S19. ^{1}H-NMR spectrum of selenate complex, [(n-$Bu_4N)_2$(2**L$_2$**·SeO_4)] in DMSO-D_6.

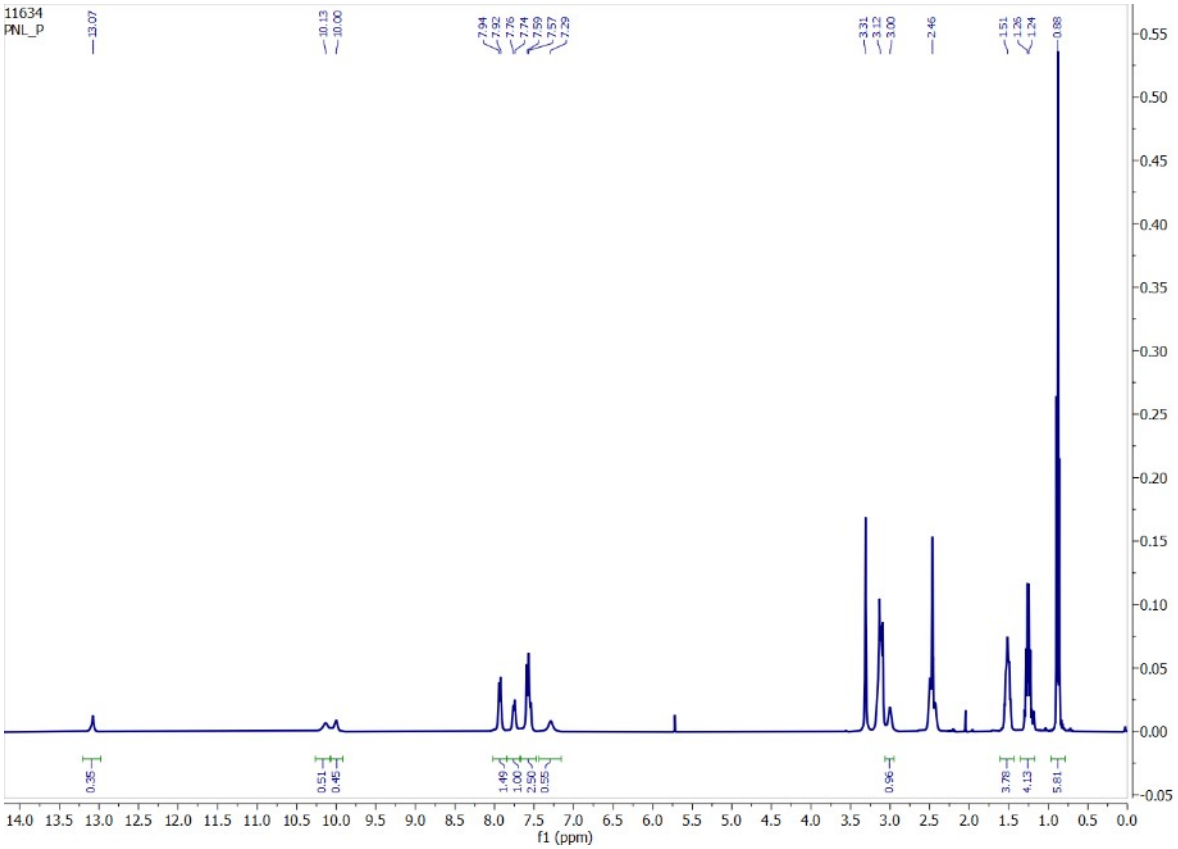

Fig. S20. ^{1}H-NMR spectrum of phosphate complex in DMSO-D_6, two sets of urea -NH and aromatic -CH signals observed due to the presence of a mixture of [(n-$Bu_4N)_2$(2**L$_2$**·HPO_4)] and [(n-$Bu_4N)_3$(2**L$_2$**·PO_4)].

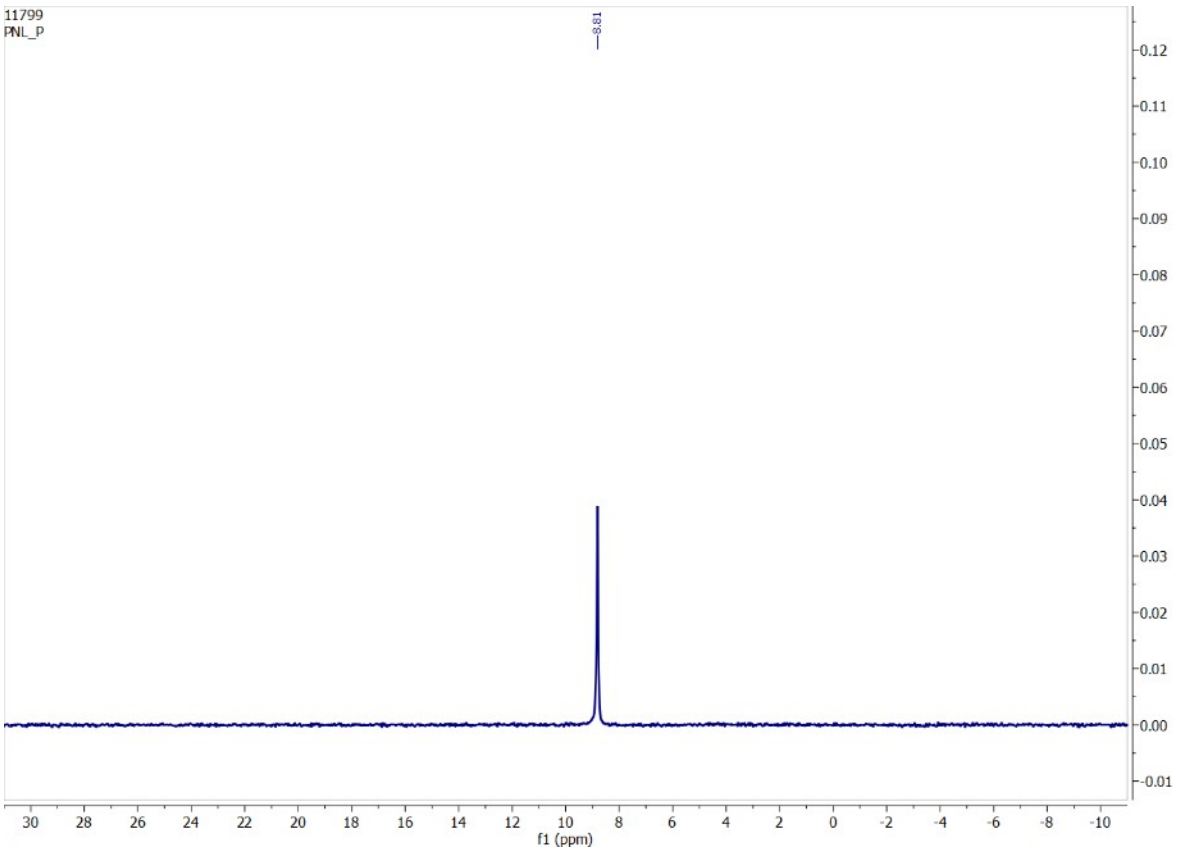

Fig. S21. ^{31}P-NMR spectrum of phosphate complex in DMSO-D_6, one signal observed for a mixture of [(n-$Bu_4N)_2$(2**L**$_2$·HPO_4)] and [(n-$Bu_4N)_3$(2**L**$_2$·PO_4)].

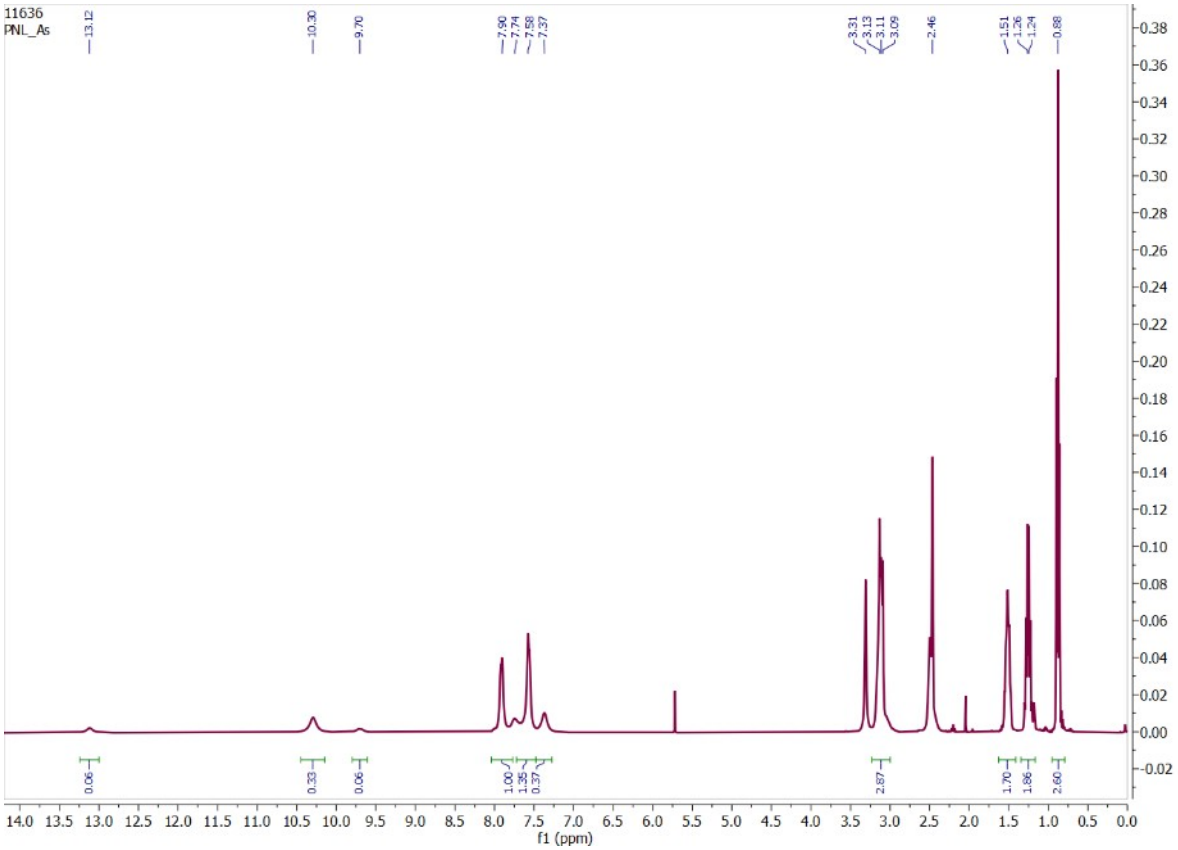

Fig. S22. ^{1}H-NMR spectrum of arsenate complex in DMSO-D_6, two sets of urea -NH and aromatic -CH signals observed due to the presence of a mixture of [(n-$Bu_4N)_2$(2**L**$_2$·$HAsO_4$)] and [(n-$Bu_4N)_3$(2**L**$_2$·AsO_4)].

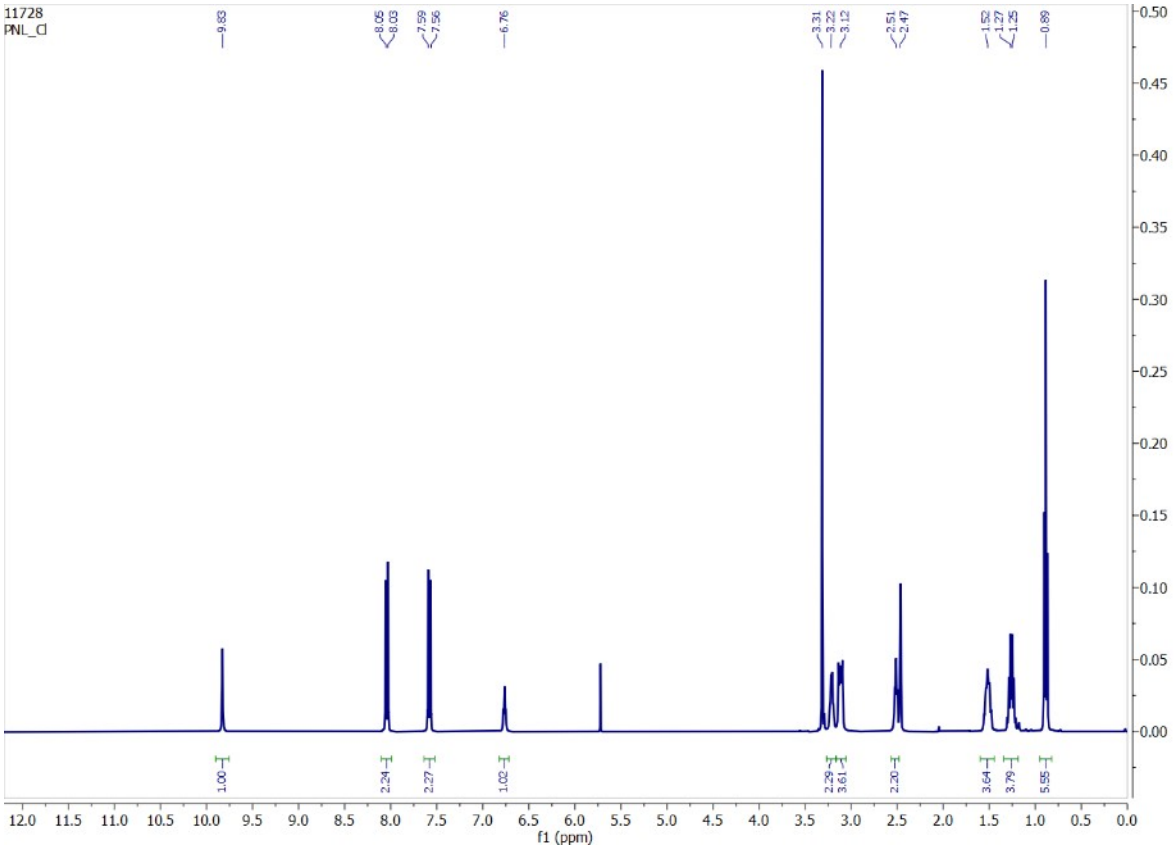

Fig. S23. ^{1}H-NMR spectrum of chloride complex, [(n-Bu_4N)(**L_2**·Cl)] in DMSO-D_6.

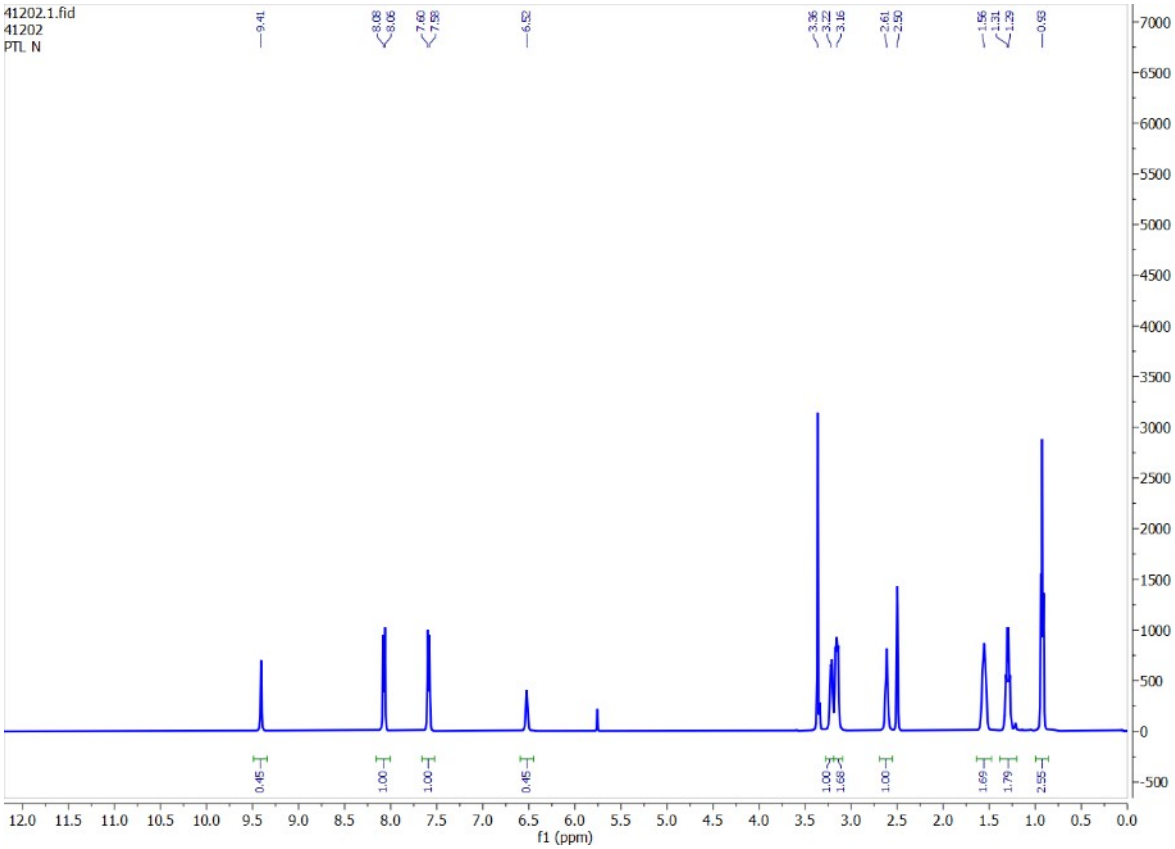

Fig. S24. ^{1}H-NMR spectrum of nitrate complex, [(n-Bu_4N)(**L_2**·NO_3)] in DMSO-D_6.

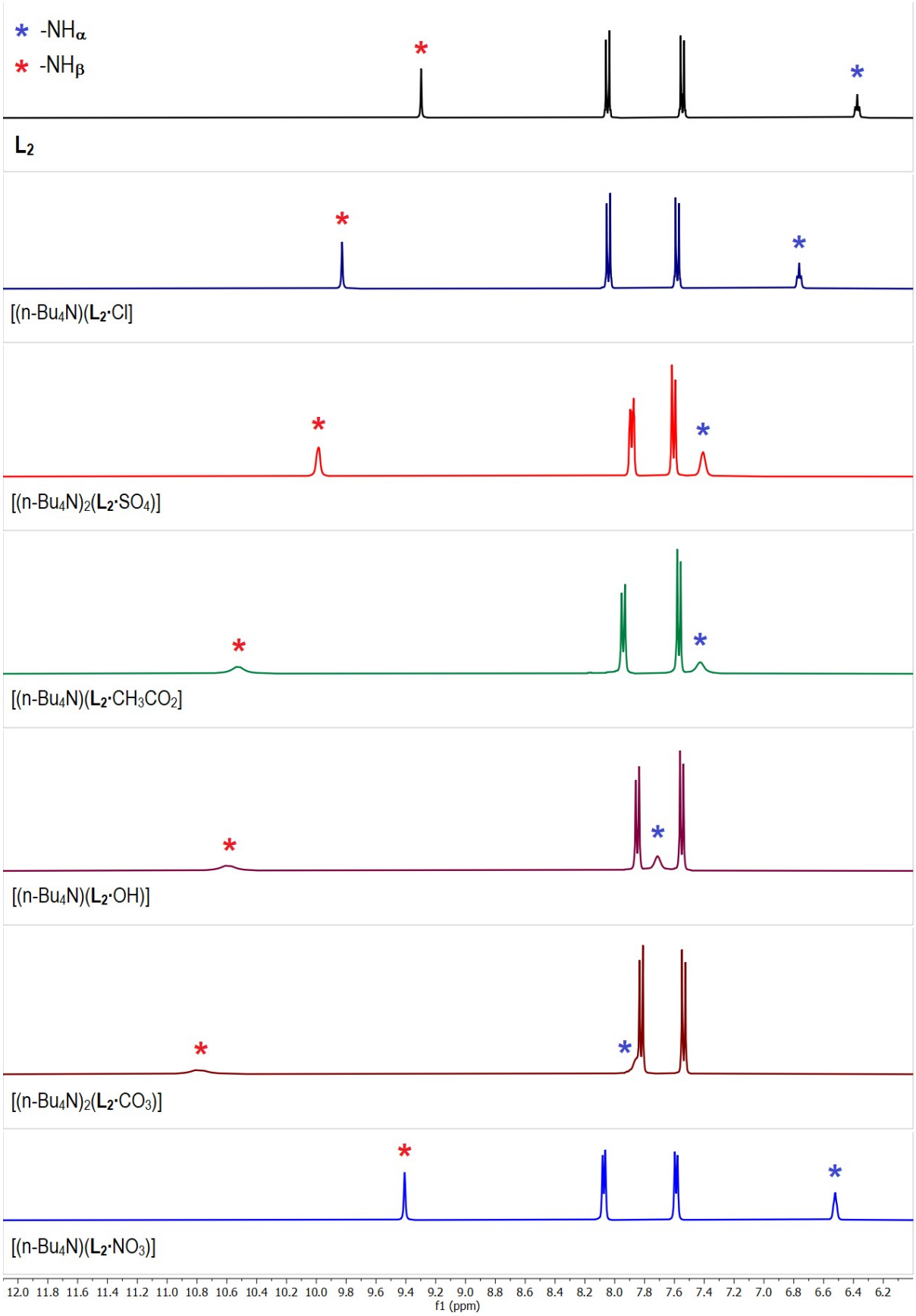

Fig S25. Aromatic region of the ^{1}H-NMR (DMSO-d_6) spectra of $\mathbf{L_2}$ and the receptor-anion complexes showing variable downfield shift of the urea -NH signals in different anion complexes relative to $\mathbf{L_2}$.

8. Anion complexes of L_3: Characterization by NMR spectroscopy

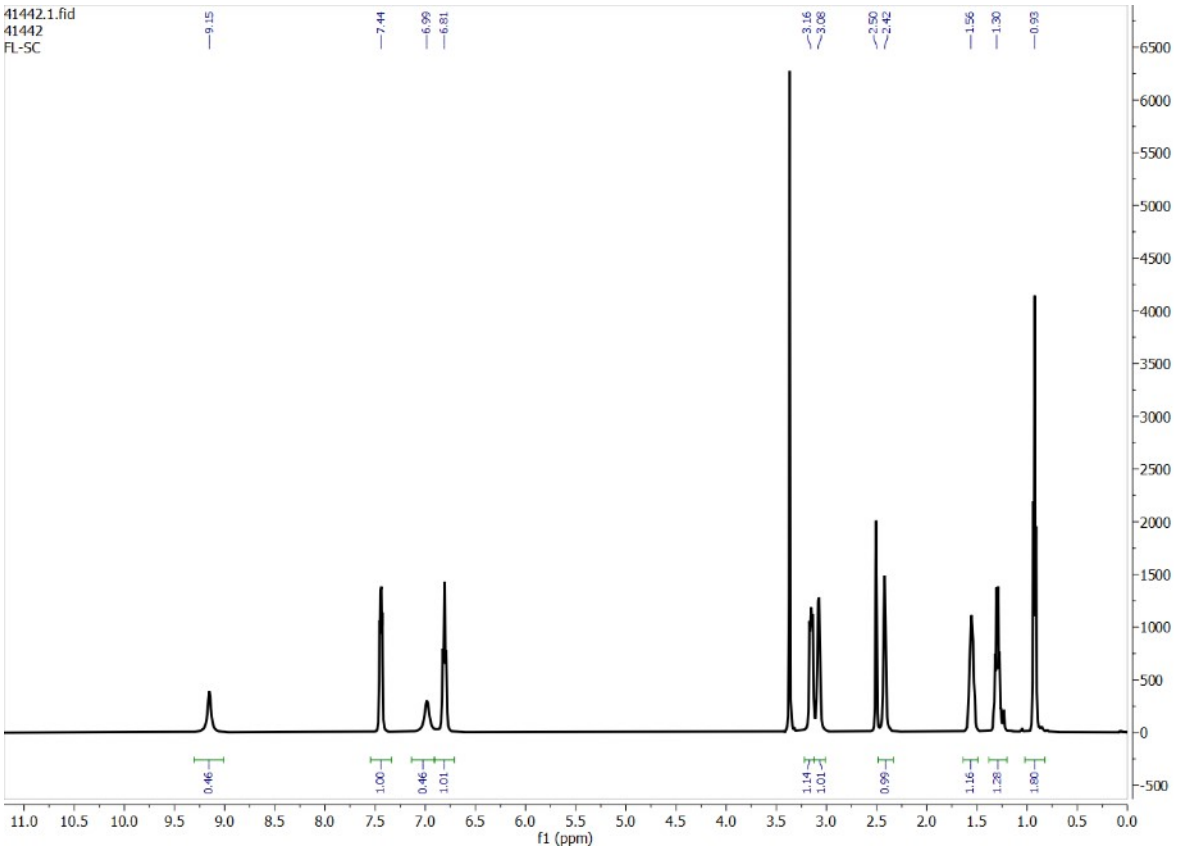

Fig. S26. ^{1}H-NMR spectrum of sulfate complex, [(n-$Bu_4N)_2$(2**L_3**·SO_4)] in DMSO-D_6.

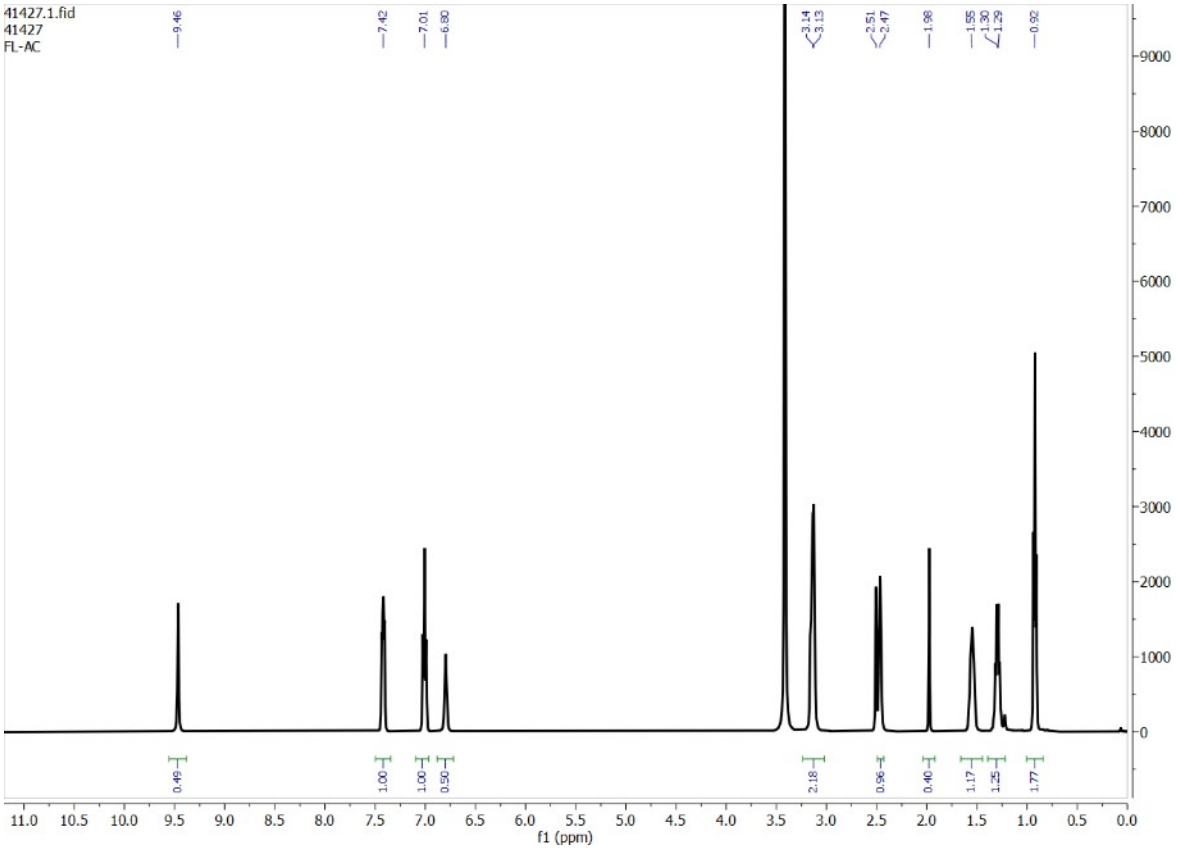

Fig. S27. ^{1}H-NMR spectrum of acetate complex, [(n-Bu_4N)(**L_3**·CH_3CO_2)] in DMSO-D_6.

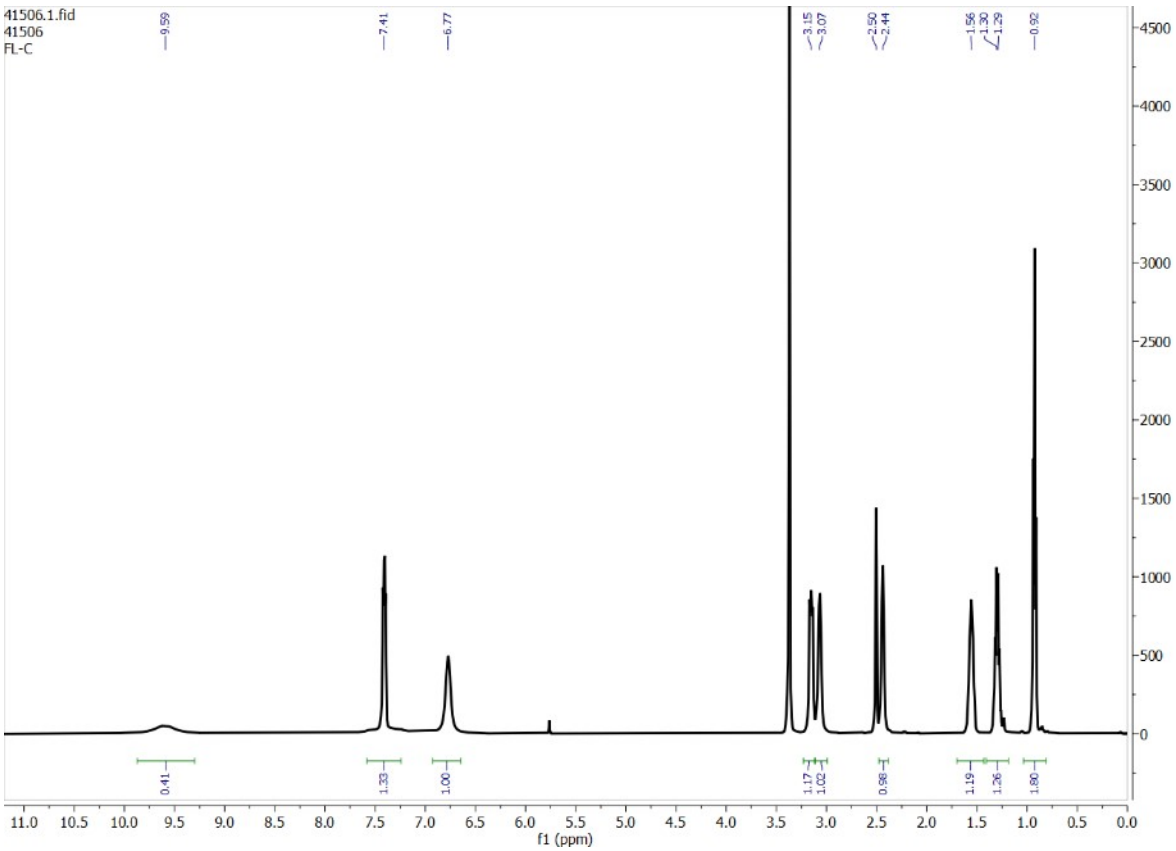

Fig. S28. ^{1}H-NMR spectrum of carbonate complex, [(n-Bu_4N)$_2$(2**L$_3$**·CO_3)] in DMSO-D_6.

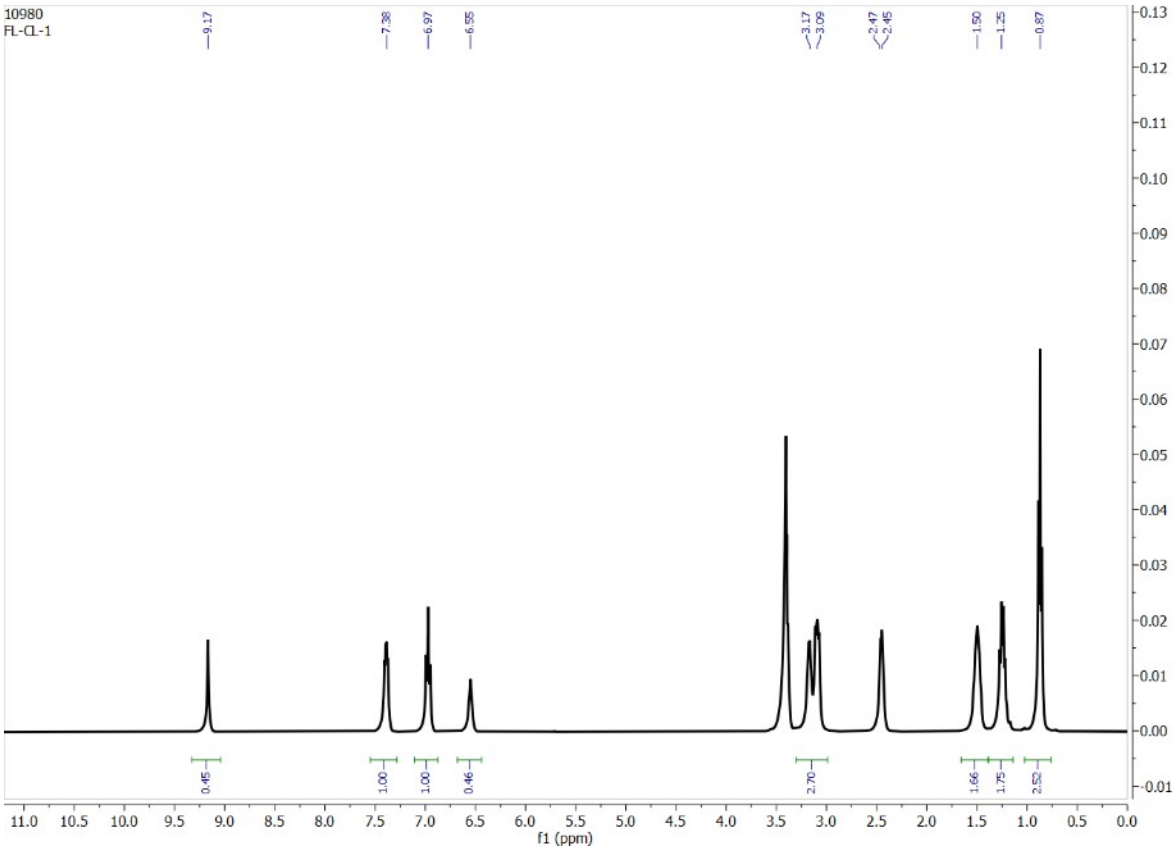

Fig. S29. ^{1}H-NMR spectrum of chloride complex, [(n-Bu_4N)(**L$_3$**·Cl)] in DMSO-D_6.

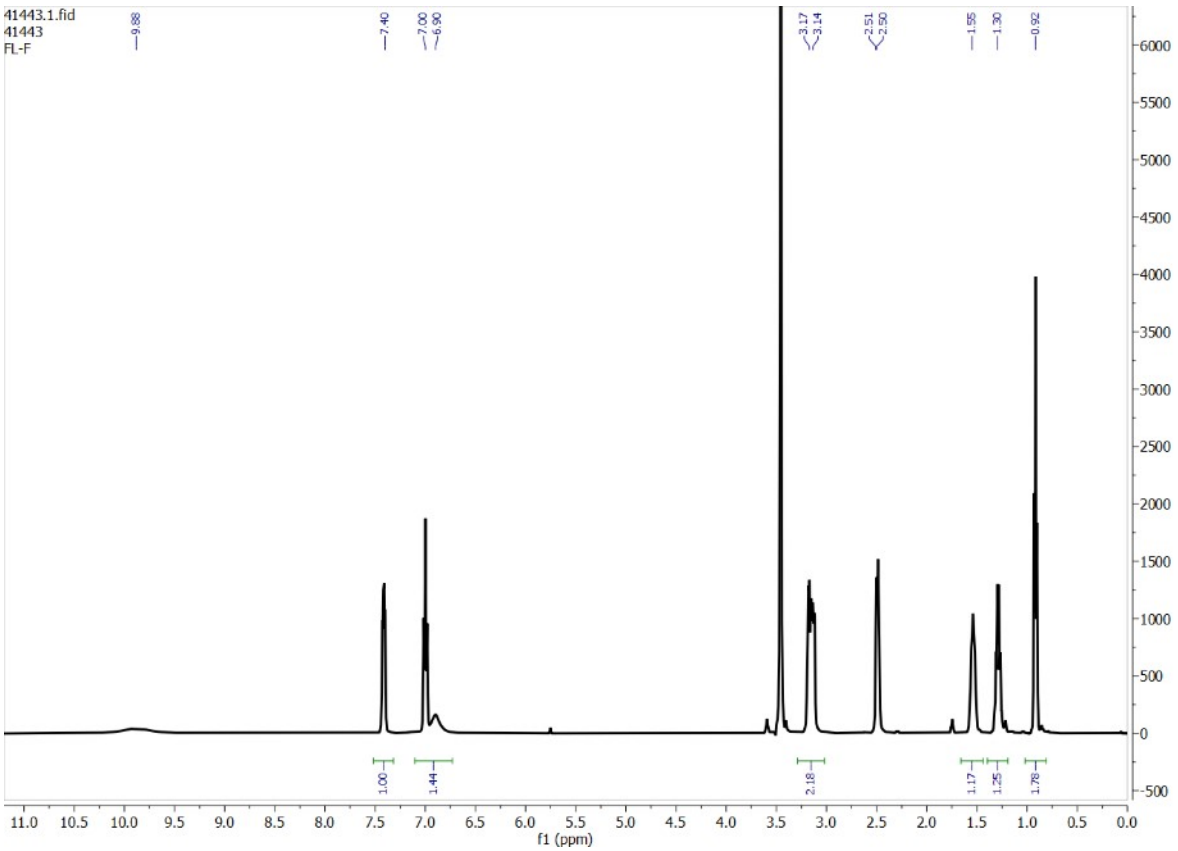

Fig. S30. ^{1}H-NMR spectrum of fluoride complex, [(n-Bu_4N)(**L_3**·F)] in DMSO-D_6.

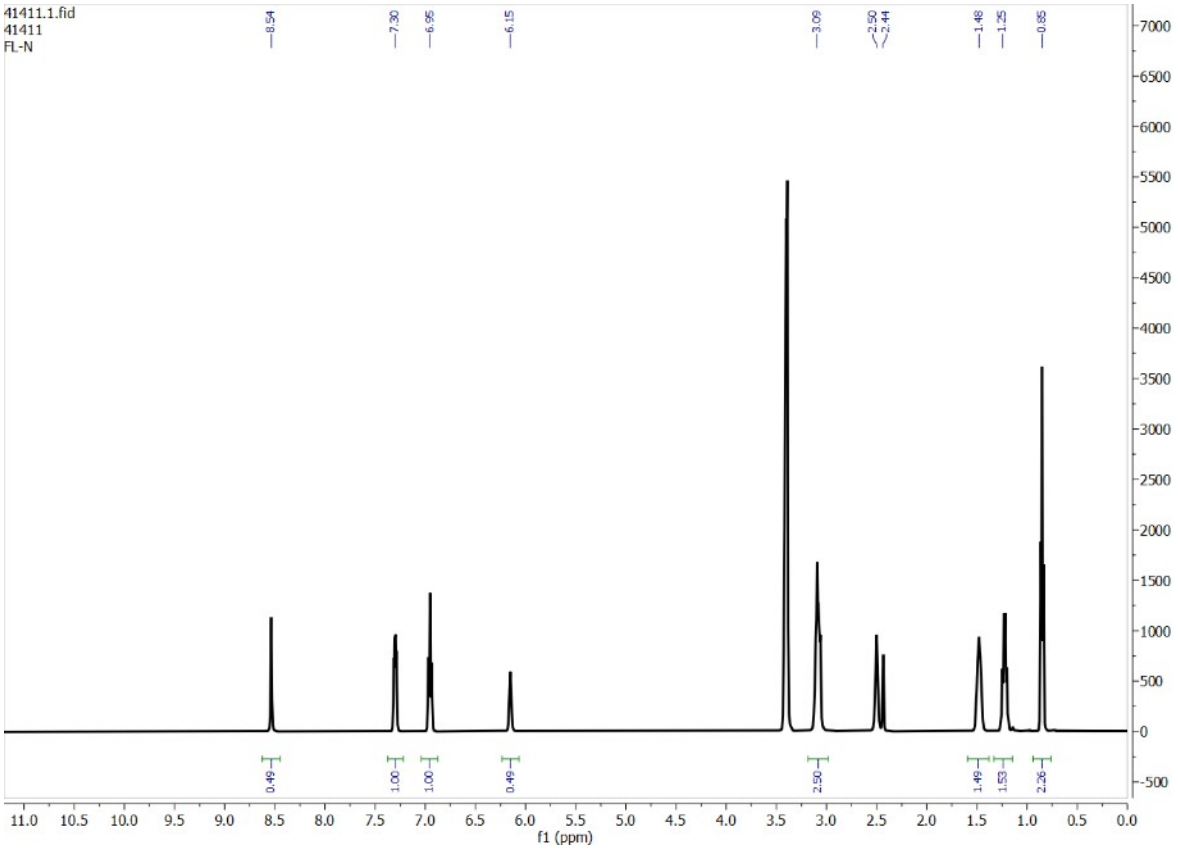

Fig. S31. ^{1}H-NMR spectrum of nitrate complex, [(n-Bu_4N)(**L_3**·NO_3)] in DMSO-D_6.

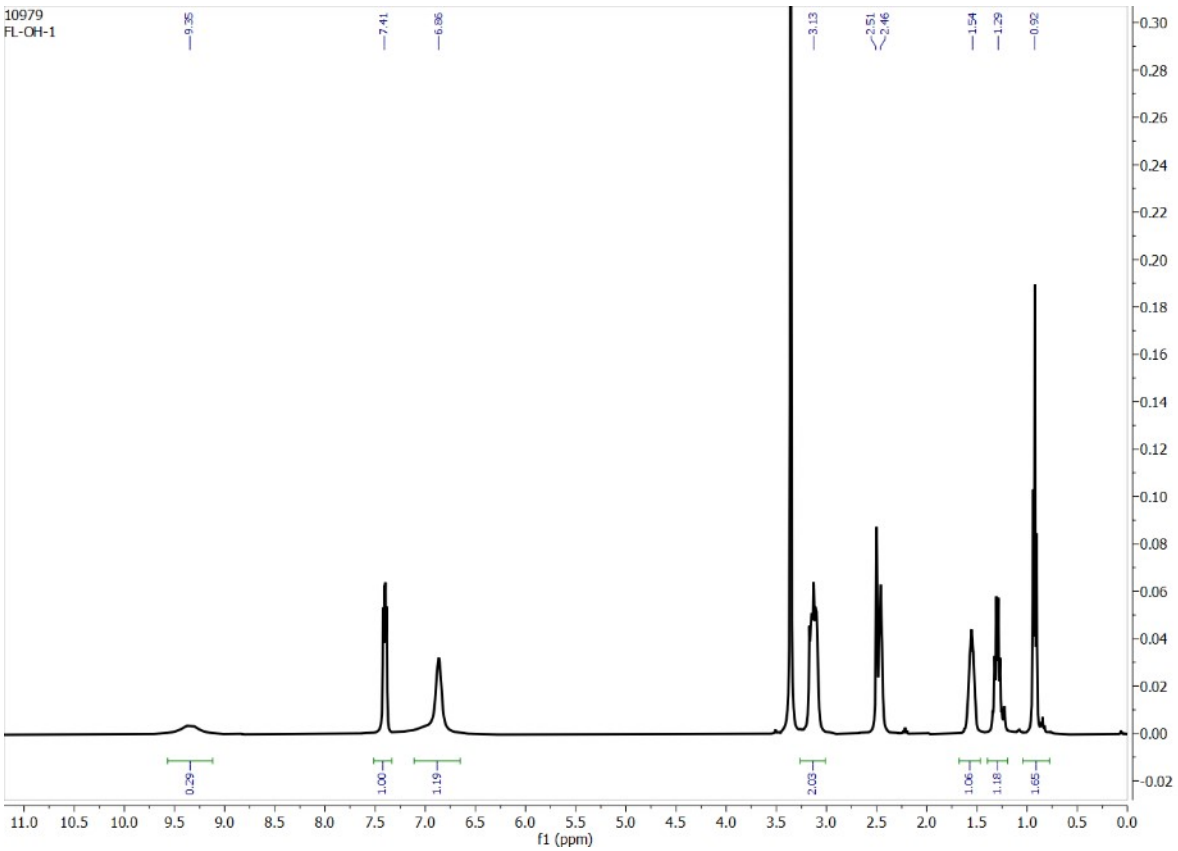

Fig. S32. ^{1}H-NMR spectrum of hydroxide complex, [(n-Bu_4N)(**L_3**·OH)] in DMSO-D_6.

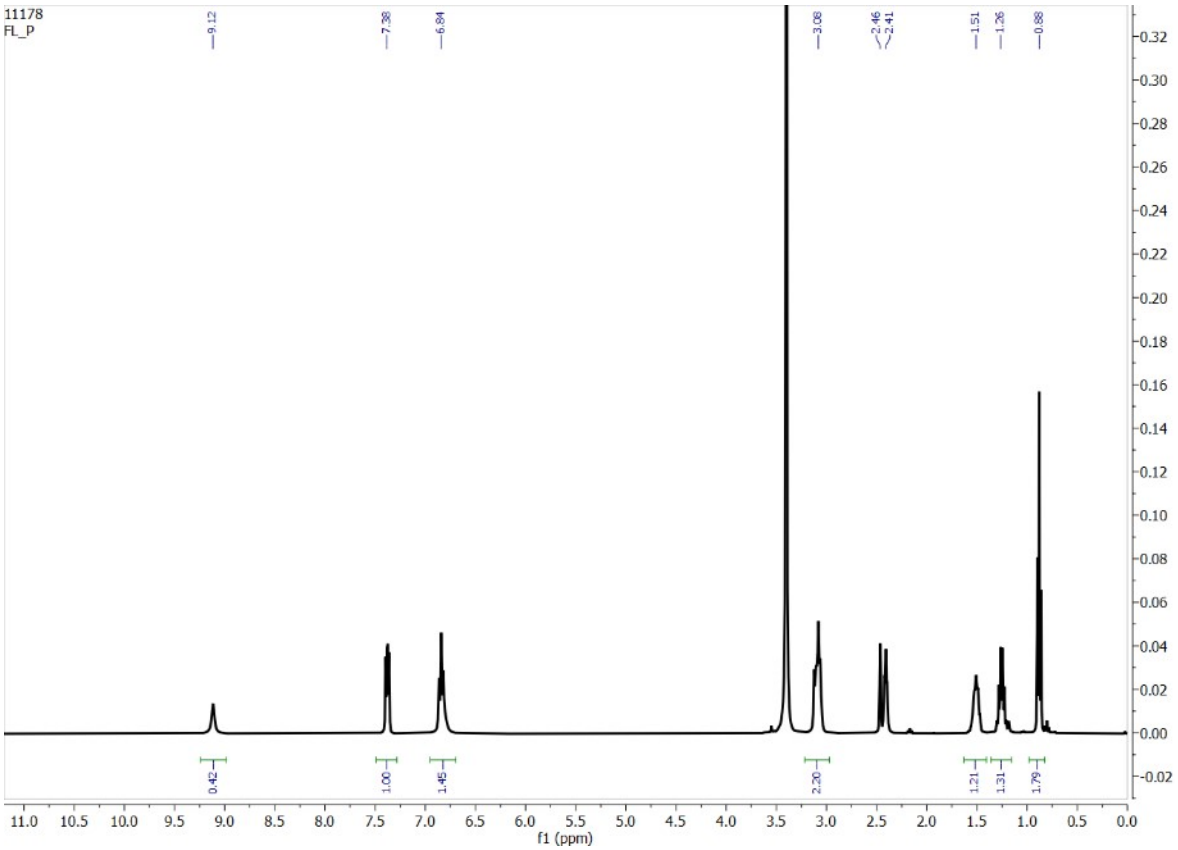

Fig. S33. ^{1}H-NMR spectrum of hydrogenphosphate complex, [(n-Bu_4N)$_2$(2**L_3**·HPO_4)] in DMSO-D_6.

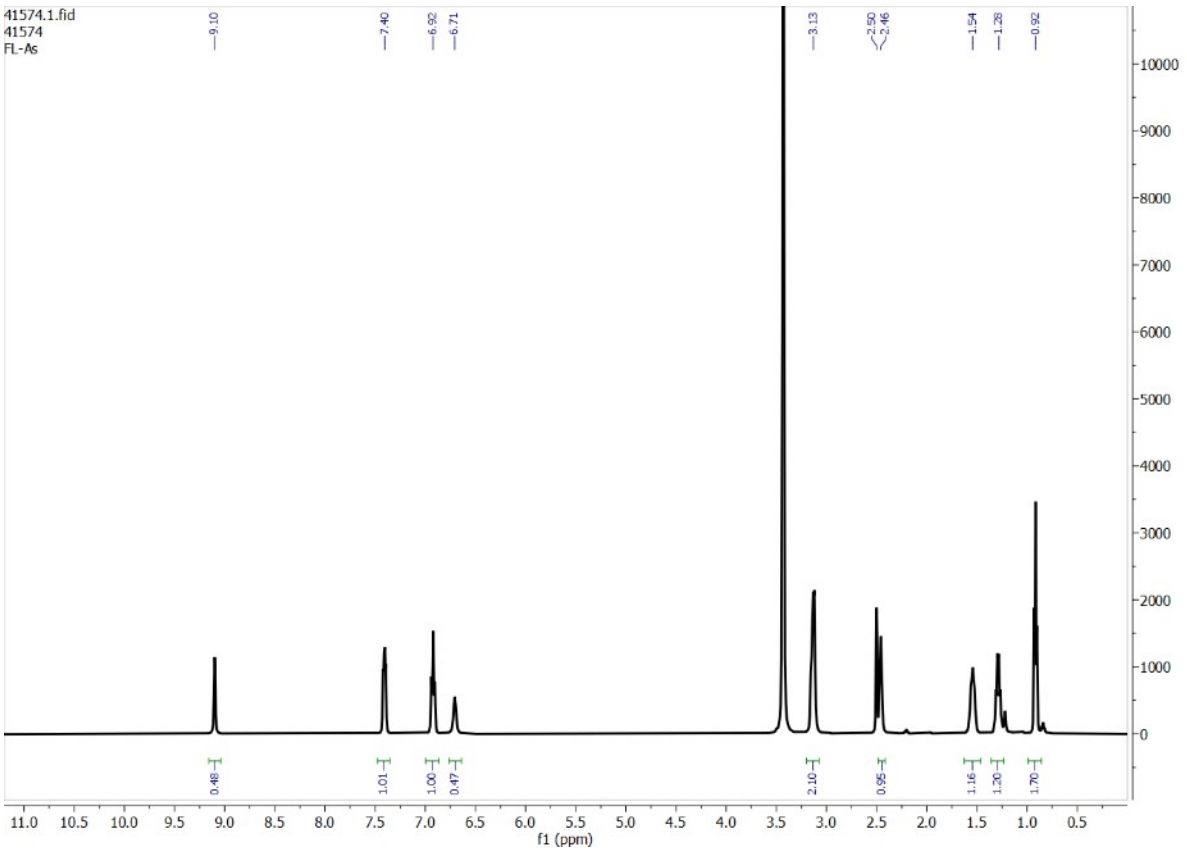

Fig. S34. ^{1}H-NMR spectrum of hydrogenarsenate complex, [(n-Bu_4N)$_2$(2**L$_3$**·$HAsO_4$)] in DMSO-D_6.

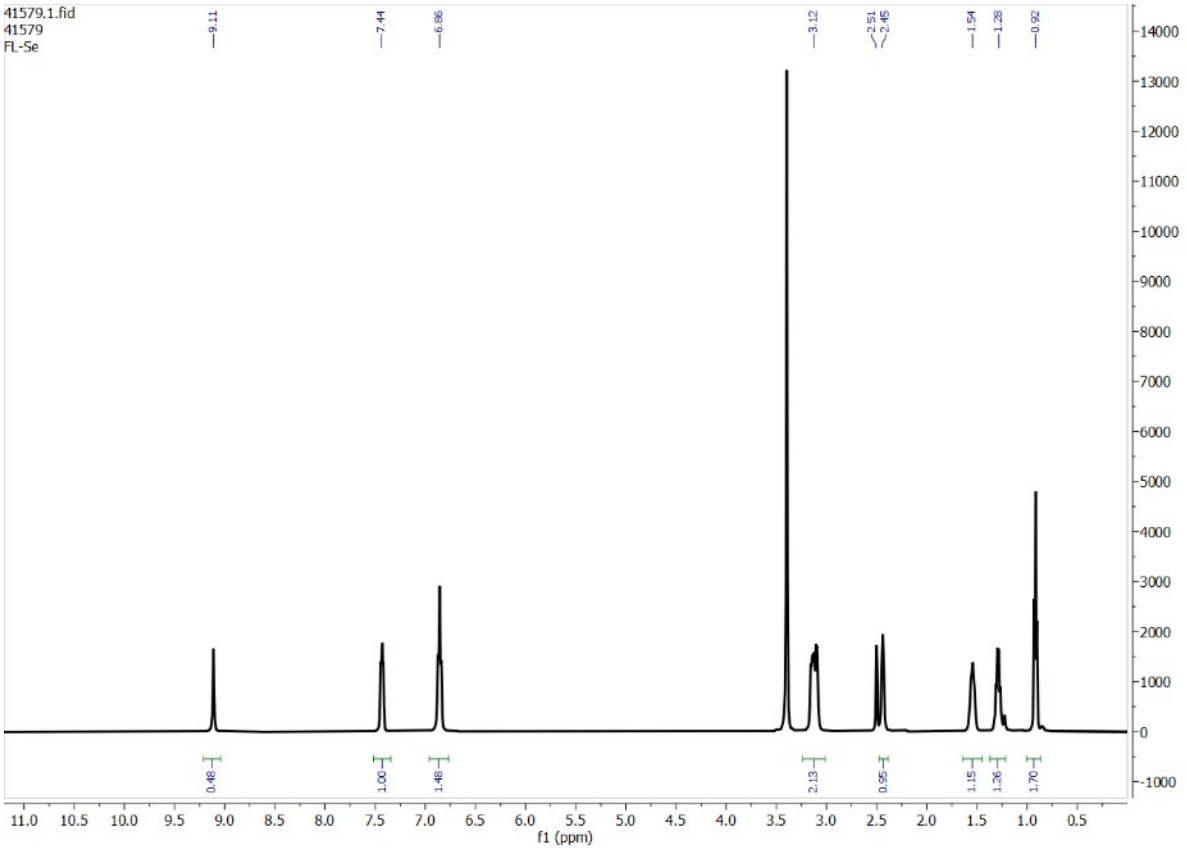

Fig. S35. ^{1}H-NMR spectrum of selenate complex, [(n-Bu_4N)$_2$(2**L$_3$**·SeO_4)] in DMSO-D_6.

9. Selective extraction of sulfate by L_1: ^{1}H-NMR spectra of LLE isolated sulfate complexes

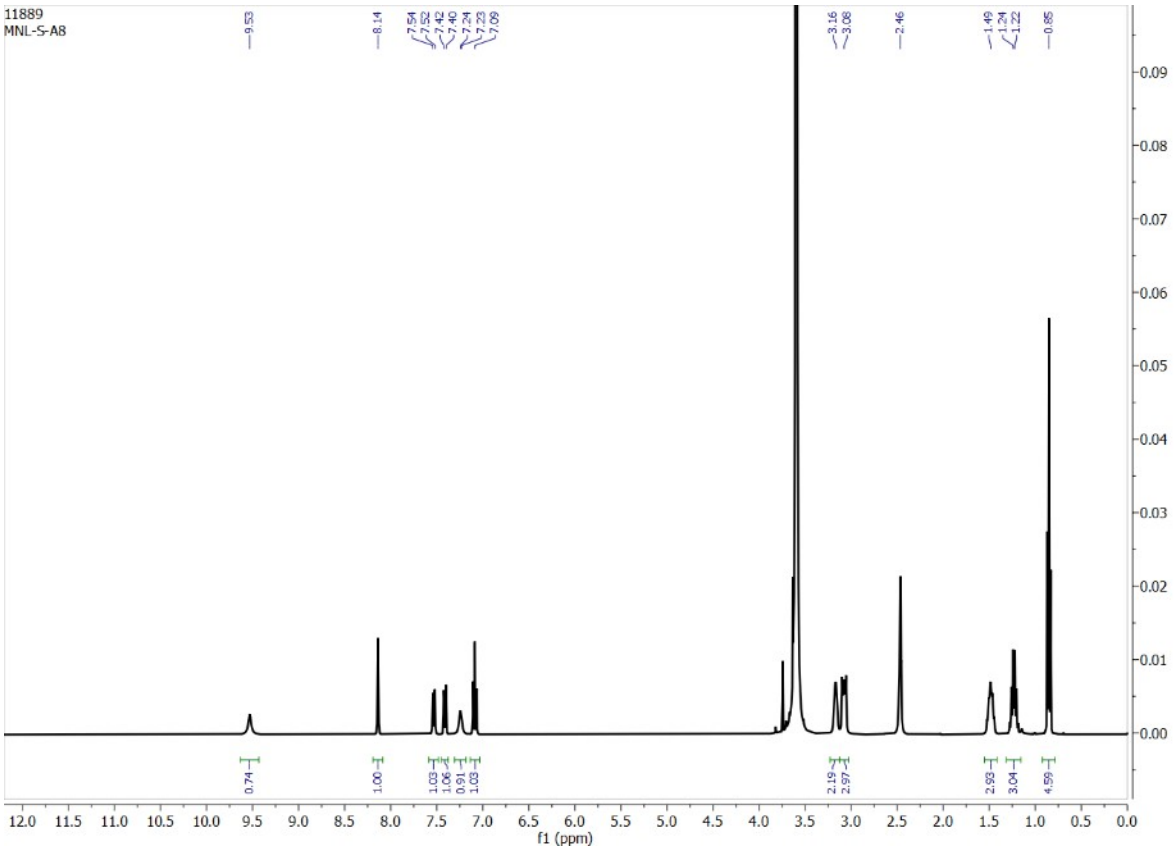

Fig. S36. ^{1}H-NMR spectrum of [(n-$Bu_4N)_2$(2$\mathbf{L_1}$·SO_4)] obtained from LLE in the presence of acetate as a competing anion.

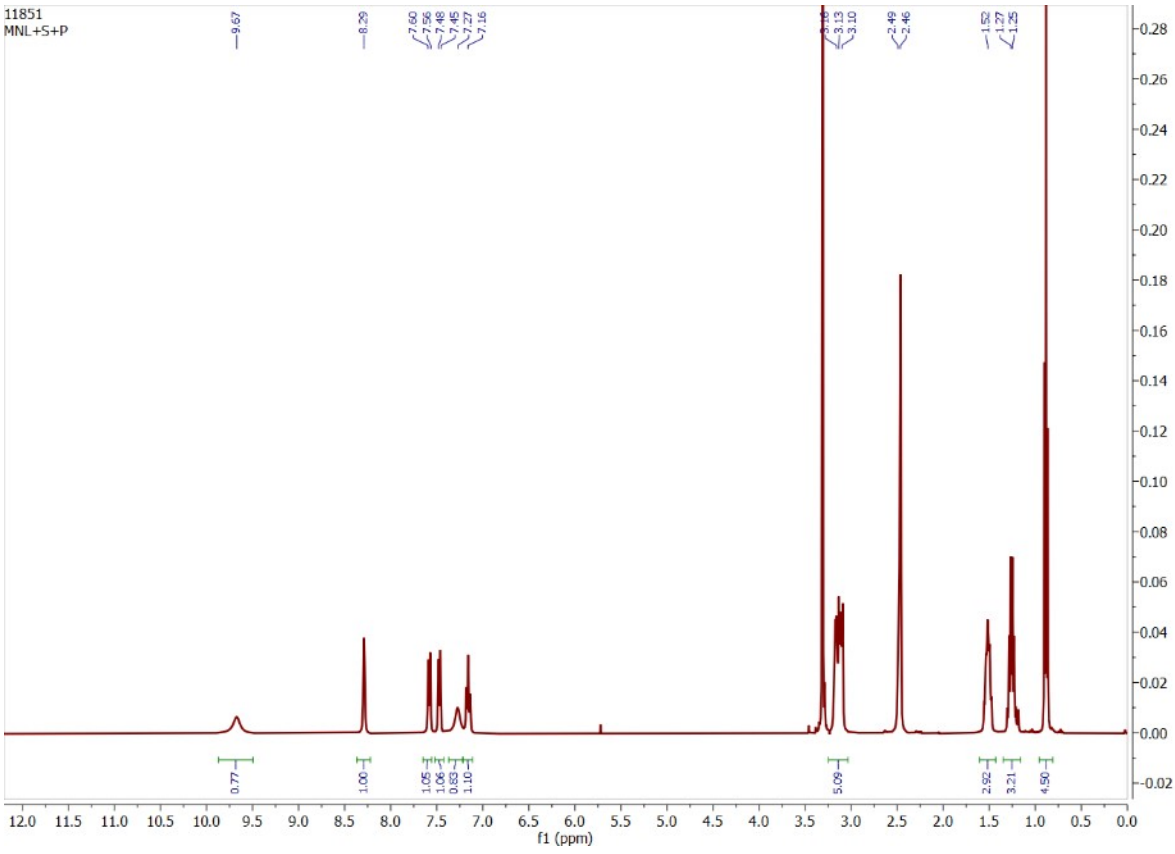

Fig. S37. ^{1}H-NMR spectrum of [(n-$Bu_4N)_2$(2**L**$_1$·SO_4)] obtained from LLE in the presence of HPO_4^{2-} as a competing anion.

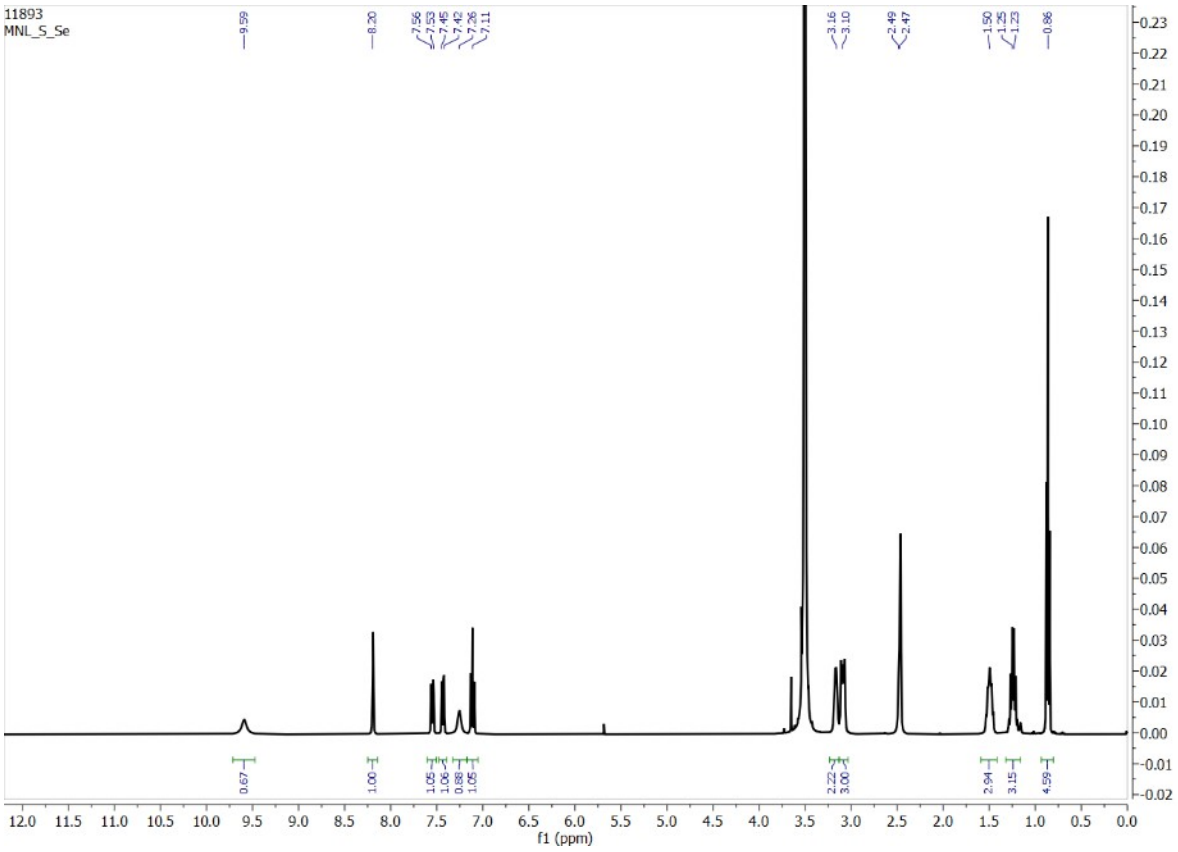

Fig. S38. ^{1}H-NMR spectrum of [(n-$Bu_4N)_2$(2**L**$_1$·SO_4)] obtained from LLE in the presence of selenate as a competing anion.

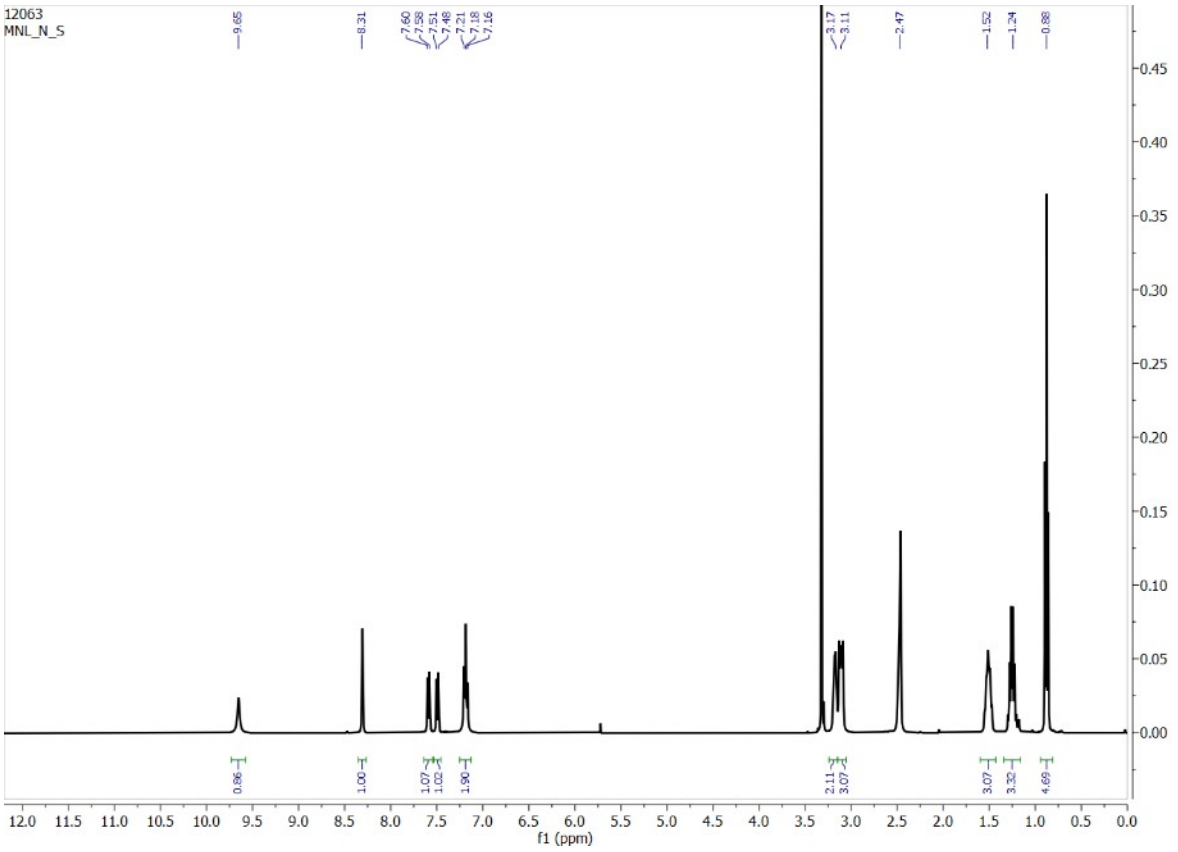

Fig. S39. ^{1}H-NMR spectrum of [(n-$Bu_4N)_2$(2**L**$_1$·SO_4)] obtained from LLE in the presence of nitrate as a competing anion.

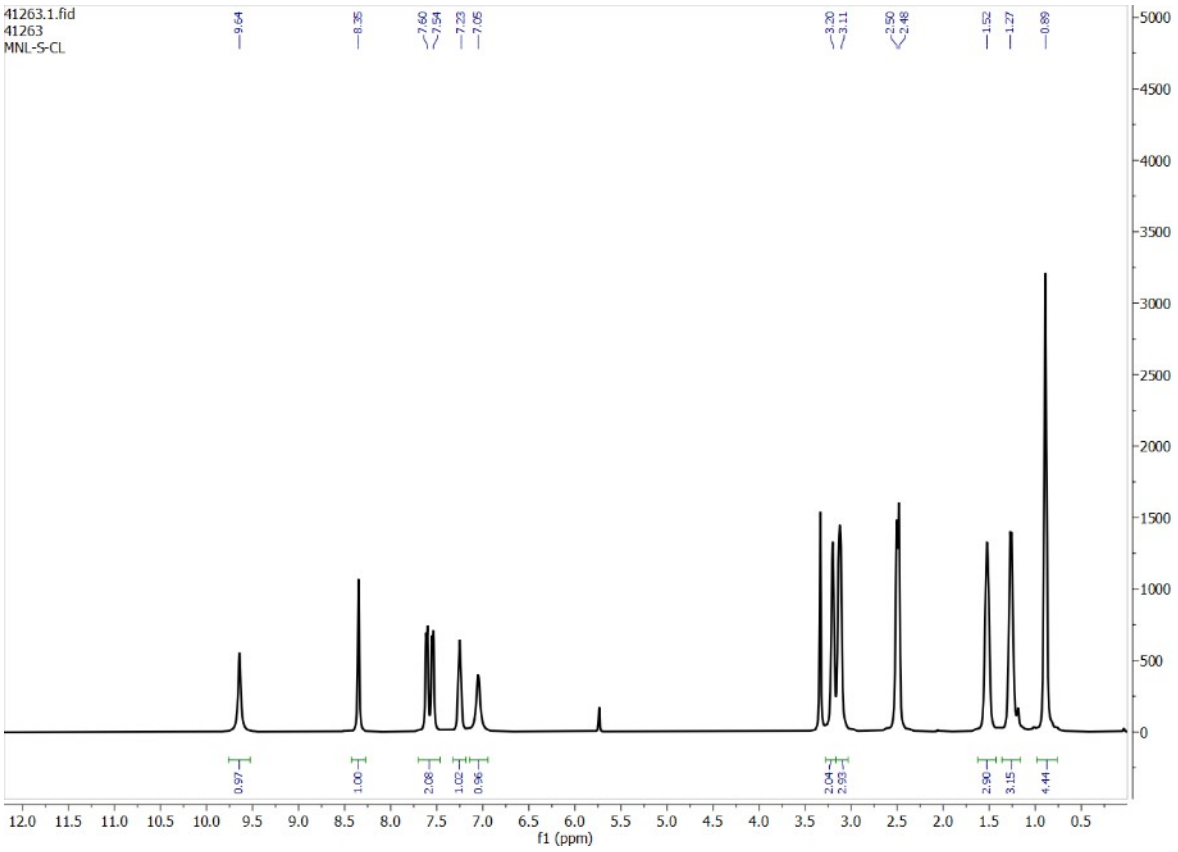

Fig. S40. ^{1}H-NMR spectrum of [(n-$Bu_4N)_2$(2**L**$_1$·SO_4)] obtained from LLE in the presence of chloride as a competing anion.

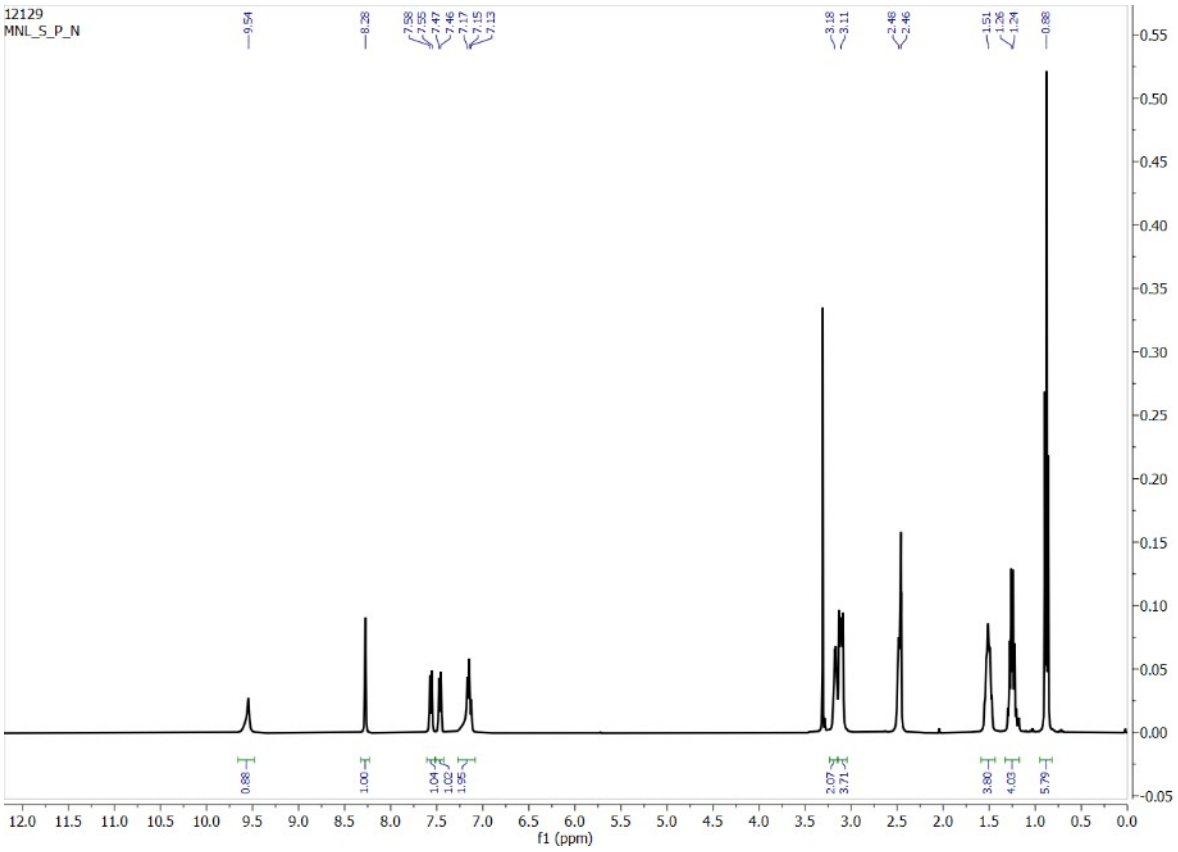

Fig. S41. ^{1}H-NMR spectrum of [(n-$Bu_4N)_2$(2$\mathbf{L_1}$·SO_4)] obtained from LLE in the presence of hydrogenphosphate and nitrate as competing anions.

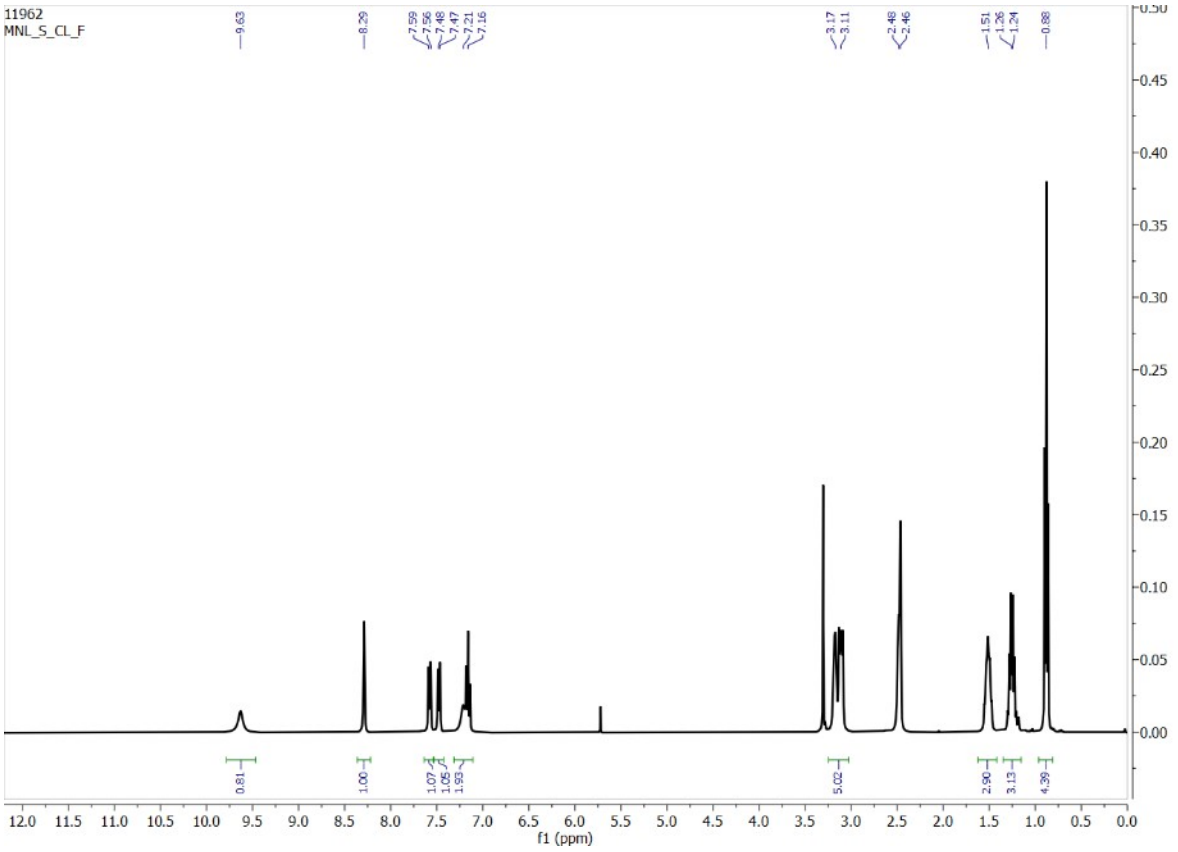

Fig. S42. ^{1}H-NMR spectrum of [(n-$Bu_4N)_2$(2$\mathbf{L_1}$·SO_4)] obtained from LLE in the presence of chloride and fluoride as competing anions (no signal for fluoride was observed in ^{19}F-NMR spectrum).

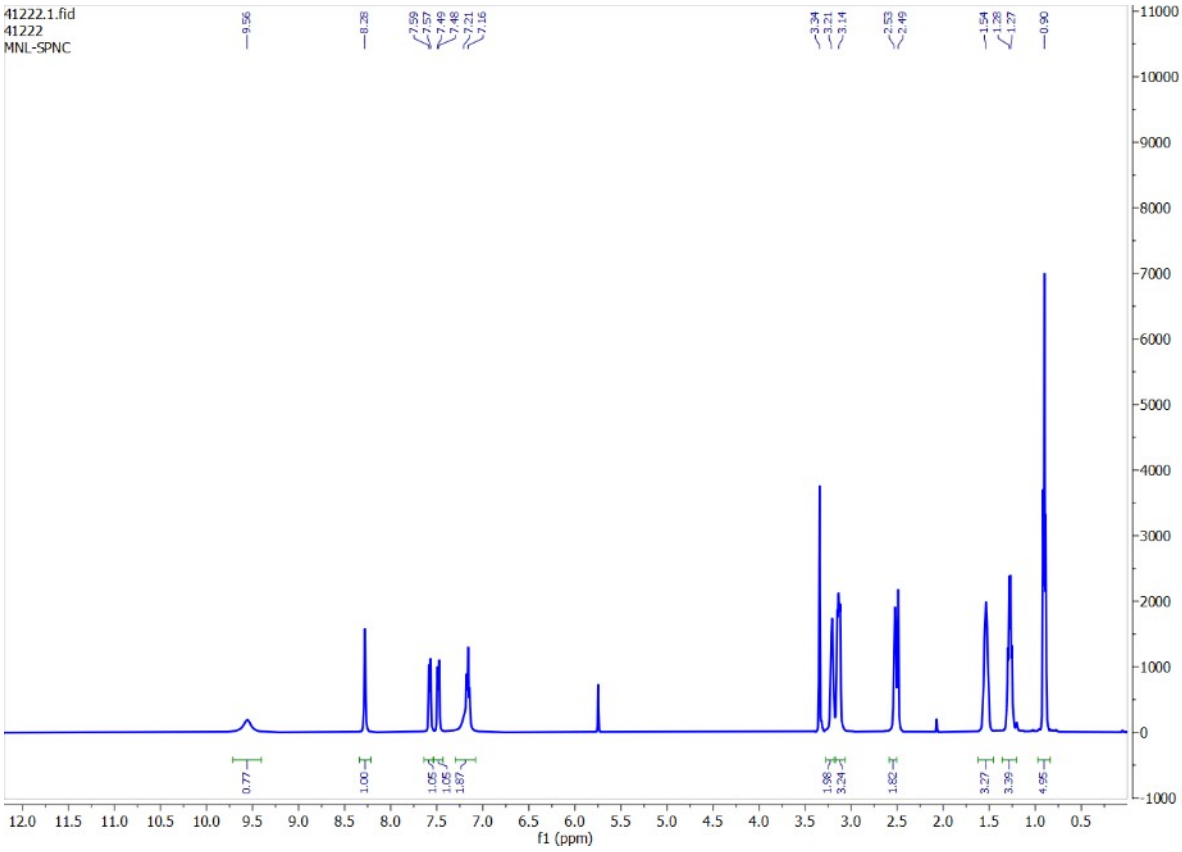

Fig. S43. ^{1}H-NMR spectrum of [(n-$Bu_4N)_2$(2**L**$_1$·SO_4)] obtained from LLE in the presence of hydrogenphosphate, carbonate and nitrate as competing anions (no signal for phosphate was observed in ^{31}P-NMR spectrum).

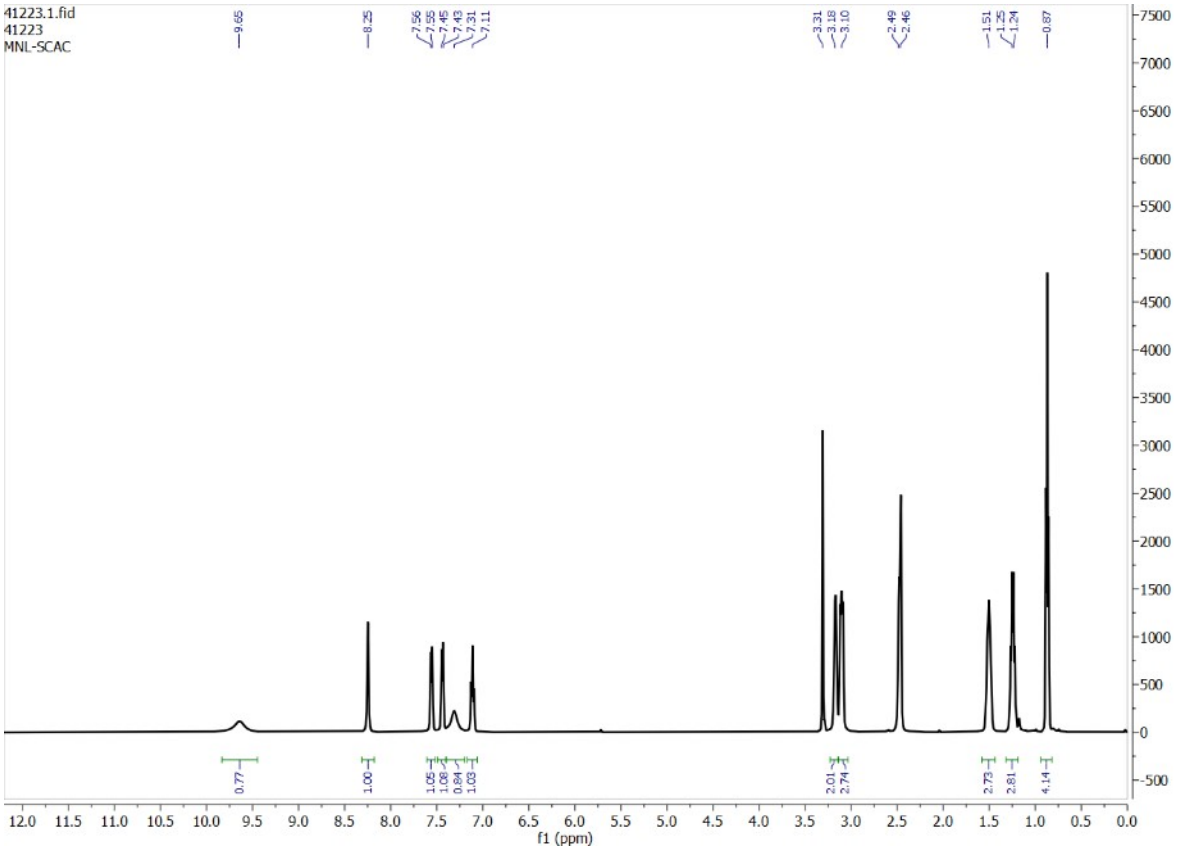

Fig. S44. ^{1}H-NMR spectrum of [(n-$Bu_4N)_2$(2**L**$_1$·SO_4)] obtained from LLE in the presence of acetate and carbonate as competing anions (no acetate -CH_3 peak observed at ≈ 1.9 ppm).

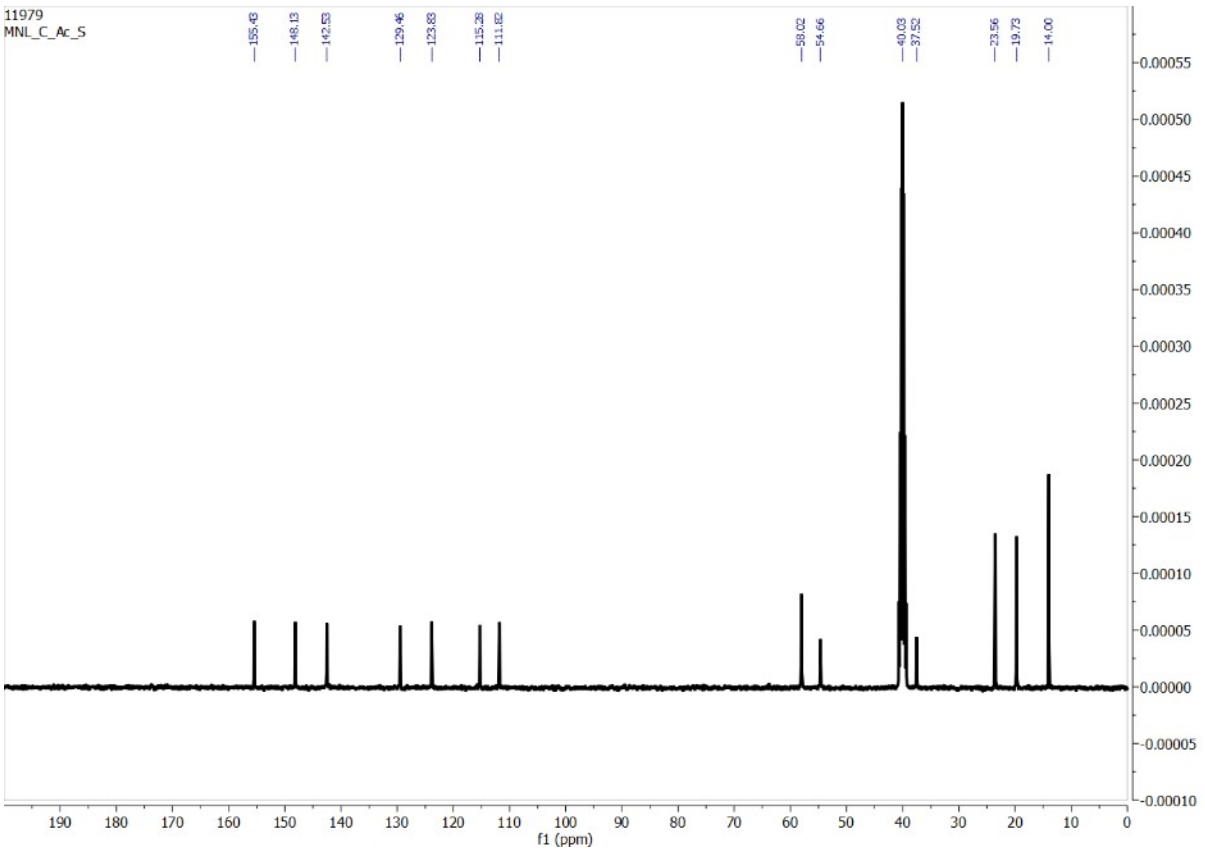

Fig. S45. ^{1}H-NMR spectrum of [(n-$Bu_4N)_2$(2$\mathbf{L_1}$·SO_4)] obtained from LLE in the presence of acetate and carbonate as competing anions (no signals for acetate and carbonate observed in the spectrum).

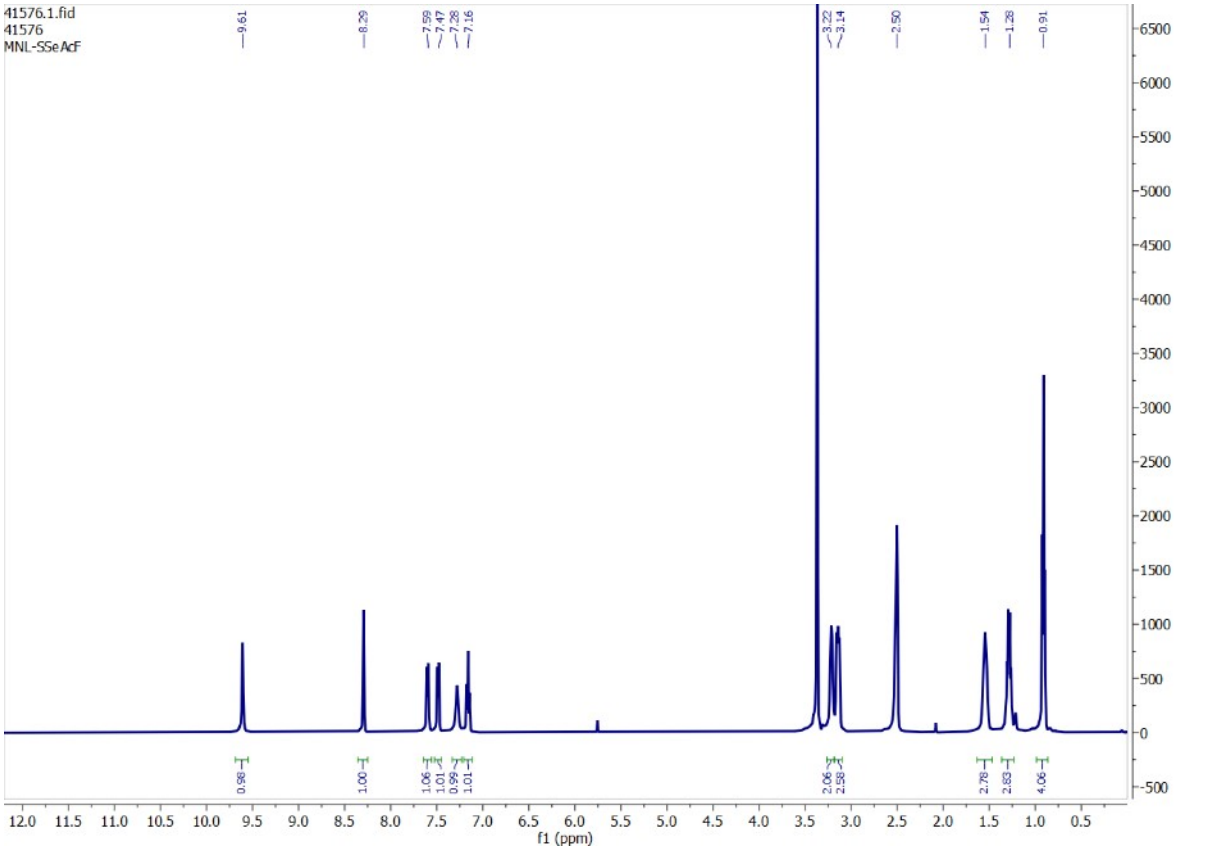

Fig. S46. ^{1}H-NMR spectrum of [(n-$Bu_4N)_2$(2$\mathbf{L_1}$·SO_4)] obtained from LLE in the presence of selenate, acetate and fluoride as competing anions (no signal for fluoride was observed in ^{19}F-NMR spectrum).

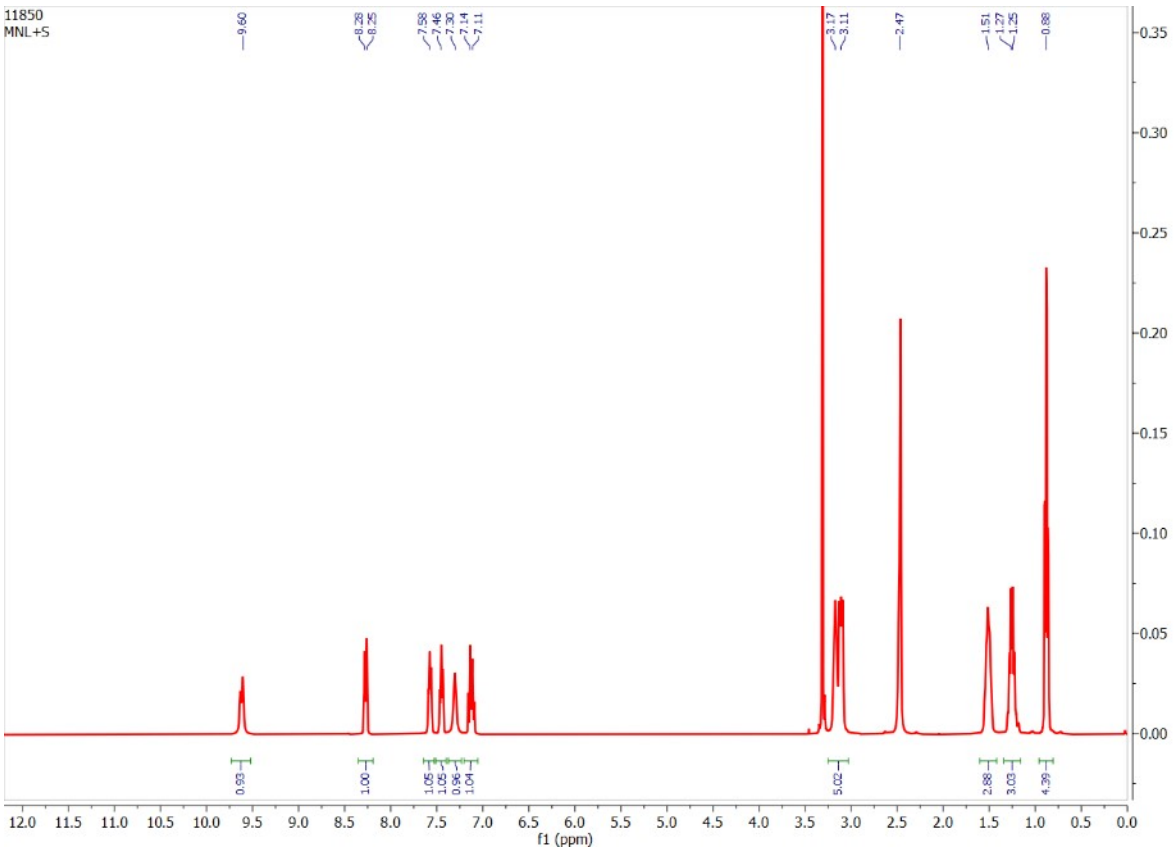

Fig. S47. ^{1}H-NMR spectrum of [(n-$Bu_4N)_2$(2$\mathbf{L_1}$·SO_4)] obtained in the presence of two equivalents of tetrabutylammonium hydrogensulfate in organic phase and one equivalent of sodium sulfate in the aqueous phase.

10. Selective extraction of sulfate by L_2: ^{1}H-NMR spectra of LLE isolated sulfate complexes

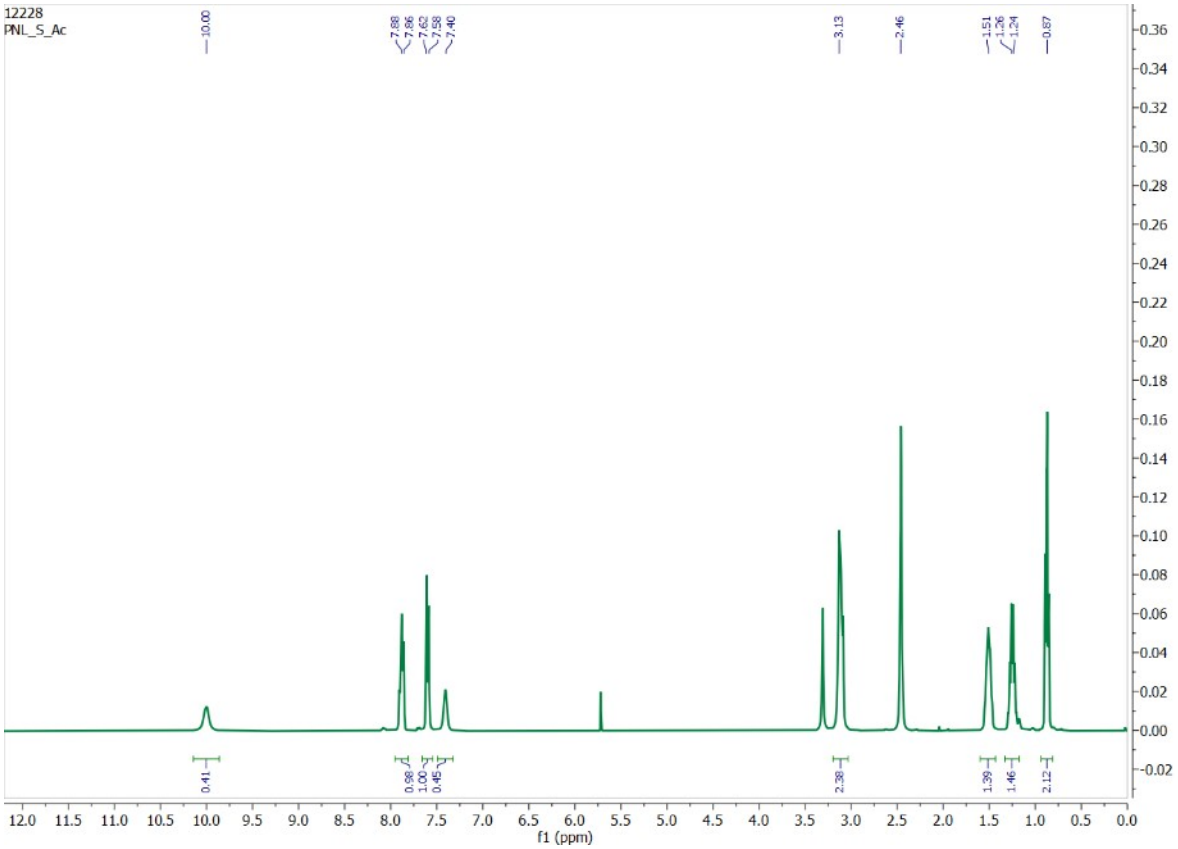

Fig. S48. ^{1}H-NMR spectrum of [(n-$Bu_4N)_2$(2$\mathbf{L_2}$·SO_4)] obtained from LLE in the presence of acetate as a competing anion.

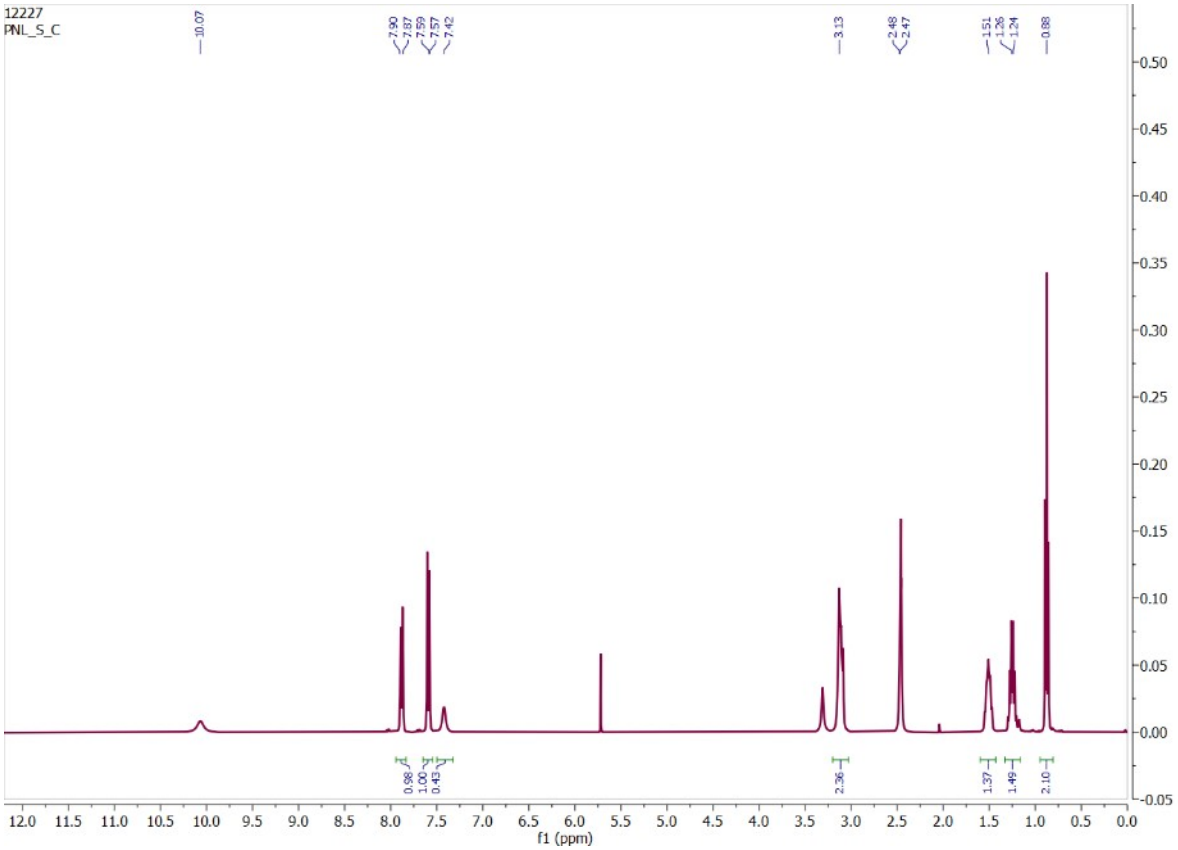

Fig. S49. ^{1}H-NMR spectrum of [(n-$Bu_4N)_2$(2$\mathbf{L_2}$·SO_4)] obtained from LLE in the presence of carbonate as a competing anion.

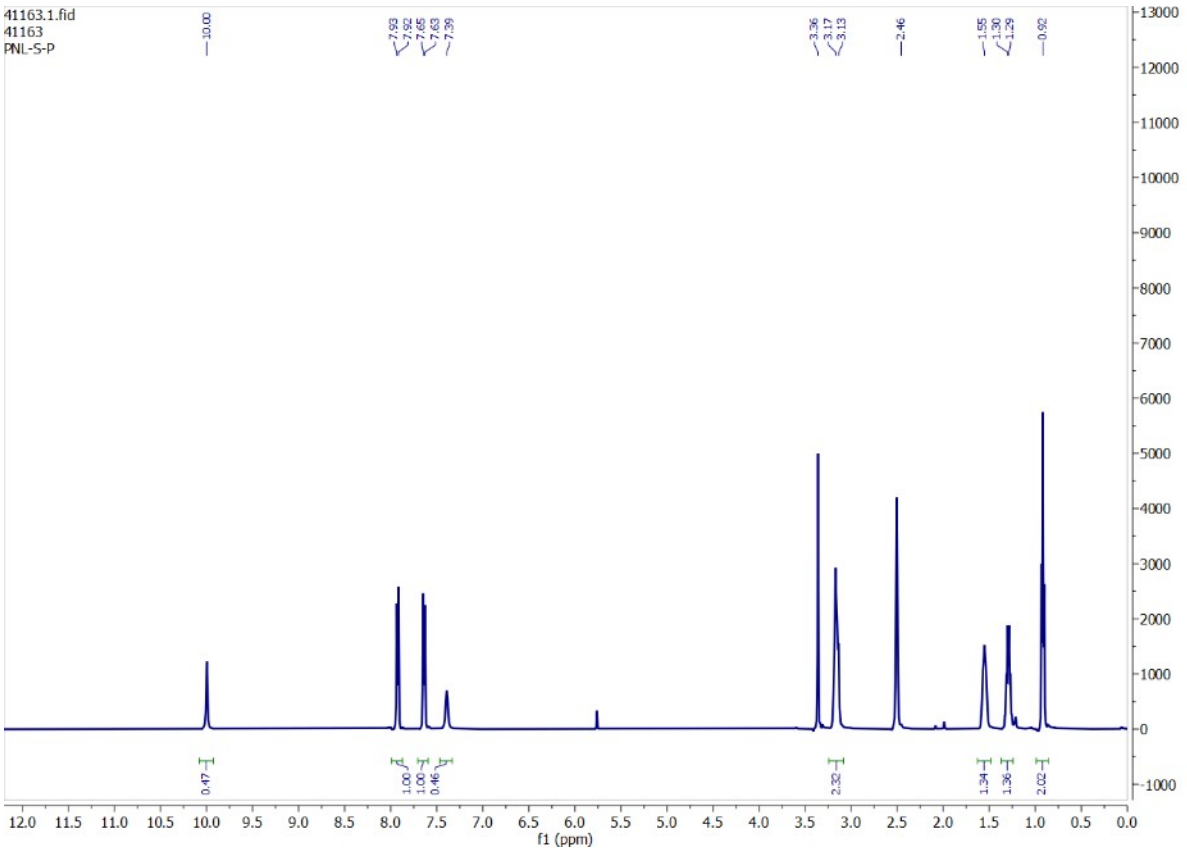

Fig. S50. ^{1}H-NMR spectrum of [(n-$Bu_4N)_2$(2**L**$_2$·SO_4)] obtained from LLE in the presence of hydrogenphosphate as a competing anion (no signal for phosphate was observed in ^{31}P-NMR spectrum).

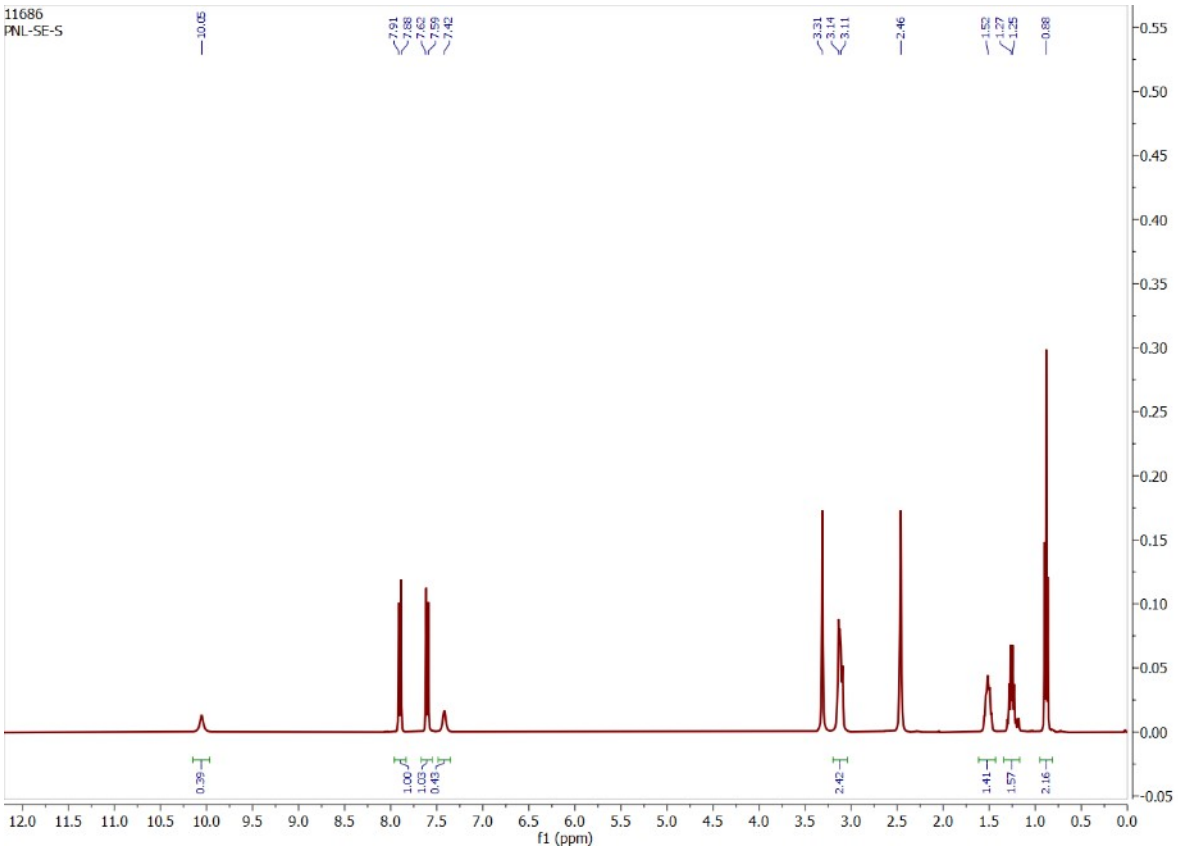

Fig. S51. ^{1}H-NMR spectrum of [(n-$Bu_4N)_2$(2**L$_2$**·SO_4)] obtained from LLE in the presence of selenate as a competing anion.

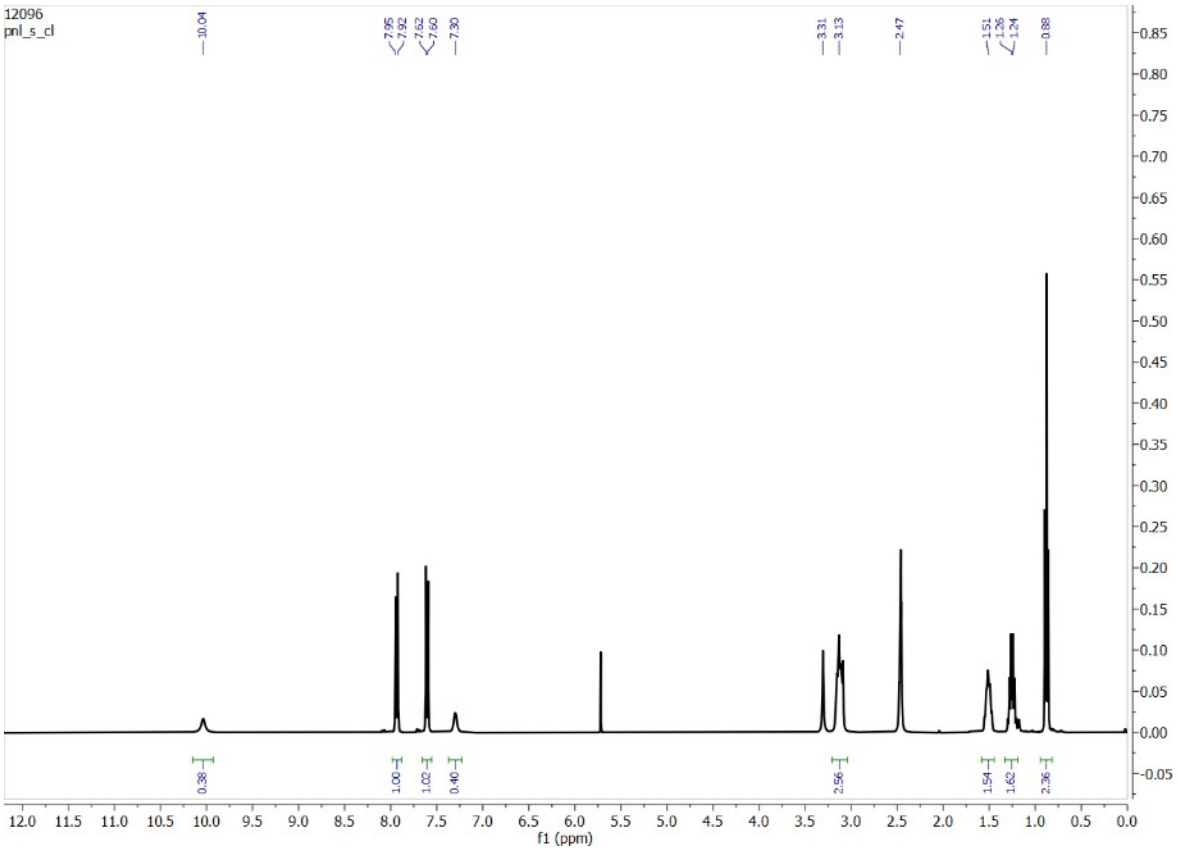

Fig. S52. ^{1}H-NMR spectrum of [(n-$Bu_4N)_2$(2**L$_2$**·SO_4)] obtained from LLE in the presence of chloride as a competing anion.

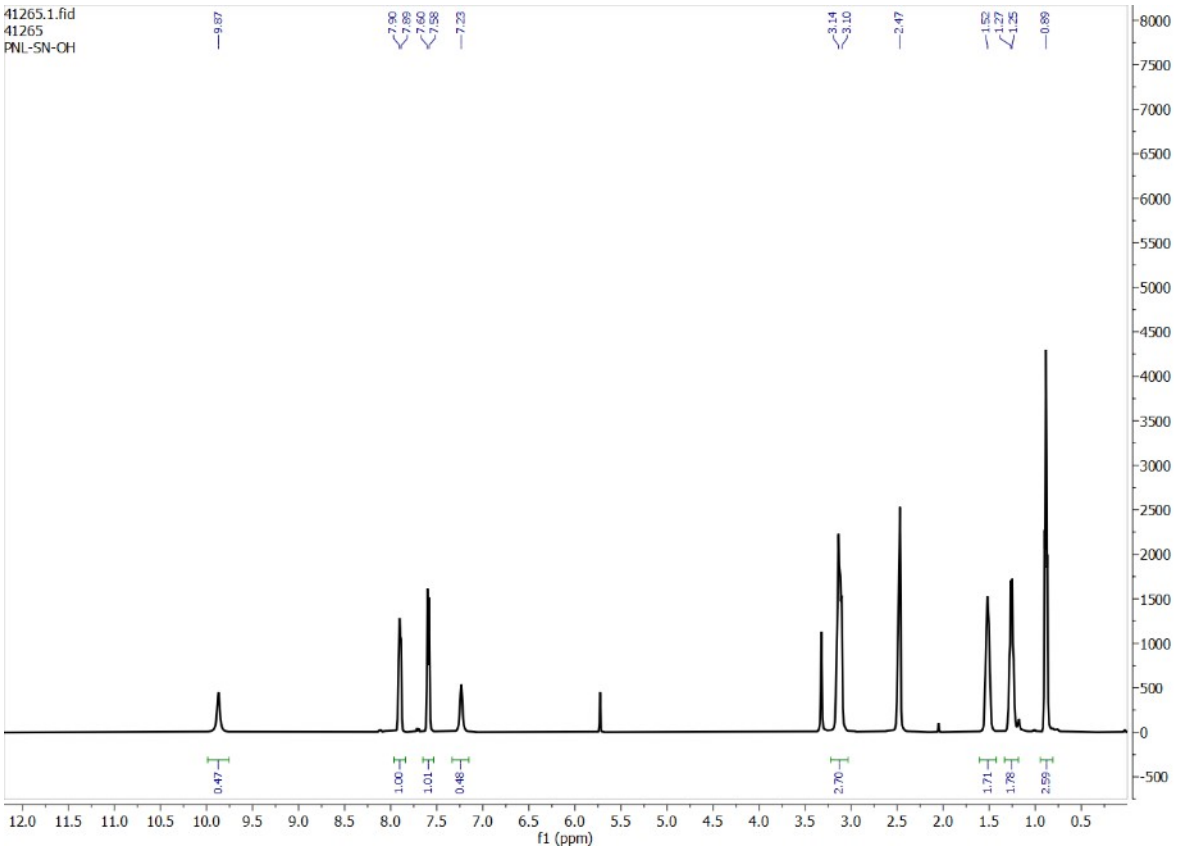

Fig. S53. ^{1}H-NMR spectrum of [(n-$Bu_4N)_2$(2**L_2**·SO_4)] obtained from LLE in the presence of nitrate as a competing anion.

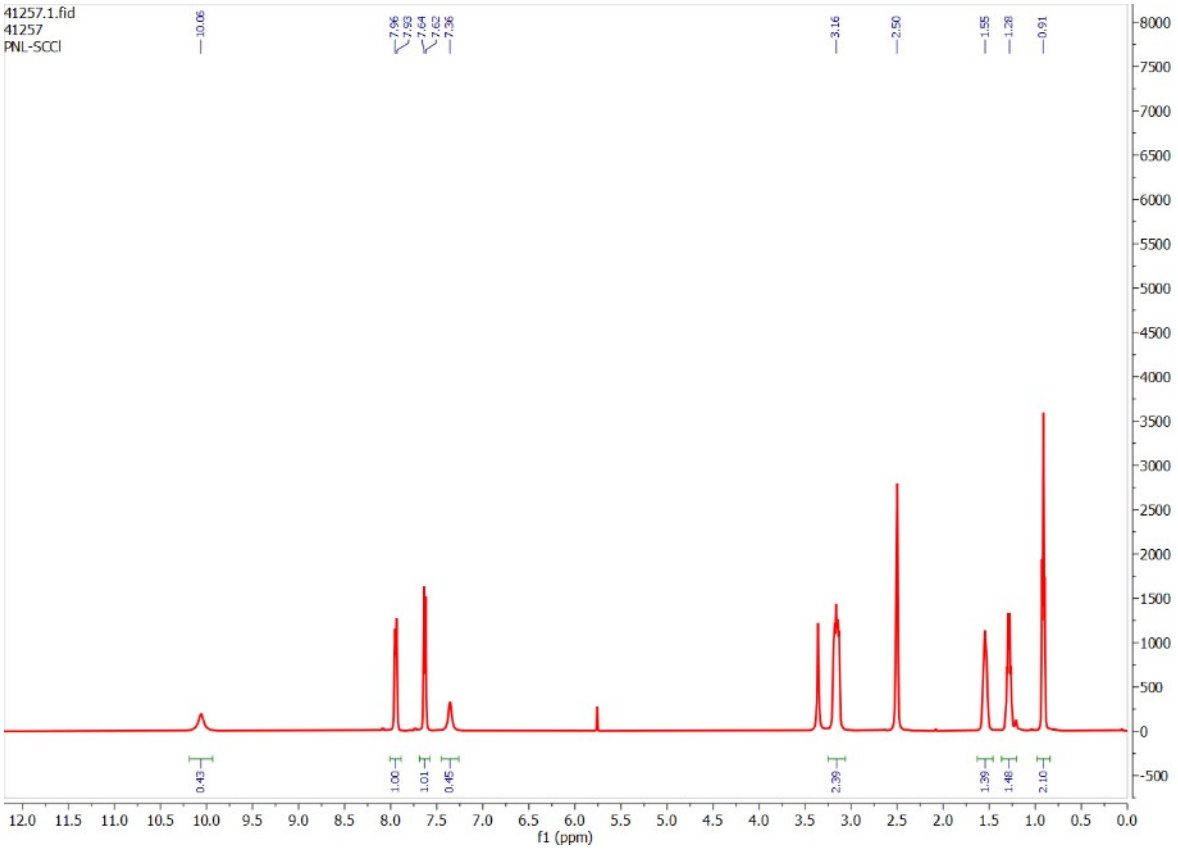

Fig. S54. ^{1}H-NMR spectrum of [(n-$Bu_4N)_2$(2**L_2**·SO_4)] obtained from LLE in the presence of carbonate and chloride as competing anions.

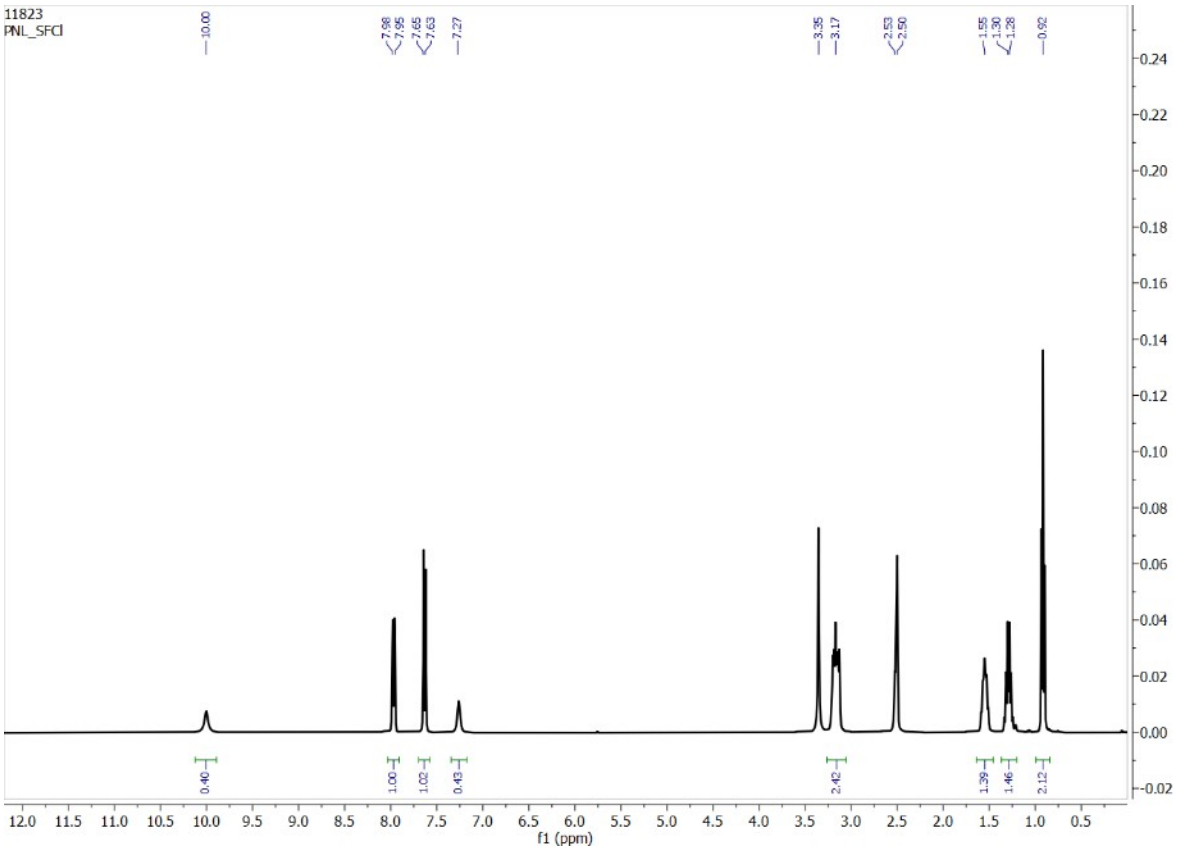

Fig. S55. ^{1}H-NMR spectrum of [(n-$Bu_4N)_2$(2**L_2**·SO_4)] obtained from LLE in the presence of chloride and fluoride as competing anions (no signal for fluoride was observed in ^{19}F-NMR spectrum).

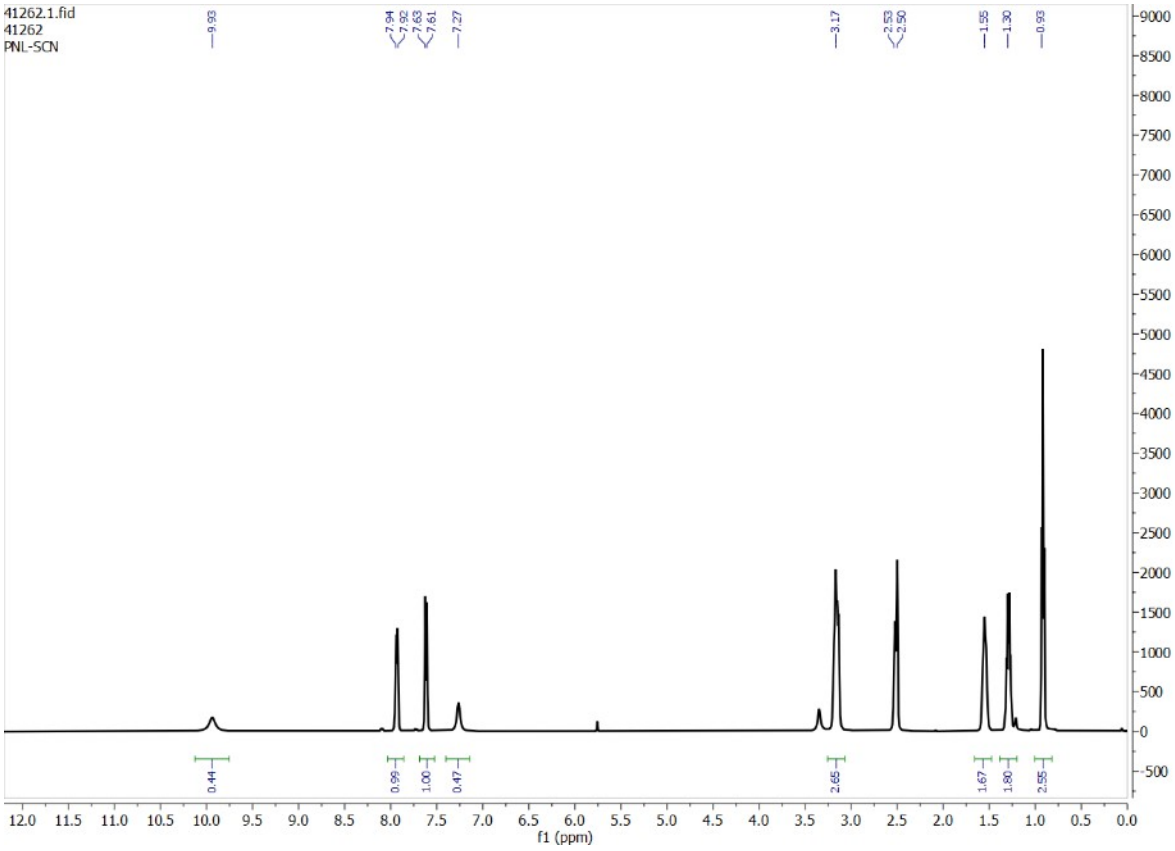

Fig. S56. ^{1}H-NMR spectrum of [(n-$Bu_4N)_2$(2**L_2**·SO_4)] obtained from LLE in the presence of carbonate and nitrate as competing anions (no signal for carbonate observed in the ^{13}C-NMR spectrum).

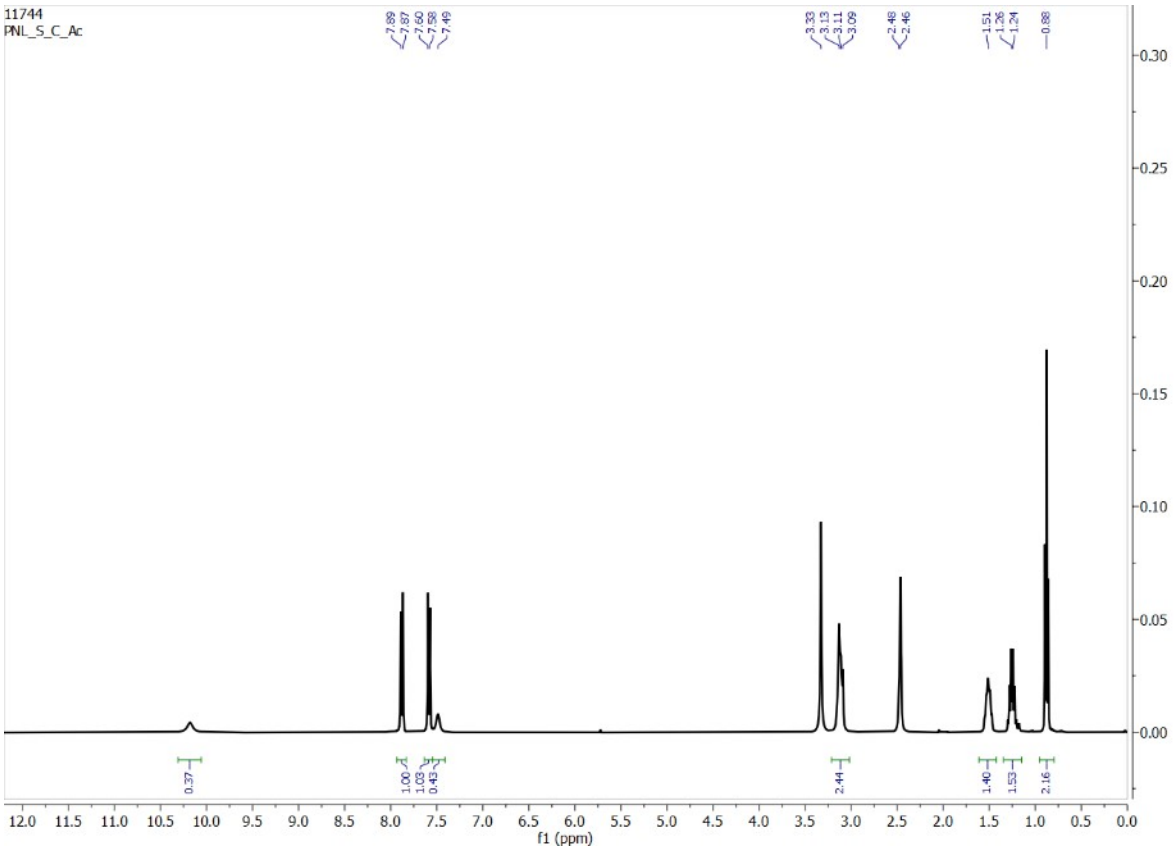

Fig. S57. ^{1}H-NMR spectrum of [(n-$Bu_4N)_2$(2**L$_2$**·SO_4)] obtained from LLE in the presence of carbonate and acetate as competing anions (no signals for acetate at ≈ 1.9 ppm observed in the spectrum).

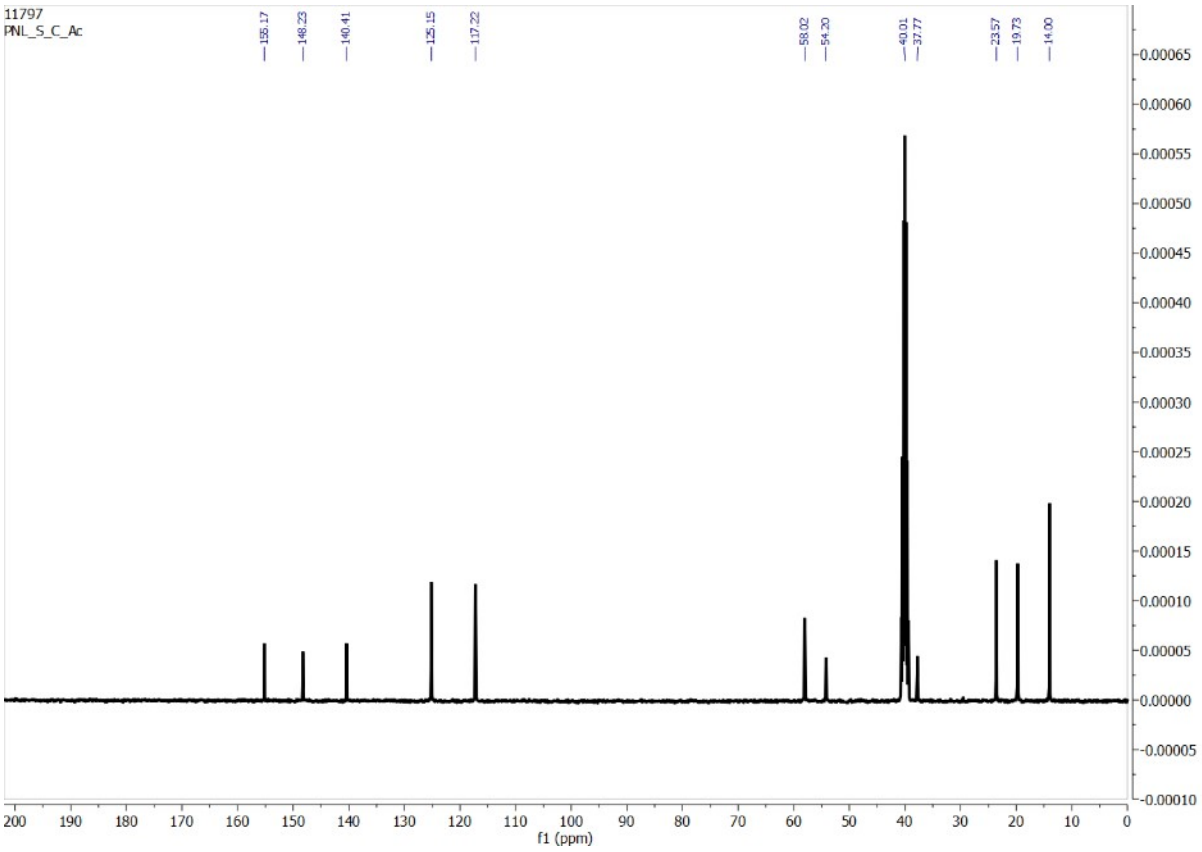

Fig. S58. ^{13}C-NMR spectrum of [(n-$Bu_4N)_2$(2**L$_2$**·SO_4)] obtained from LLE in the presence of carbonate and acetate as competing anions (no signals for acetate and carbonate observed in the spectrum).

11. Selective extraction of sulfate by L_3: ^{1}H-NMR spectra of LLE isolated sulfate complexes

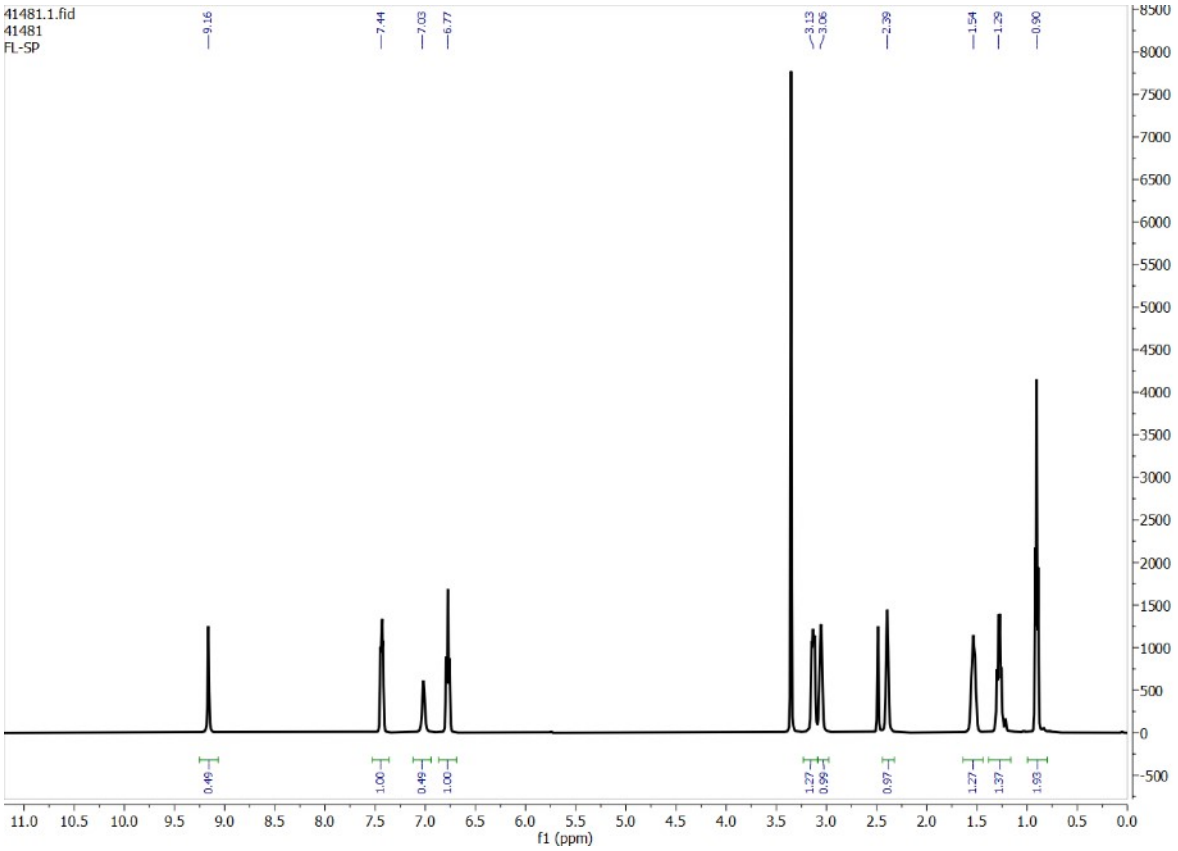

Fig. S59. ^{1}H-NMR spectrum of [(n-$Bu_4N)_2$(2**L_3**·SO_4)] obtained from LLE in the presence of HPO_4^{2-} as a competing anion.

Fig. S60. ^{1}H-NMR spectrum of [(n-$Bu_4N)_2$(2**L$_3$**·SO_4)] obtained from LLE in the presence of CO_3^{2-} as a competing anion.

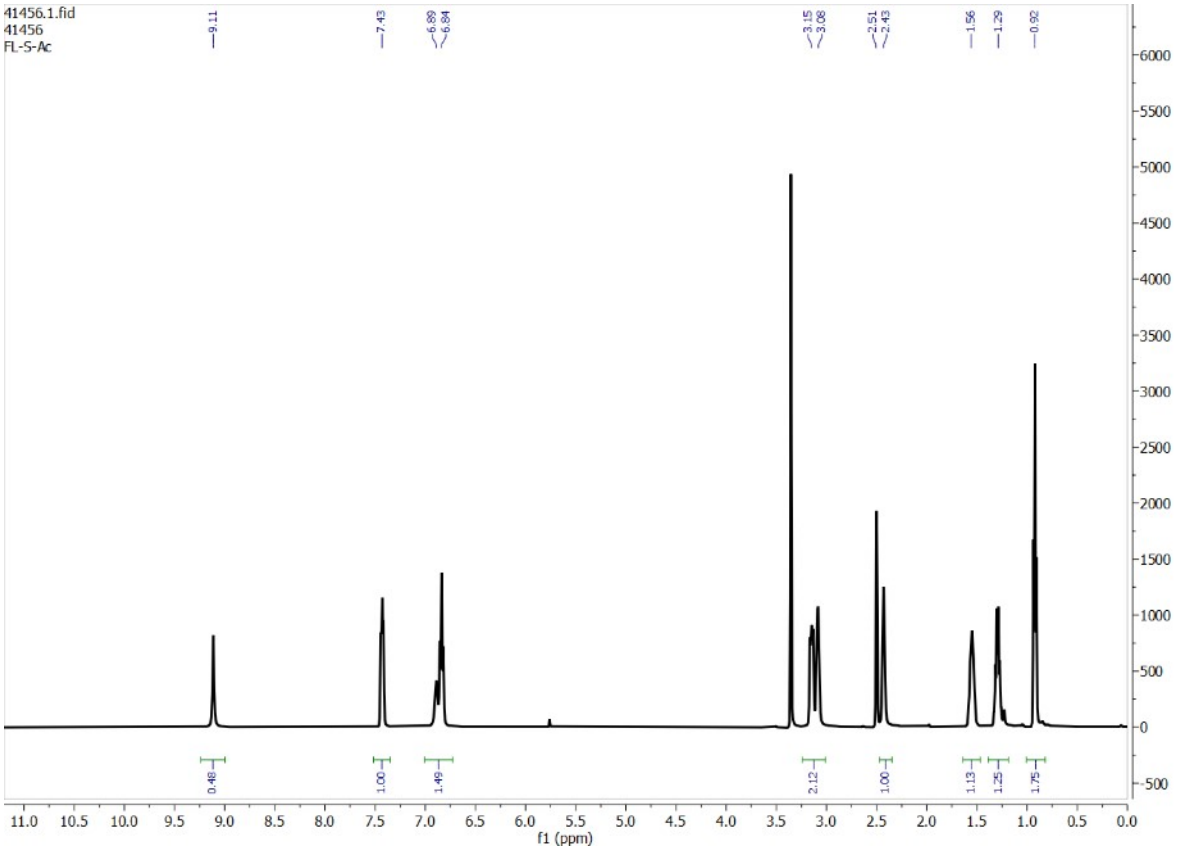

Fig. S61. ^{1}H-NMR spectrum of [(n-$Bu_4N)_2$(2**L$_3$**·SO_4)] obtained from LLE in the presence of $CH_3CO_2^-$ as a competing anion.

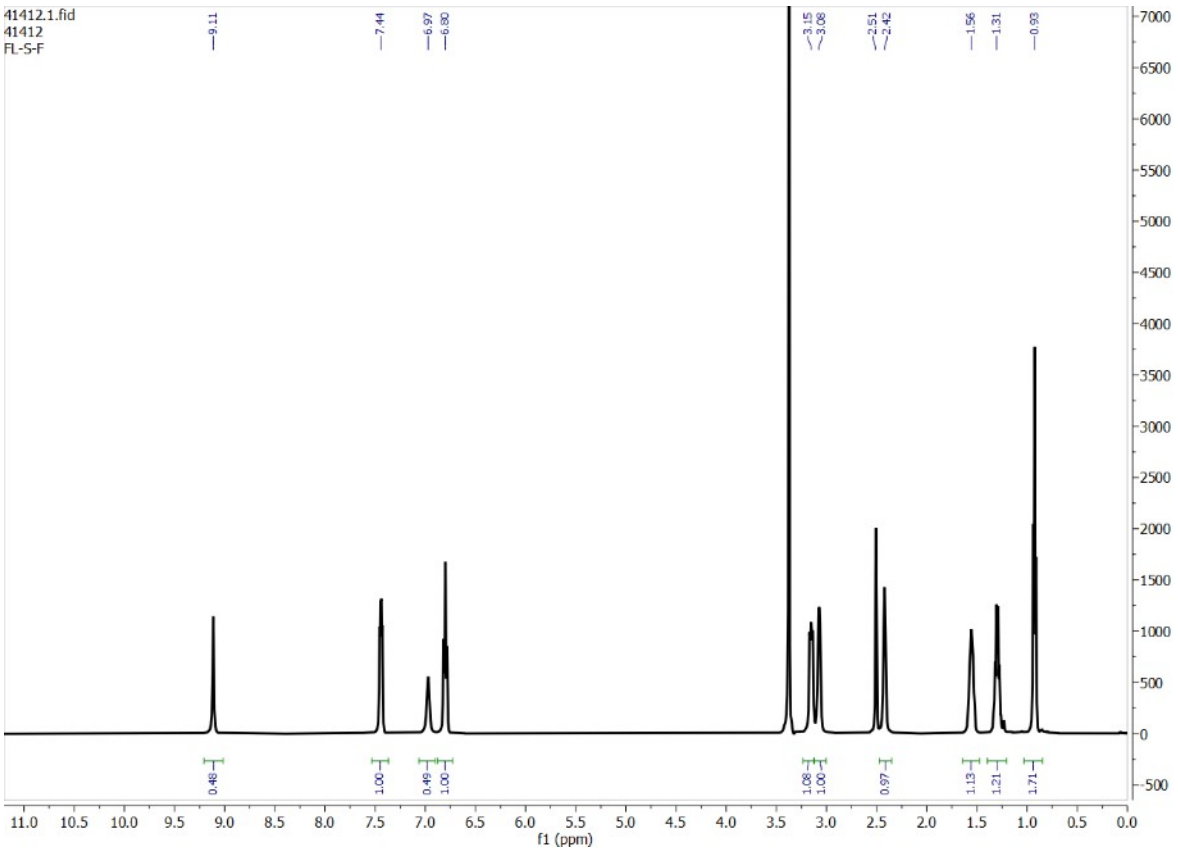

Fig. S62. ^{1}H-NMR spectrum of [(n-$Bu_4N)_2$(2**L**$_3$·SO_4)] obtained from LLE in the presence of F^- as a competing anion.

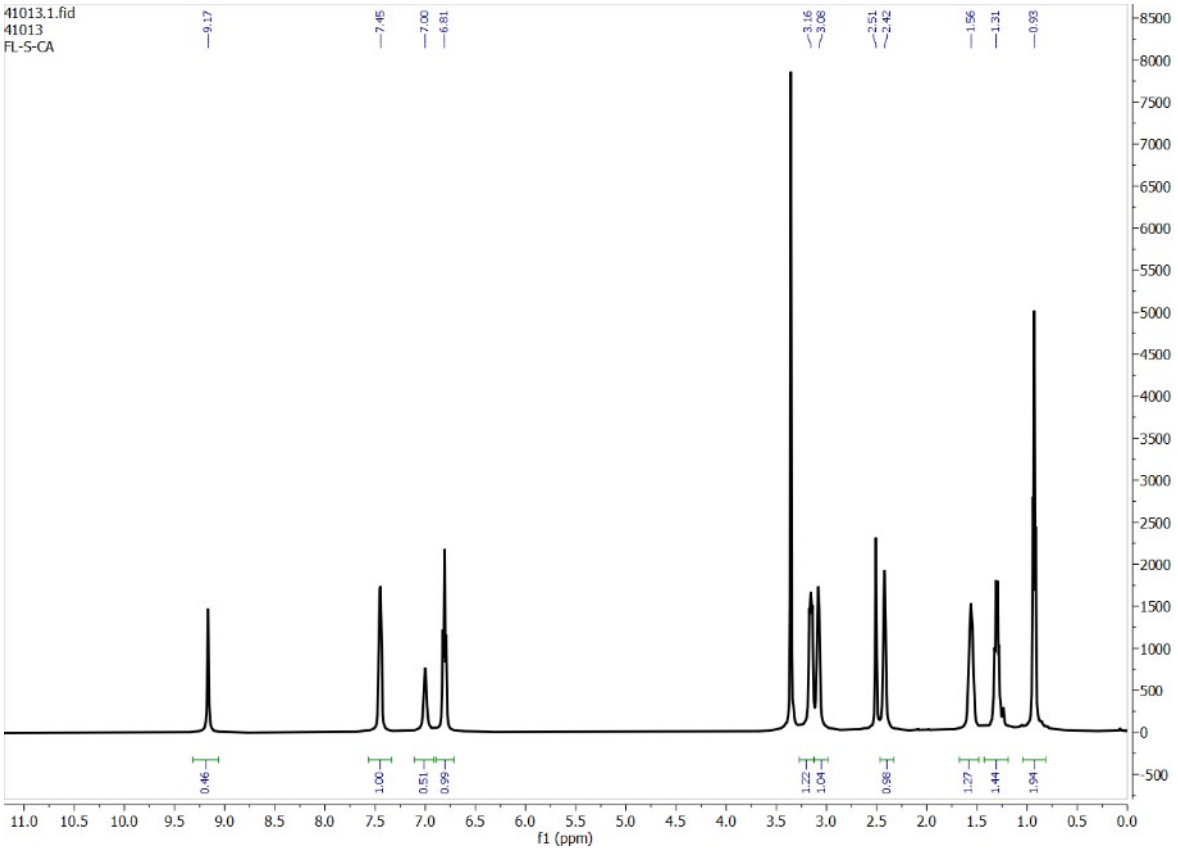

Fig. S63. ^{1}H-NMR of [(n-$Bu_4N)_2$(2**L**$_3$·SO_4)] obtained from LLE in the presence of CO_3^{2-} and $CH_3CO_2^-$ as competing anions.

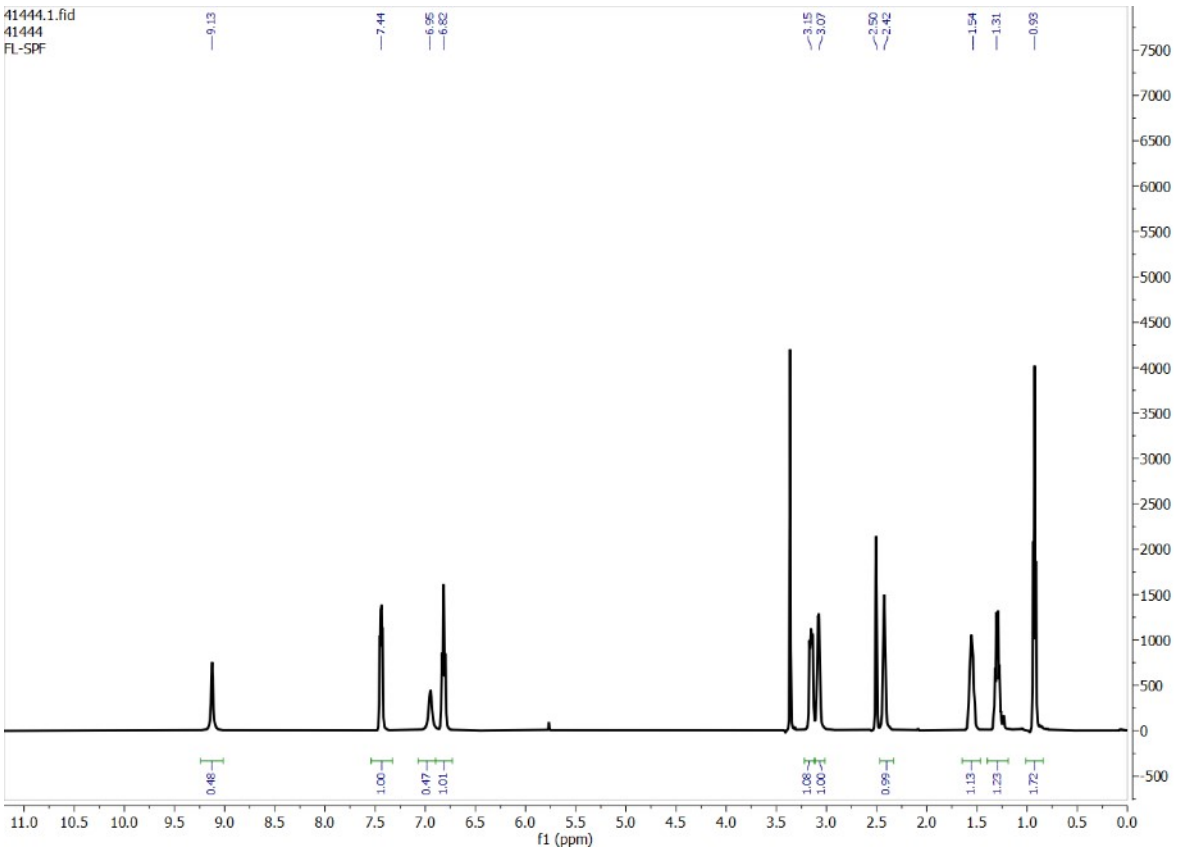

Fig. S64. ^{1}H-NMR of [(n-$Bu_4N)_2$(2**L$_3$**·SO_4)] obtained from LLE in the presence of HPO_4^{2-} and F^- as competing anions.

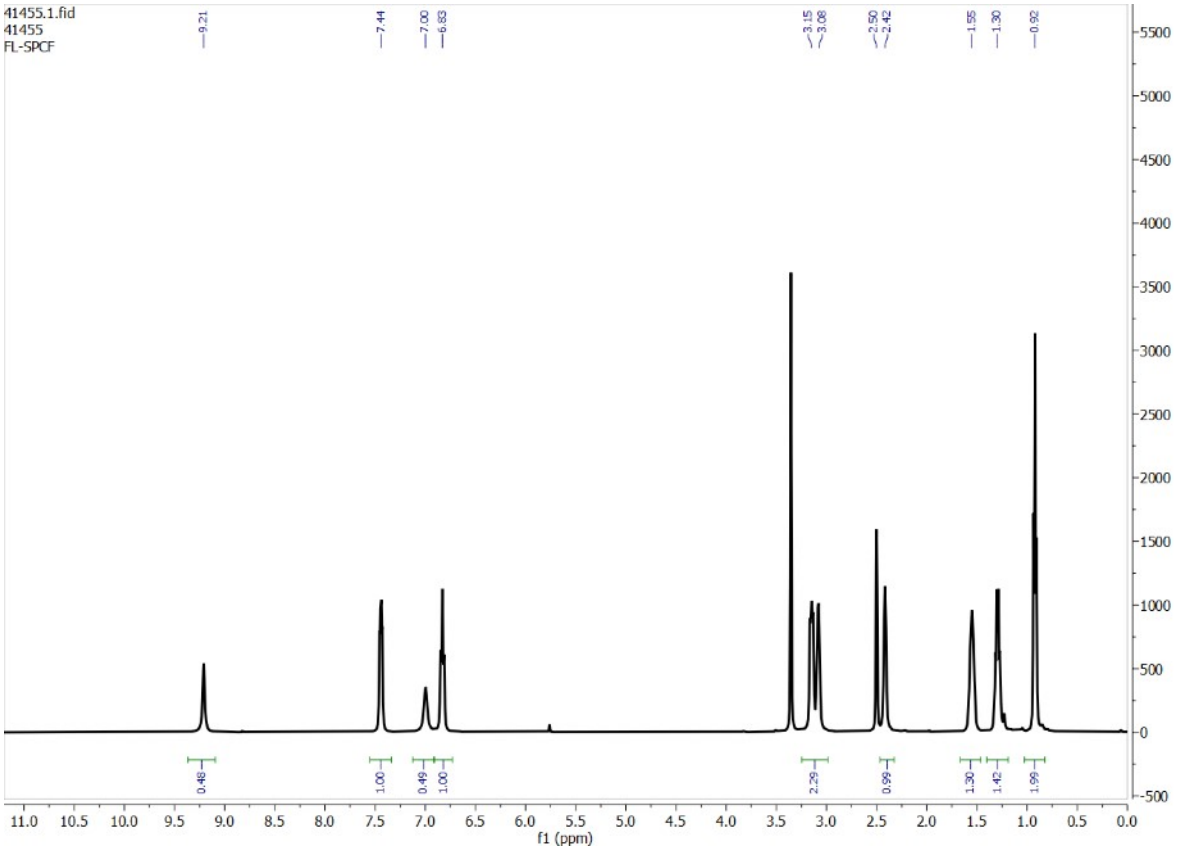

Fig. S65. ^{1}H-NMR of [(n-$Bu_4N)_2$(2**L$_3$**·SO_4)] obtained from LLE in the presence of HPO_4^{2-}, CO_3^{2-} and F^- as competing anions (no signals for phosphate and carbonate were observed in ^{31}P and ^{13}C-NMR spectra).

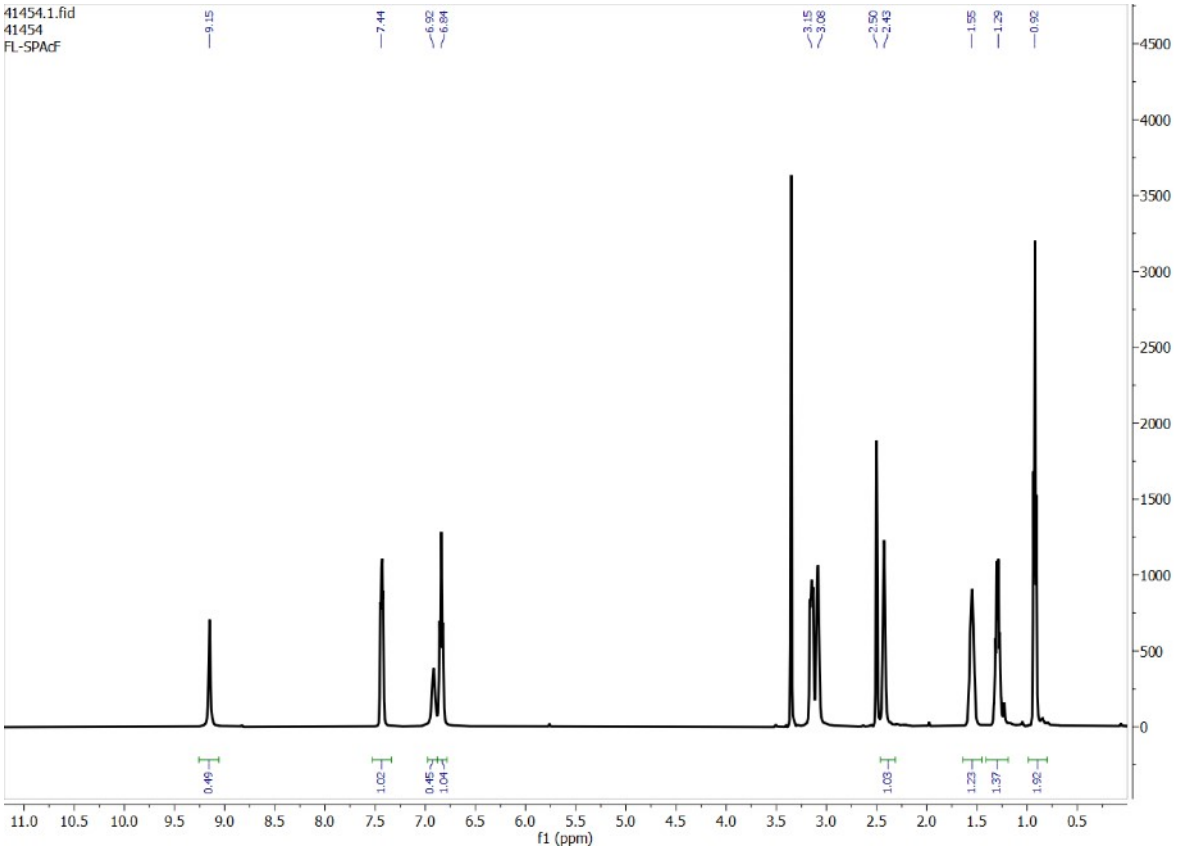

Fig. S66. ^{1}H-NMR of [(n-$Bu_4N)_2$(2**L$_3$**·SO_4)] obtained from LLE in the presence of HPO_4^{2-}, $CH_3CO_2^-$ and F^- as competing anions (no signal for phosphate was observed in ^{31}P-NMR spectrum).

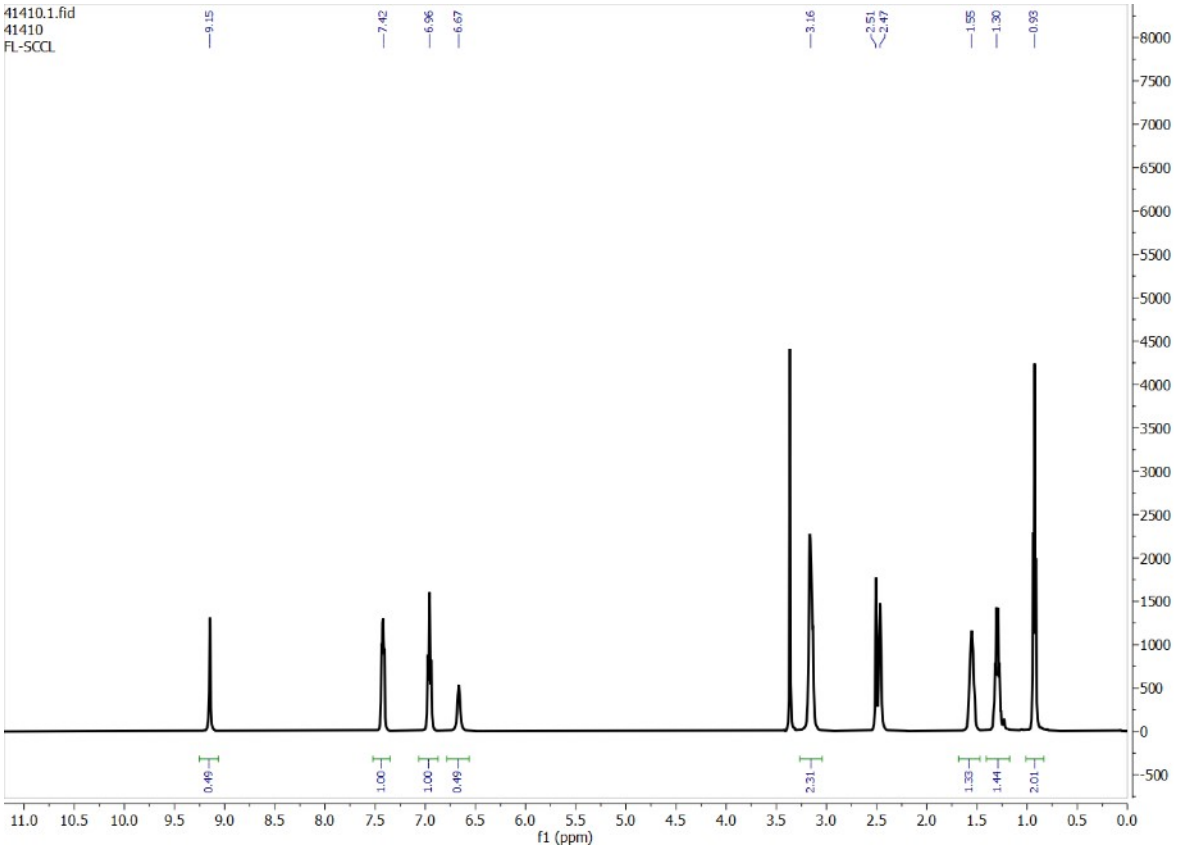

Fig. S67. ^{1}H-NMR spectrum showing inefficient extraction of SO_4^{2-} by **L_3** from LLE in the presence of Cl^- and CO_3^{2-} as competing anions.

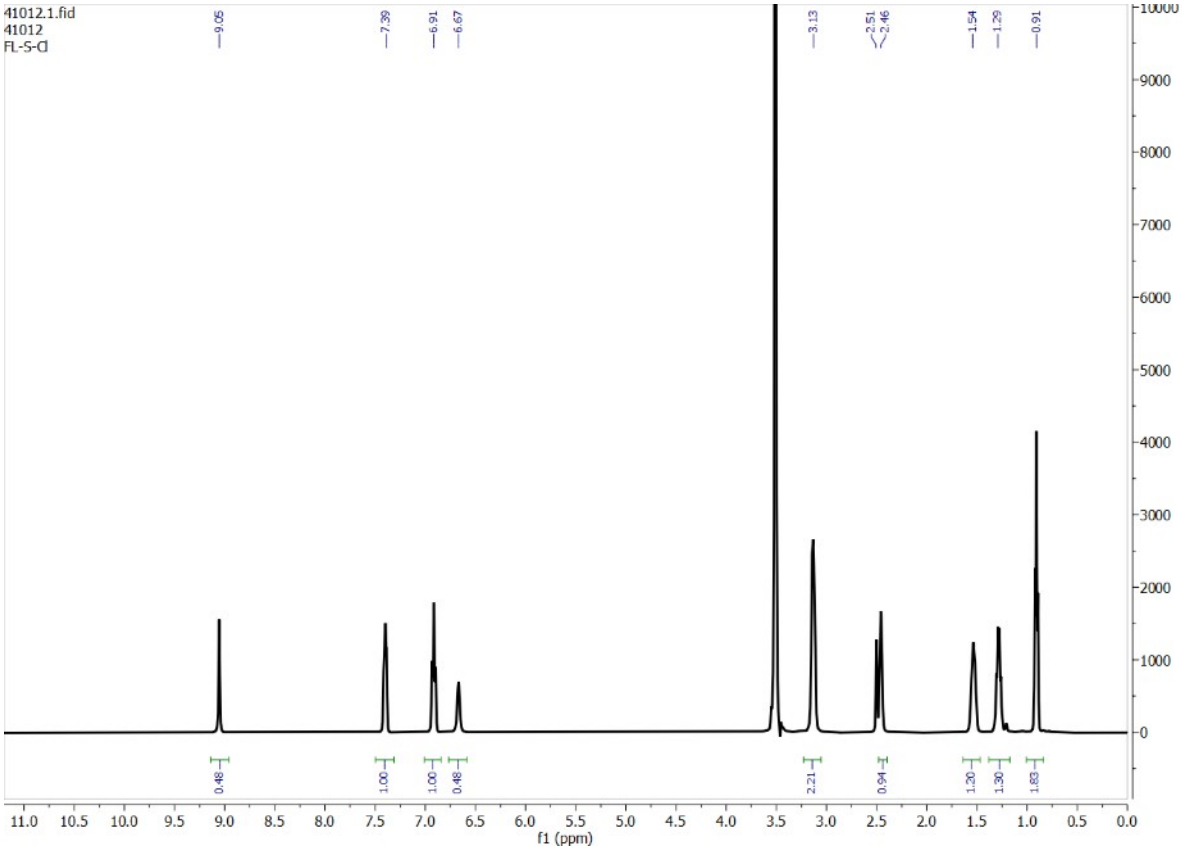

Fig. S68. ^{1}H-NMR spectrum showing inefficient extraction of SO_4^{2-} by **L_3** from LLE in the presence of Cl^- as competing anion.

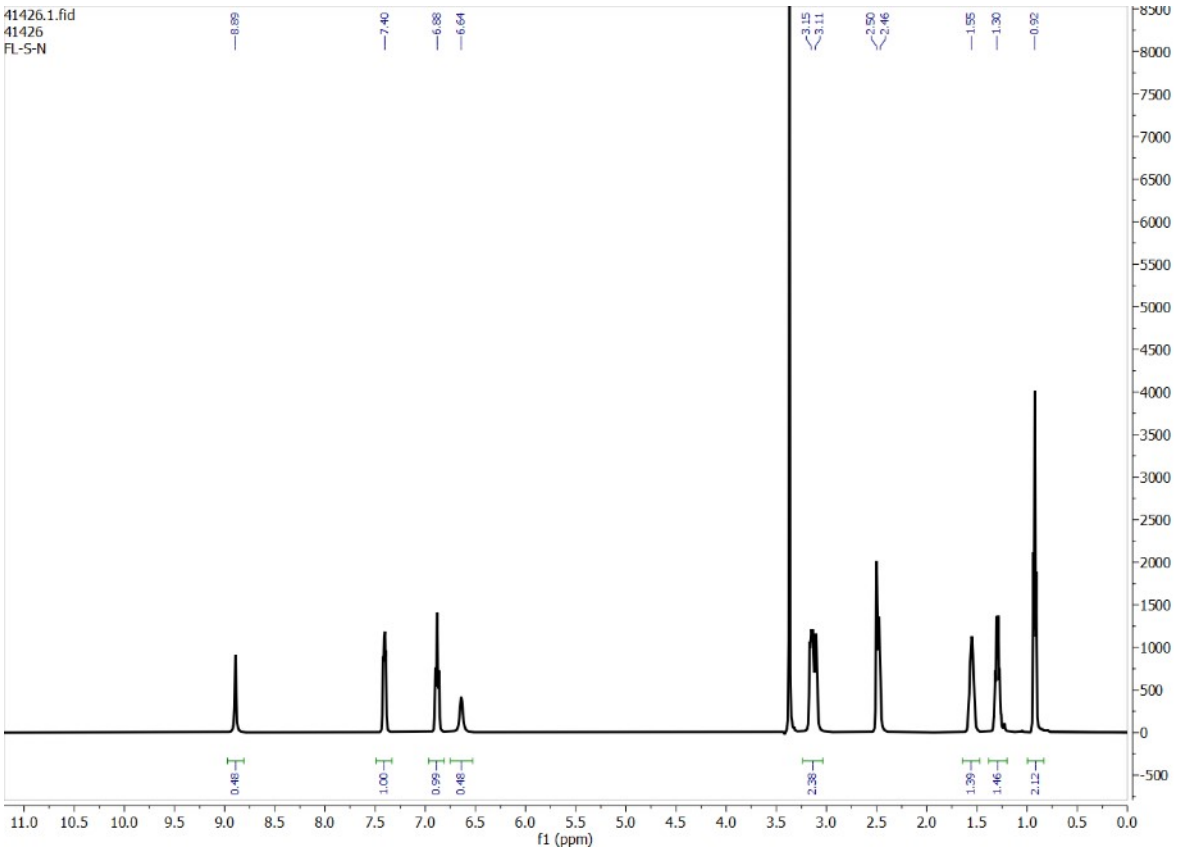

Fig. S69. ^{1}H-NMR spectrum showing inefficient extraction of SO_4^{2-} by **L_3** from LLE in the presence of NO_3^- as competing anion.

12. Anion complexes of L_4: Characterization by NMR spectroscopy

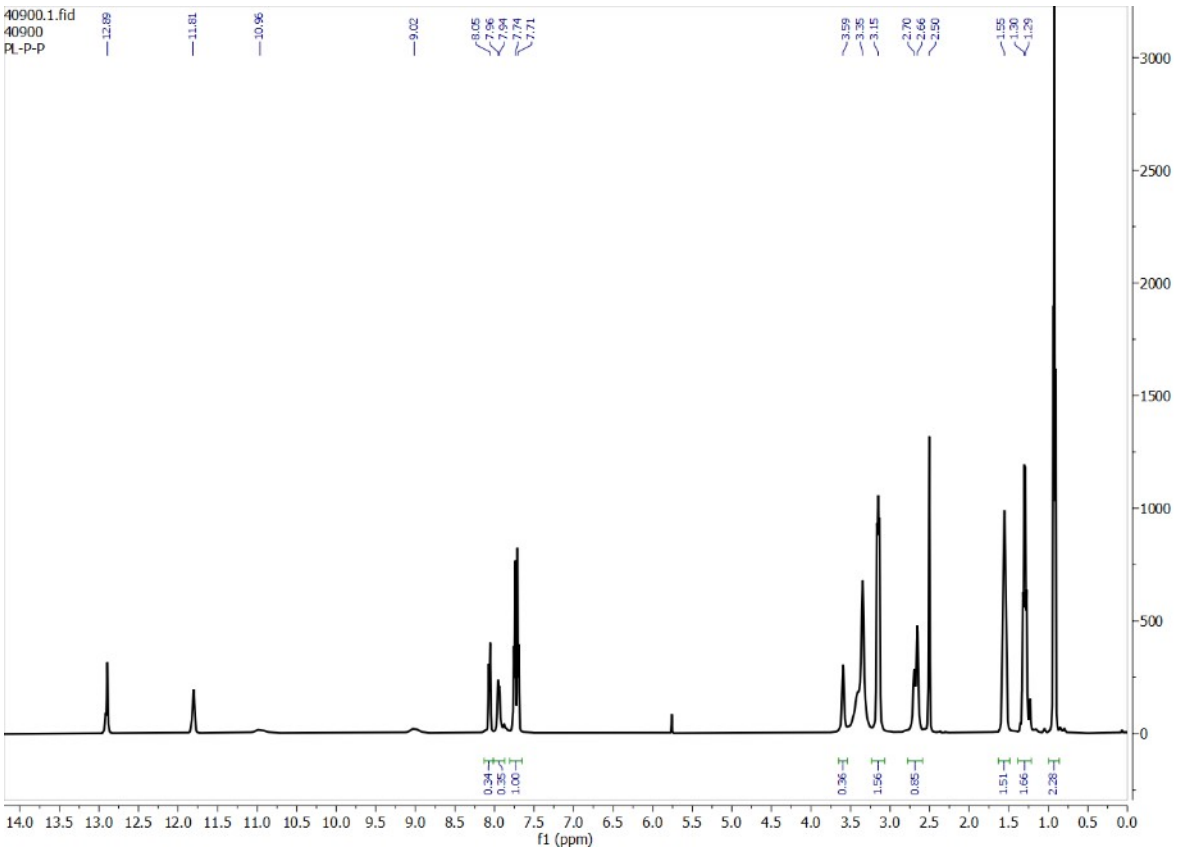

Fig. S70. ^{1}H-NMR spectrum of phosphate complex (DMSO-D_6) showing two sets of -NH and -CH signals for a mixture of [(n-$Bu_4N)_2$(2**L**$_4$·HPO_4)] and [(n-$Bu_4N)_3$(2**L**$_4$·PO_4)] with 40:60 ratio.

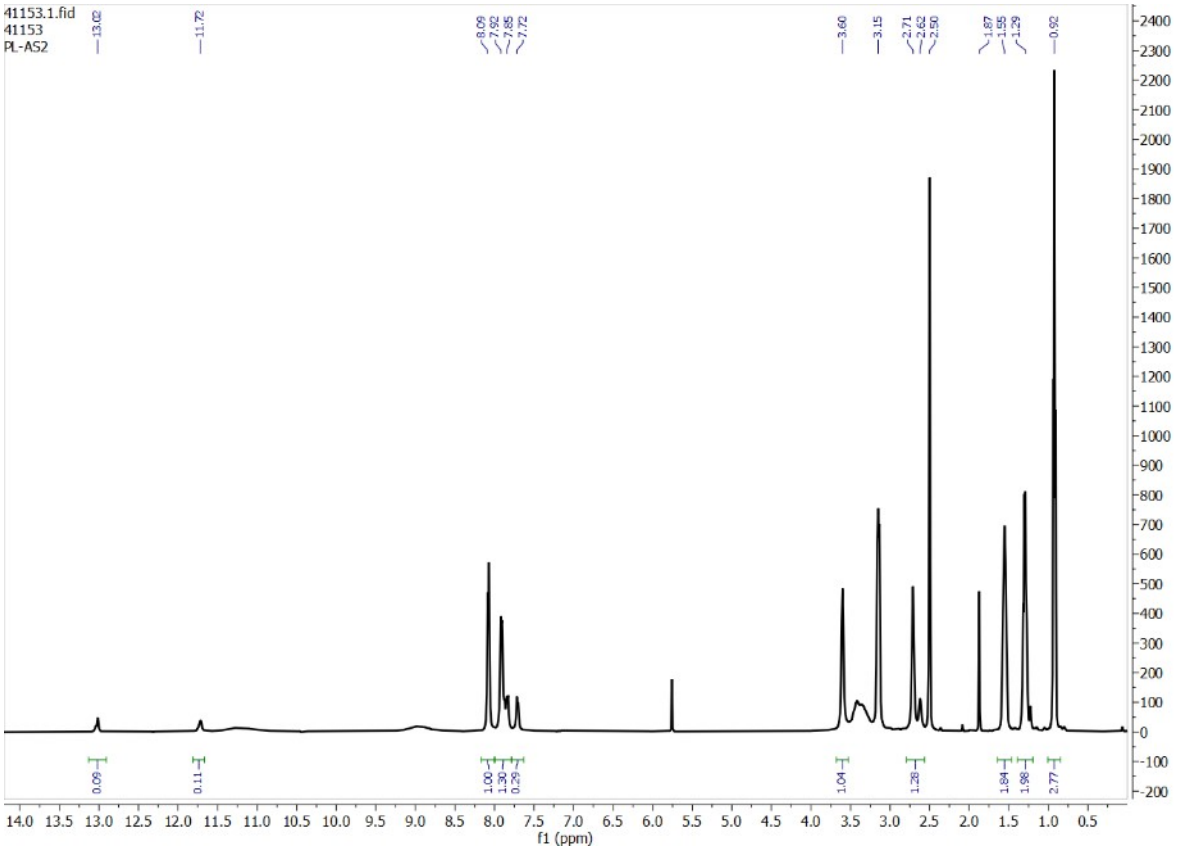

Fig. S71. ^{1}H-NMR spectrum of arsenate complex (DMSO-D_6) showing two sets of -NH and -CH signals for a mixture of [(n-$Bu_4N)_2$(2**L**$_4$·$HAsO_4$)] and [(n-$Bu_4N)_3$(2**L**$_4$·AsO_4)].

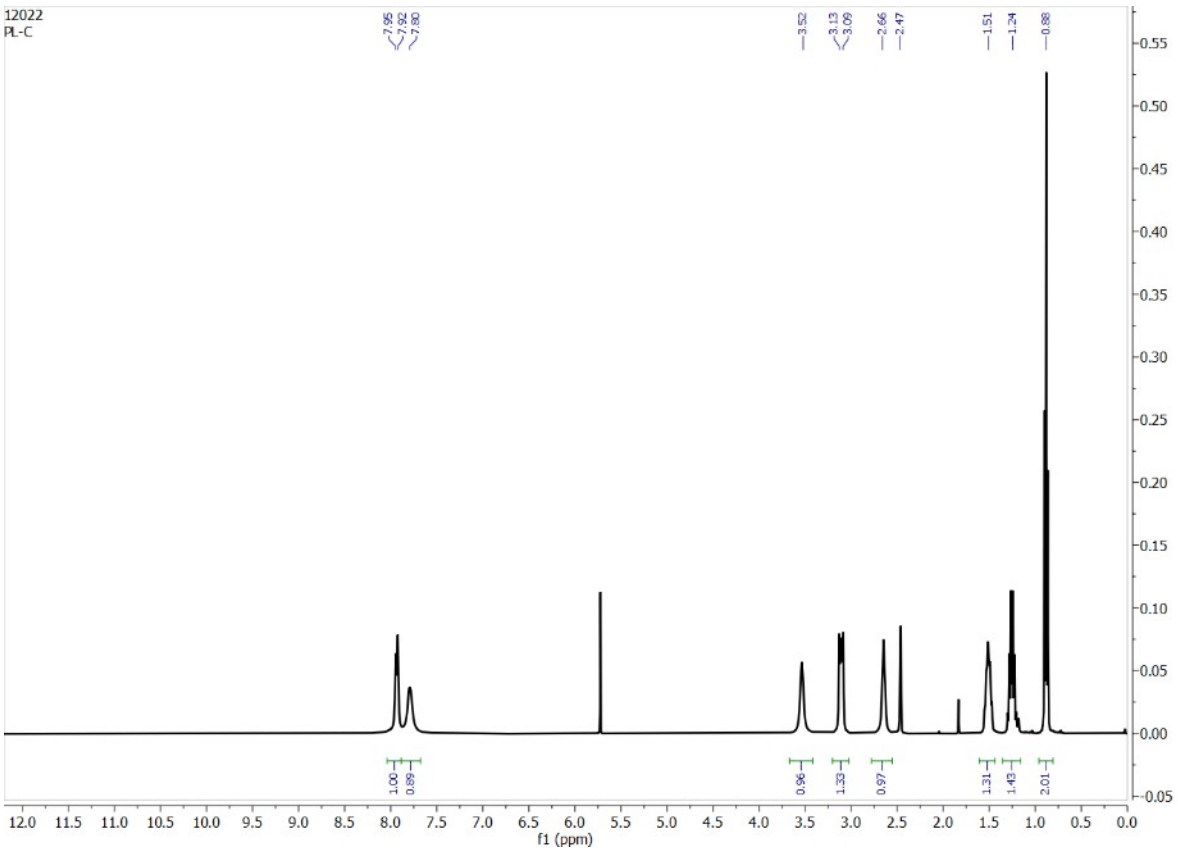

Fig. S72. ^{1}H-NMR spectrum of carbonate complex, [(n-$Bu_4N)_2$(2**L$_4$**·CO_3)] in DMSO-D_6.

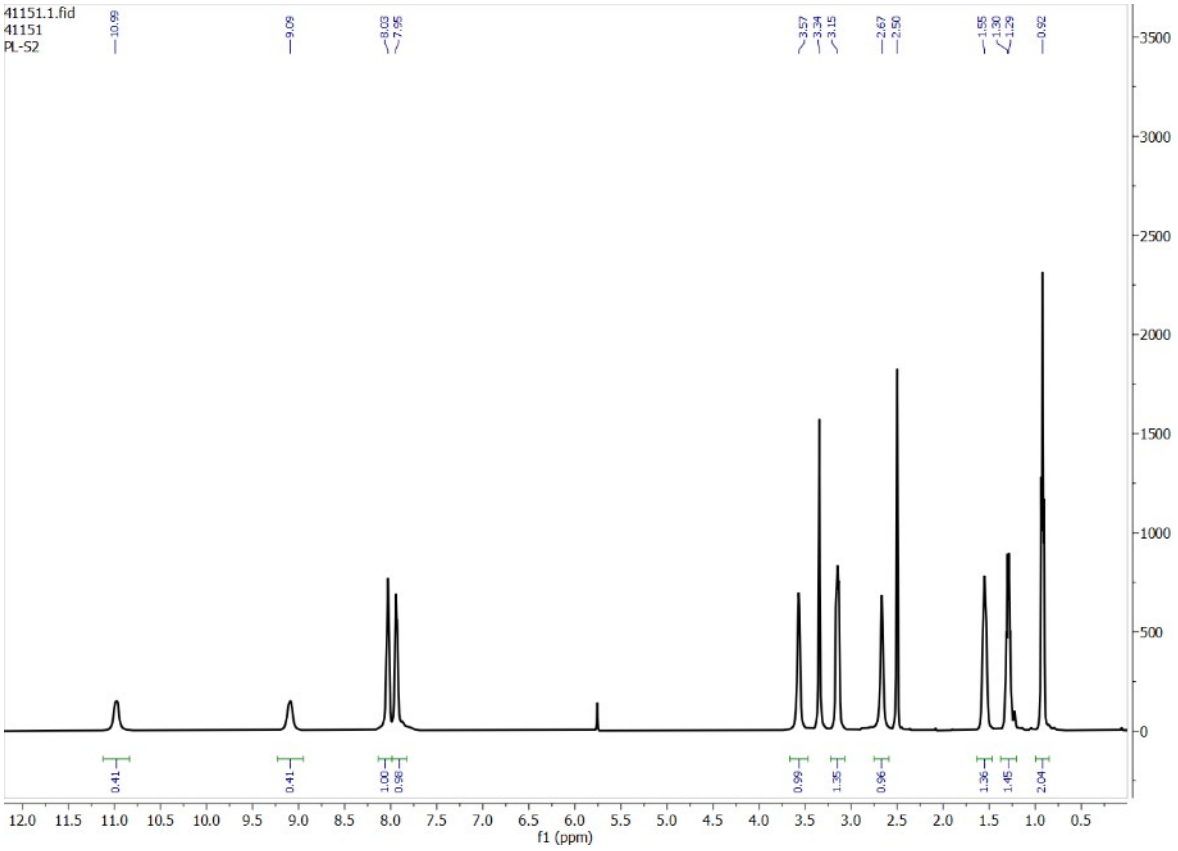

Fig. S73. ^{1}H-NMR spectrum of sulfate complex, [(n-$Bu_4N)_2$(2**L$_4$**·SO_4)] in DMSO-D_6.

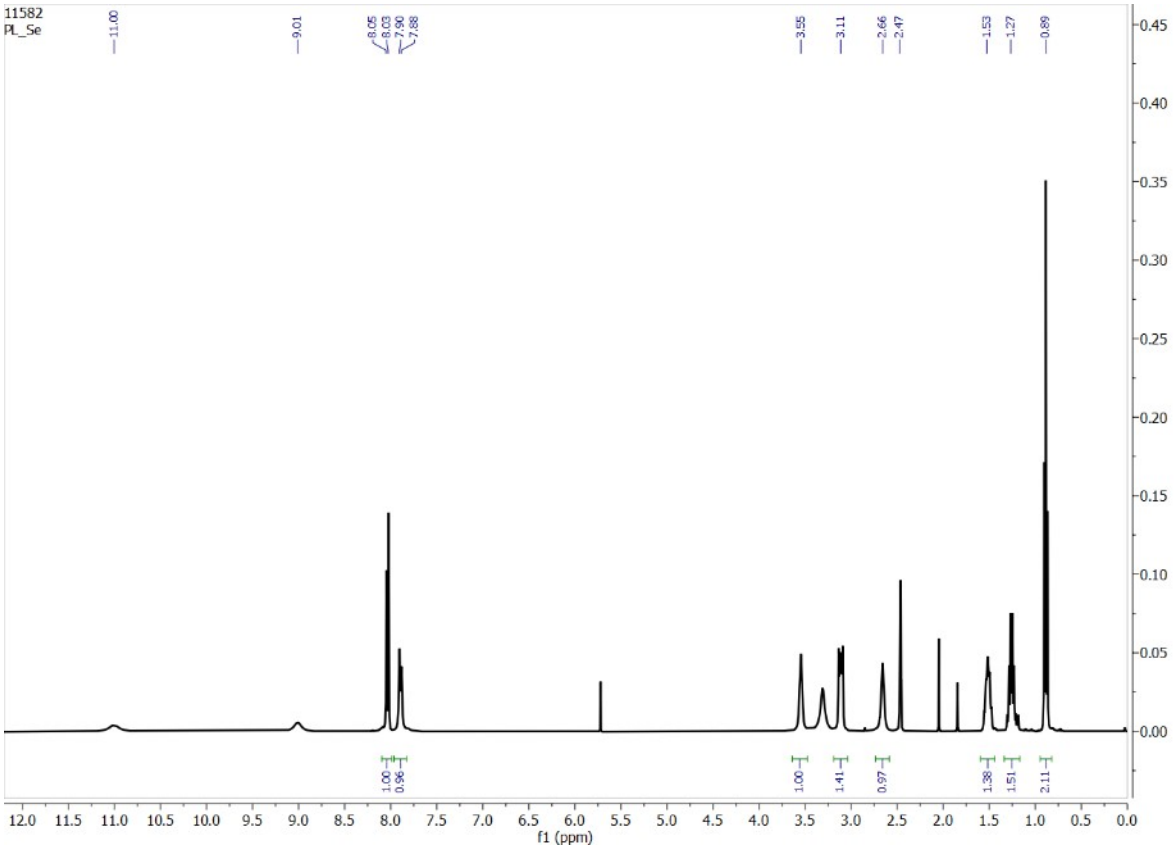

Fig. S74. ^{1}H-NMR spectrum of selenate complex, [(n-$Bu_4N)_2$(2$\mathbf{L_4}$·SeO_4)] in DMSO-D_6.

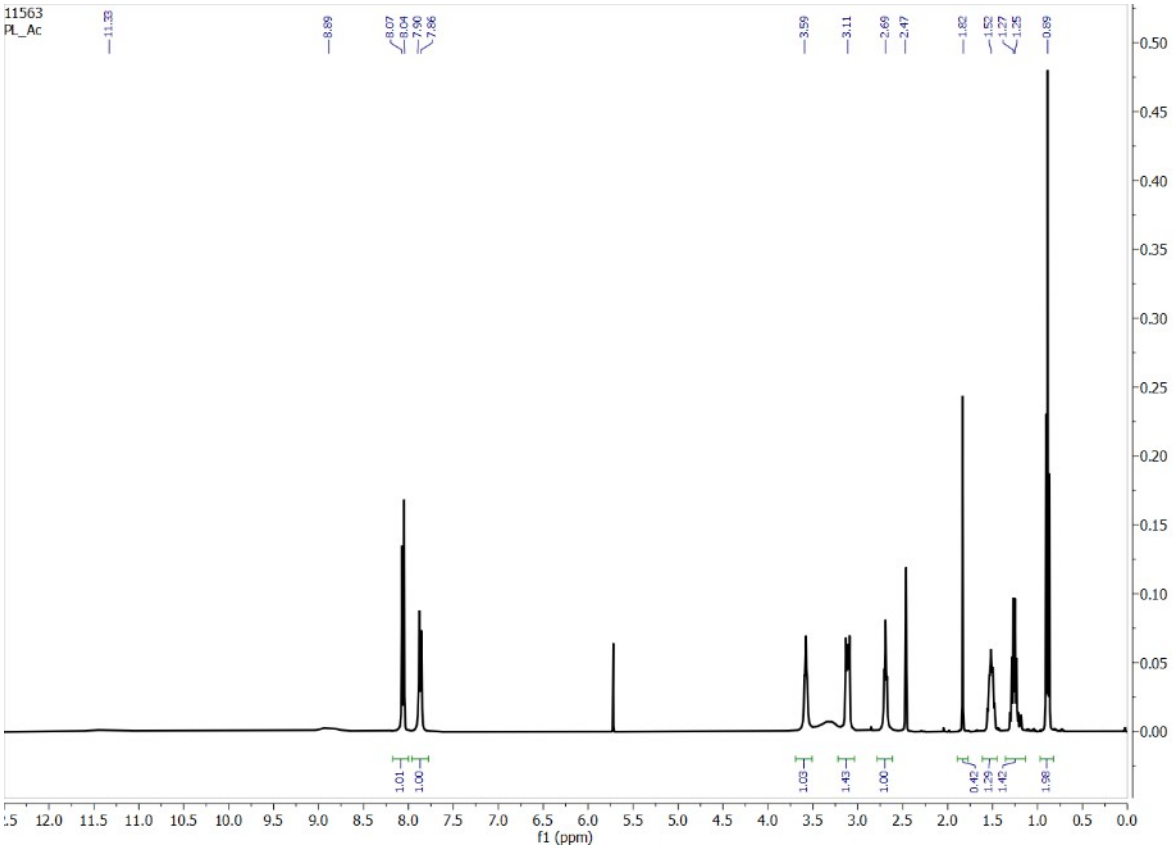

Fig. S75. ^{1}H-NMR spectrum of acetate complex, [(n-Bu_4N)($\mathbf{L_4}$·CH_3CO_2)] in DMSO-D_6.

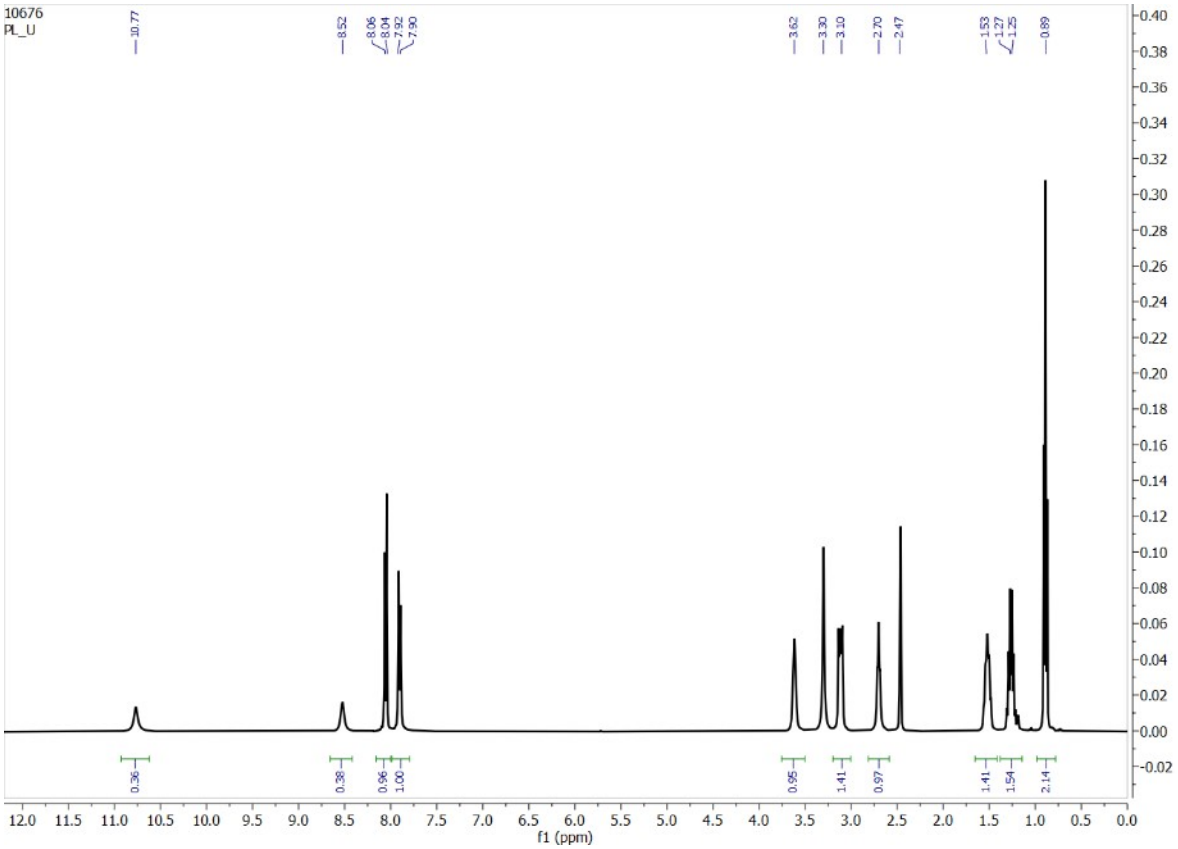

Fig. S76. ^{1}H-NMR spectrum of chloride complex, [(n-Bu_4N)(**L_4**·Cl)] in DMSO-D_6.

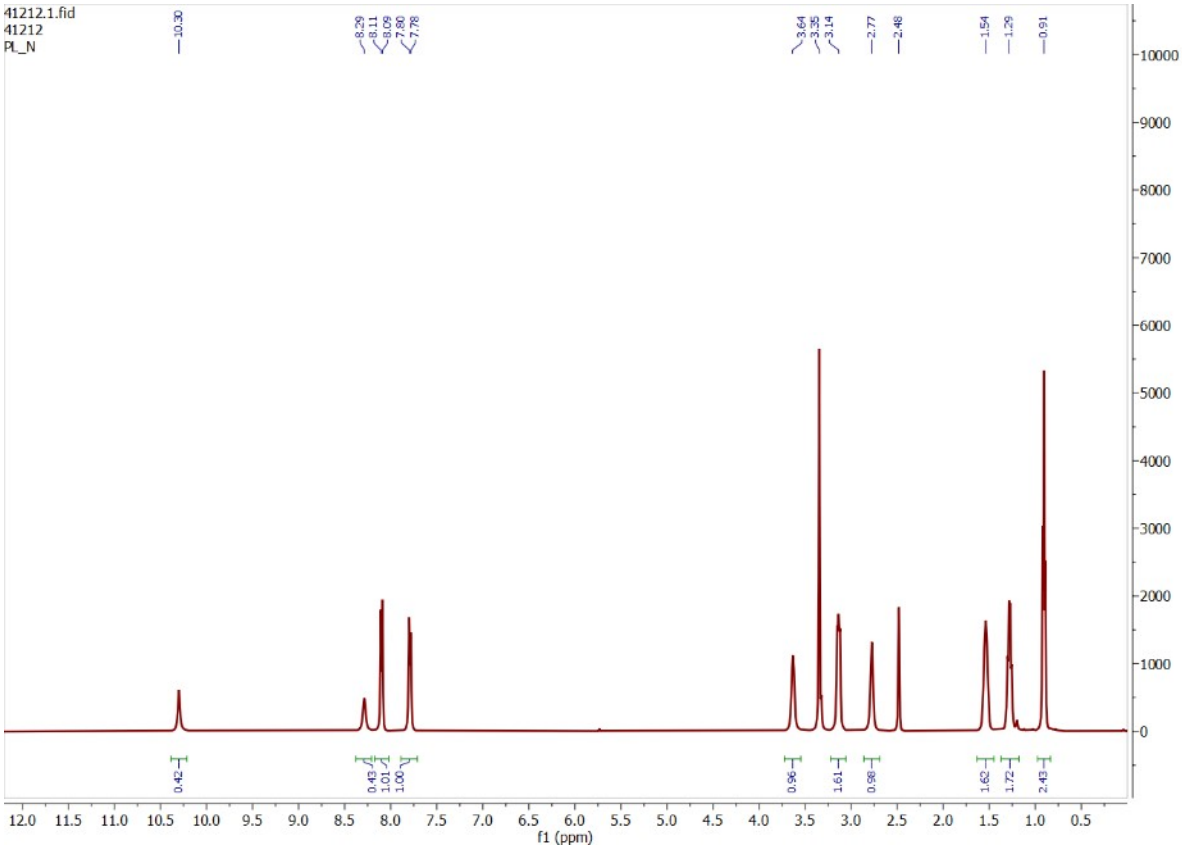

Fig. S77. ^{1}H-NMR spectrum of nitrate complex, [(n-Bu_4N)(**L_4**·NO_3)] in DMSO-D_6.

13. Selective extraction of phosphate by L_4: ^1H and ^{31}P-NMR spectra of isolated phosphate complexes

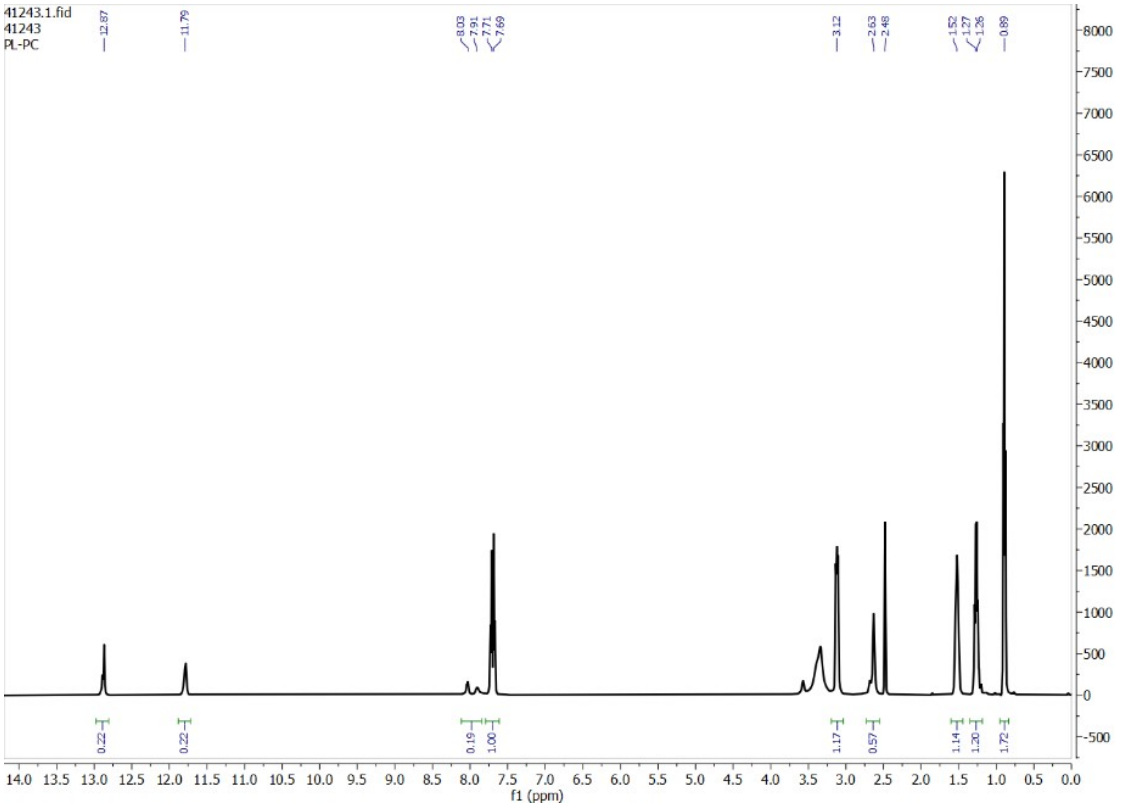

Fig. S78. ^1H-NMR spectrum of phosphate complex obtained from LLE in the presence of carbonate as a competing anion, two sets of aromatic -CH signals observed for a mixture of $[(n\text{-}Bu_4N)_2(2\mathbf{L_4}\cdot HPO_4)]$ and $[(n\text{-}Bu_4N)_3(2\mathbf{L_4}\cdot PO_4)]$ with ≈ 10:90 ratio.

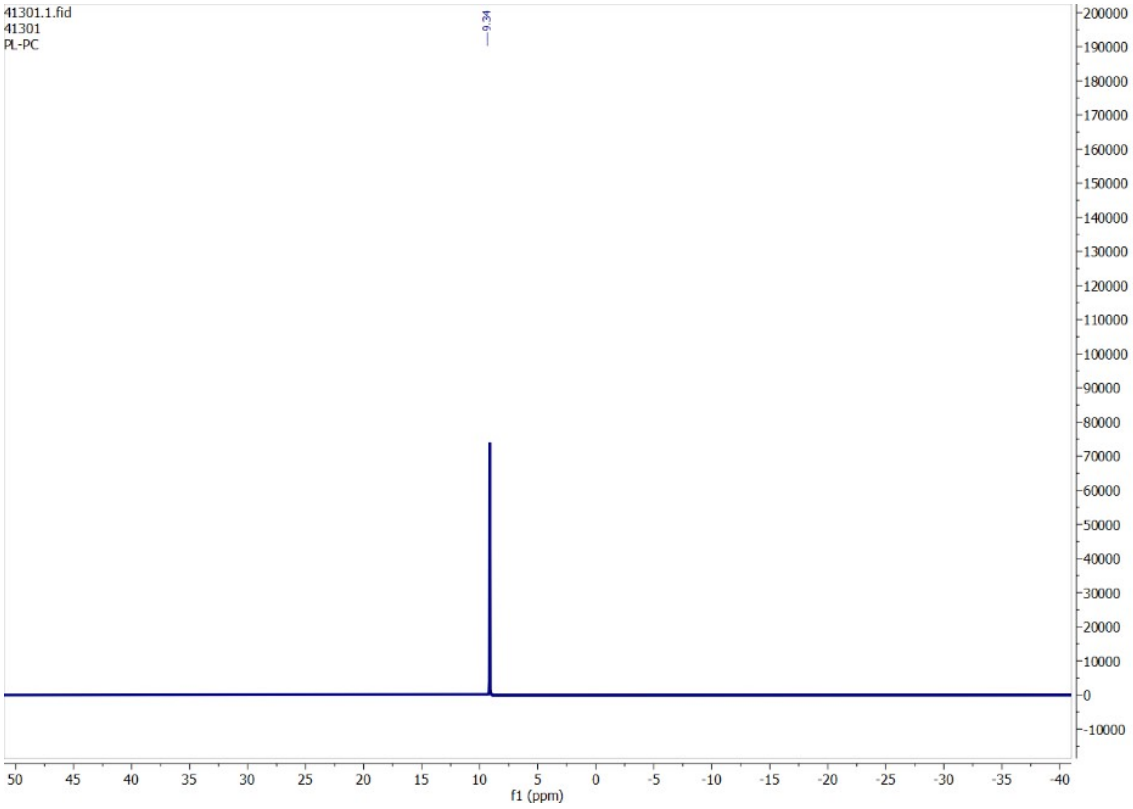

Fig. S79. ^{31}P-NMR spectrum of phosphate complex obtained from LLE in the presence of carbonate as a competing anion.

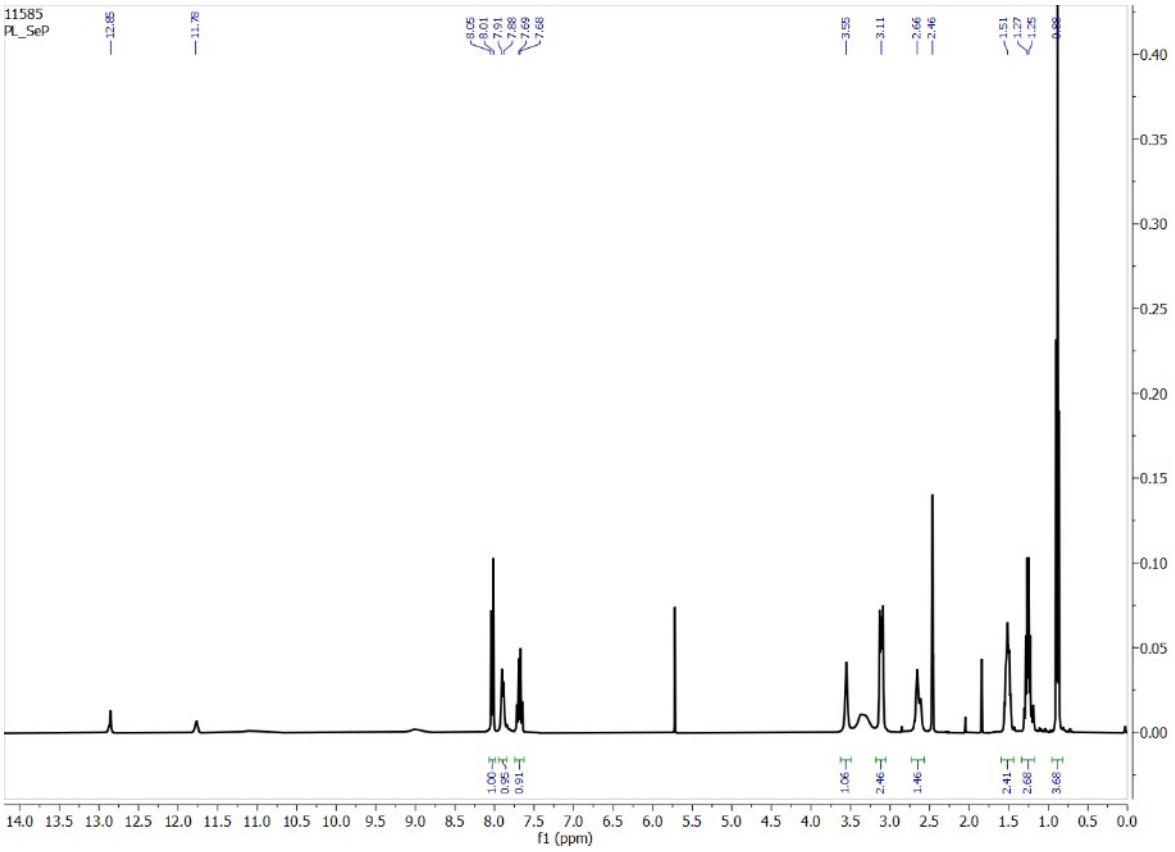

Fig. S80. ^{1}H-NMR spectrum of phosphate complex obtained from LLE in the presence of selenate, two sets of -NH and aromatic -CH signals were observed for a mixture of $[(n\text{-}Bu_4N)_2(2\mathbf{L_4}\cdot HPO_4)]$ and $[(n\text{-}Bu_4N)_3(2\mathbf{L_4}\cdot PO_4)]$ with ≈ 70:30 ratio.

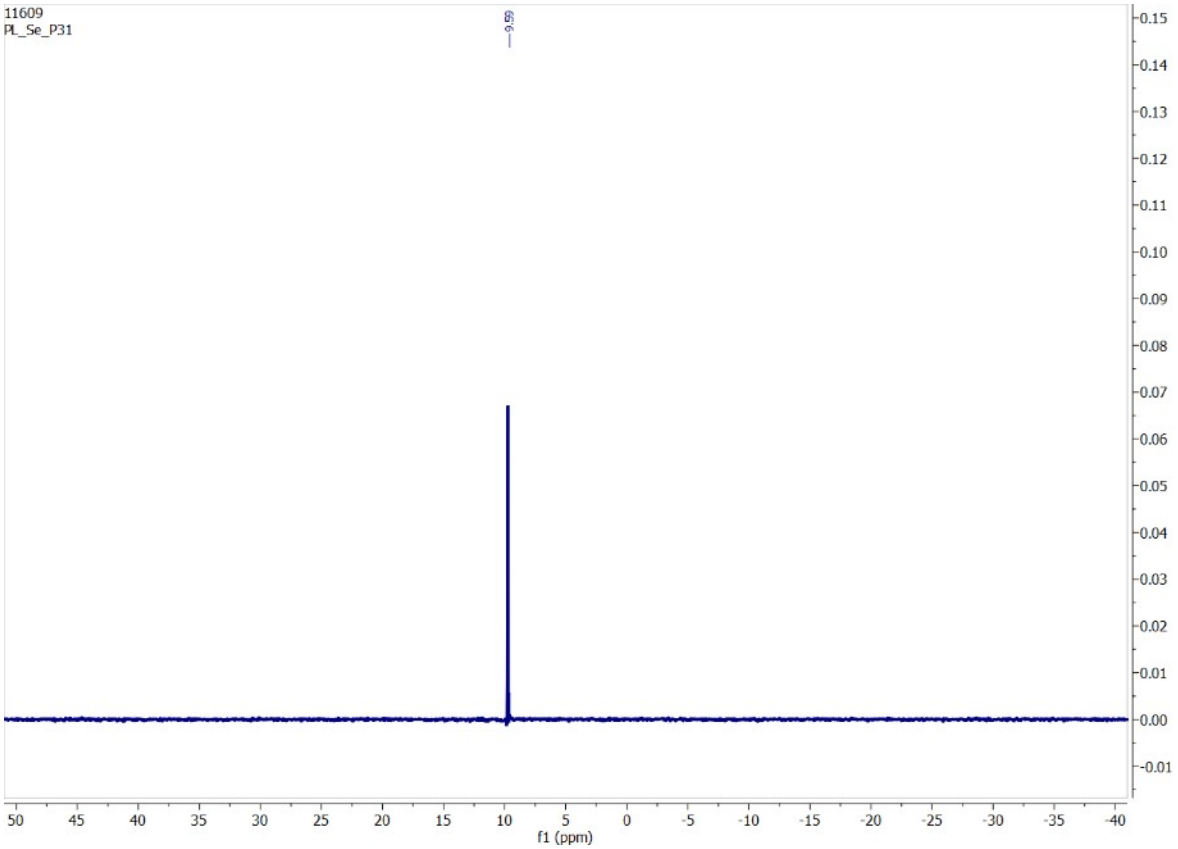

Fig. S81. ^{31}P-NMR spectrum of phosphate complex obtained from LLE in the presence of selenate as competing anion.

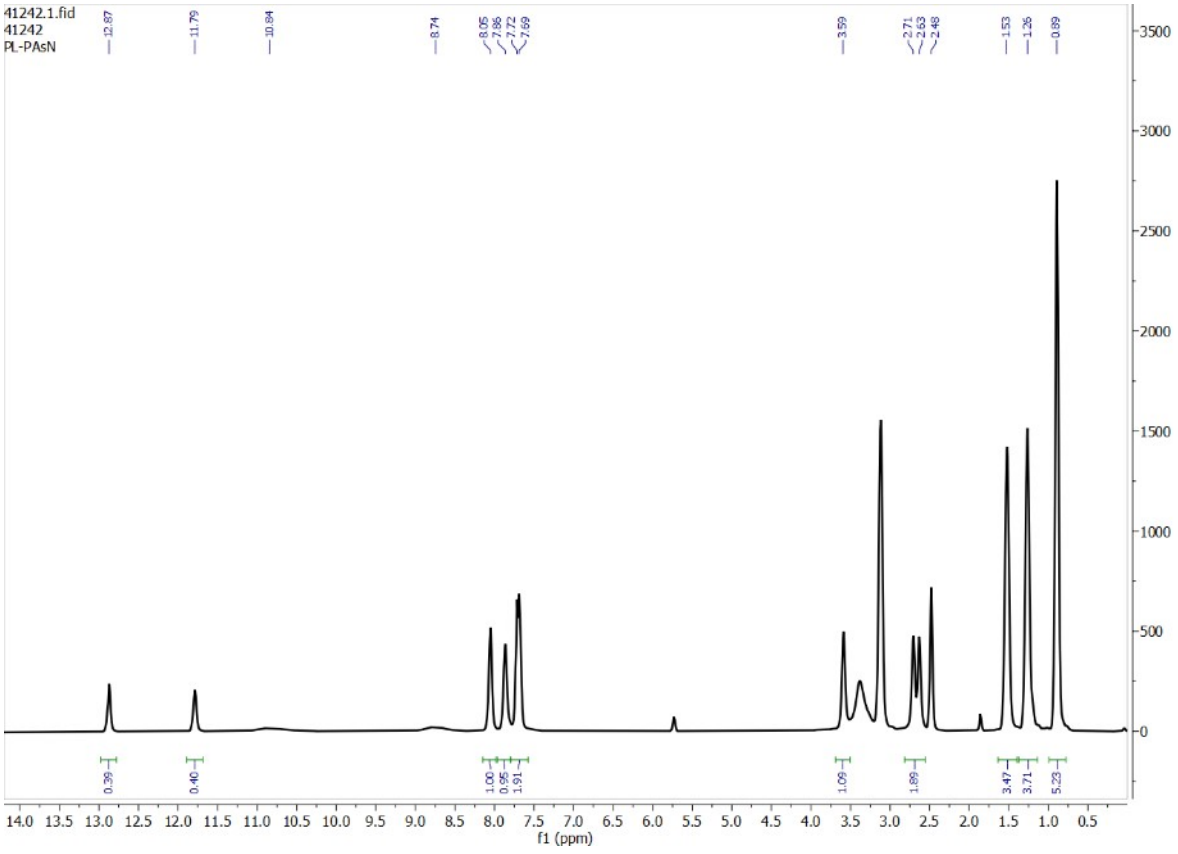

Fig. S82. ^{1}H-NMR spectrum of phosphate complex obtained from LLE in the presence of $HAsO_4^{2-}$ and NO_3^-, two sets of -NH and aromatic -CH signals observed for a mixture of $[(n\text{-}Bu_4N)_2(2\mathbf{L_4}\cdot HPO_4)]$ and $[(n\text{-}Bu_4N)_3(2\mathbf{L_4}\cdot PO_4)]$ with ≈ 50:50 ratio.

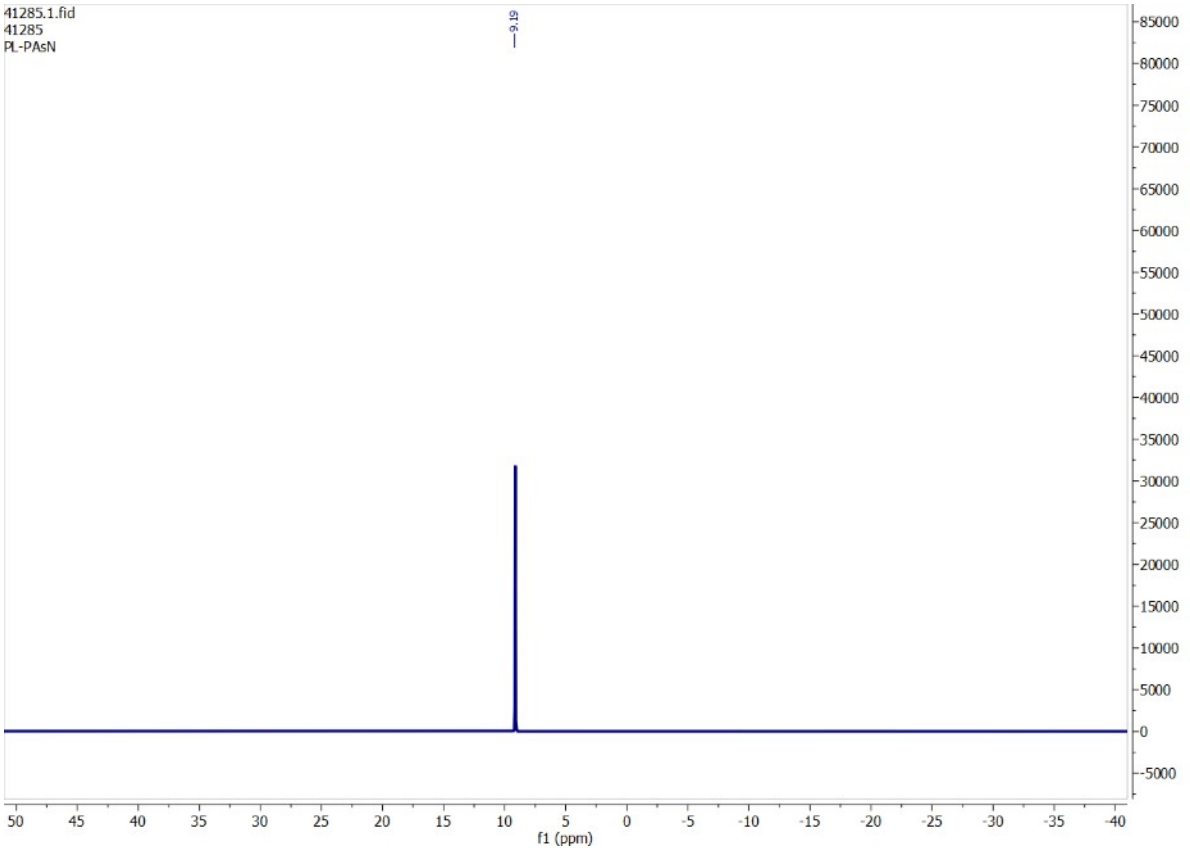

Fig. S83. ^{31}P-NMR spectrum of phosphate complex obtained from LLE in the presence of $HAsO_4^{2-}$ and NO_3^- as competing anions.

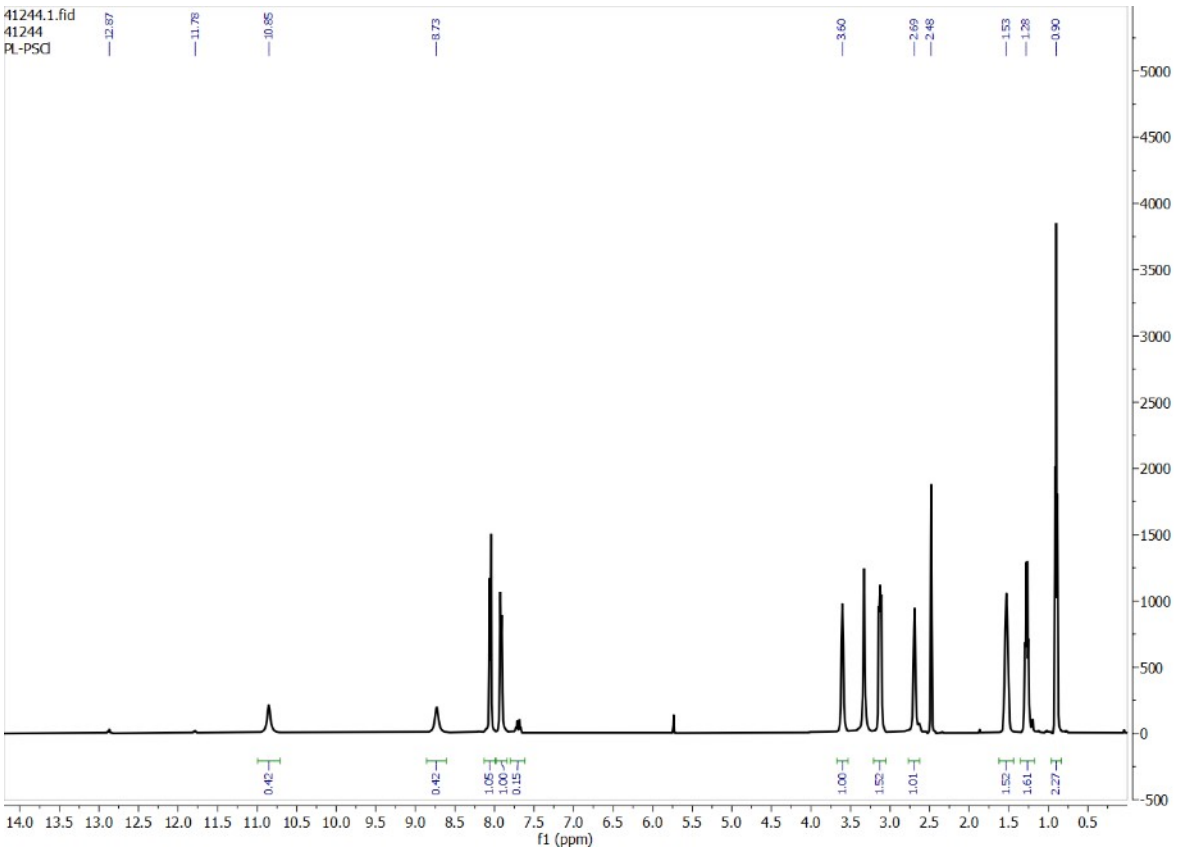

Fig. S84. ^{1}H-NMR spectrum of phosphate complex obtained from LLE in the presence of SO_4^{2-} and Cl^-, two sets of -NH and aromatic -CH signals observed for a mixture of [(n-$Bu_4N)_2$(2**L**$_4$·HPO_4)] and [(n-$Bu_4N)_3$(2**L**$_4$·PO_4)] with ≈ 90:10 ratio.

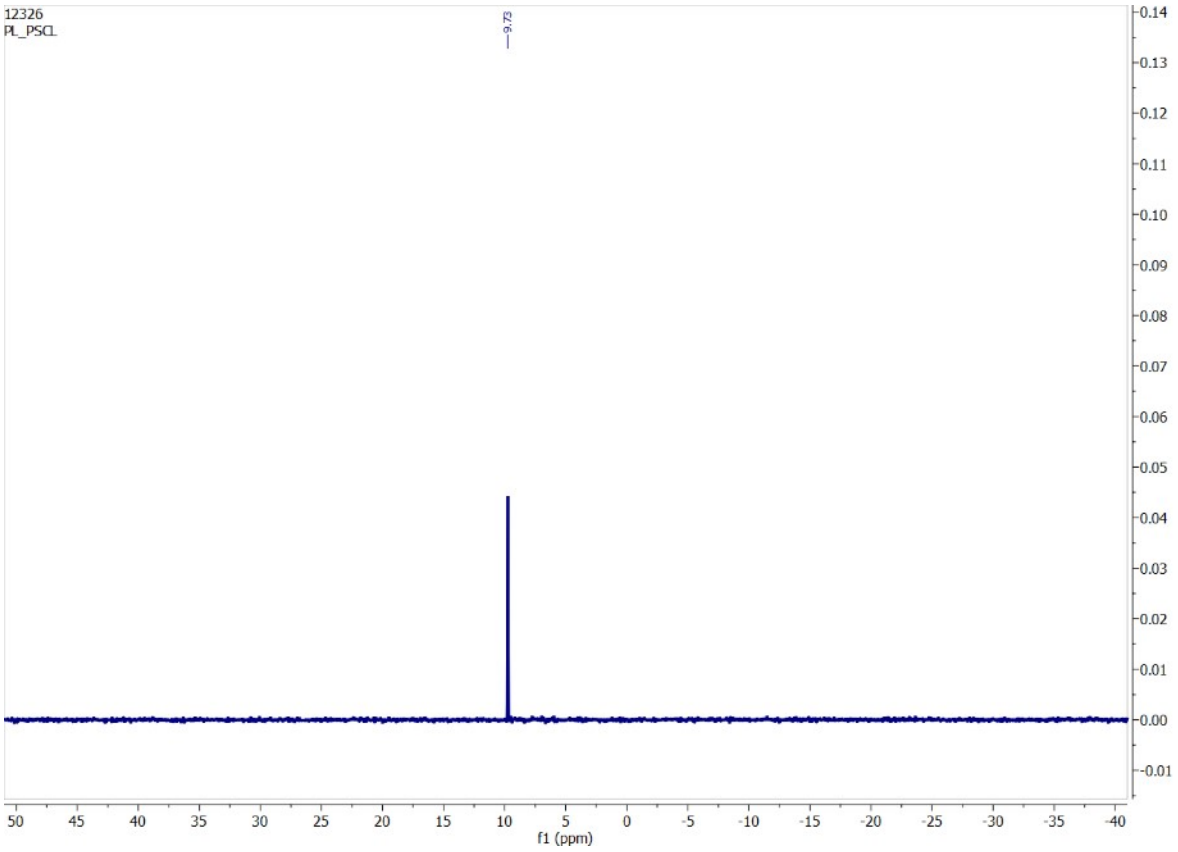

Fig. S85. ^{31}P-NMR spectrum of phosphate complex obtained from LLE in the presence of sulfate and chloride as competing anions.

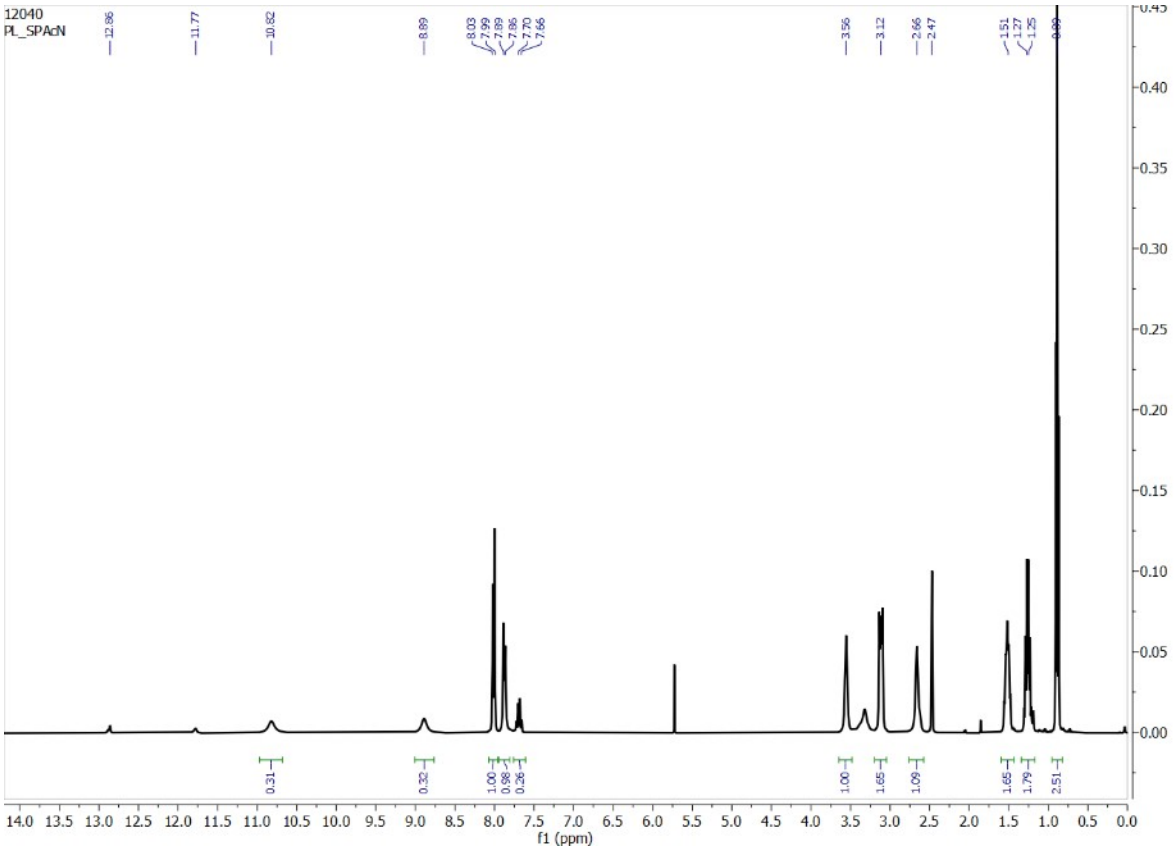

Fig. S86. ^{1}H-NMR spectrum of phosphate complex obtained from LLE in the presence of SO_4^{2-} and NO_3^-, two sets of -NH and aromatic -CH signals observed for a mixture of $[(n\text{-}Bu_4N)_2(2\mathbf{L_4}\cdot HPO_4)]$ and $[(n\text{-}Bu_4N)_3(2\mathbf{L_4}\cdot PO_4)]$ with ≈ 90:10 ratio.

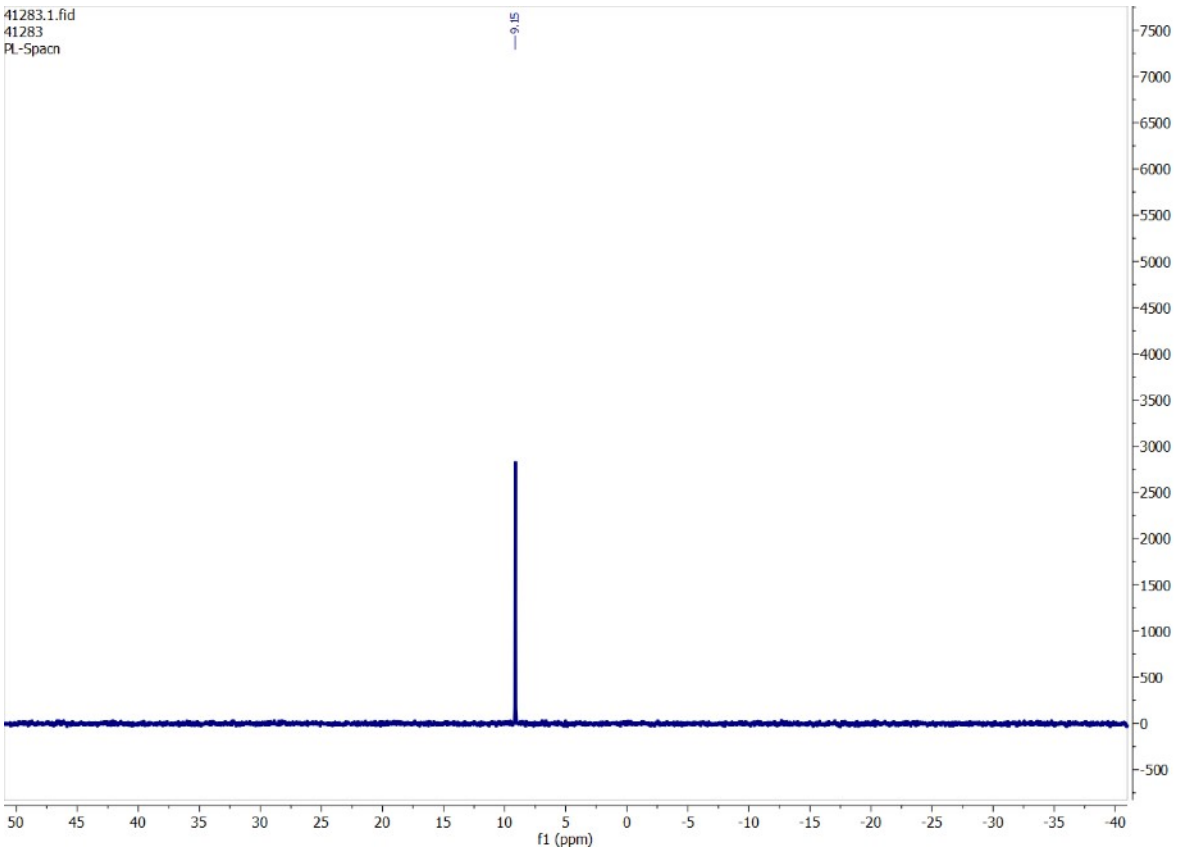

Fig. S87. ^{31}P-NMR spectrum of phosphate complex obtained from LLE in the presence of sulfate and nitrate as competing anions.

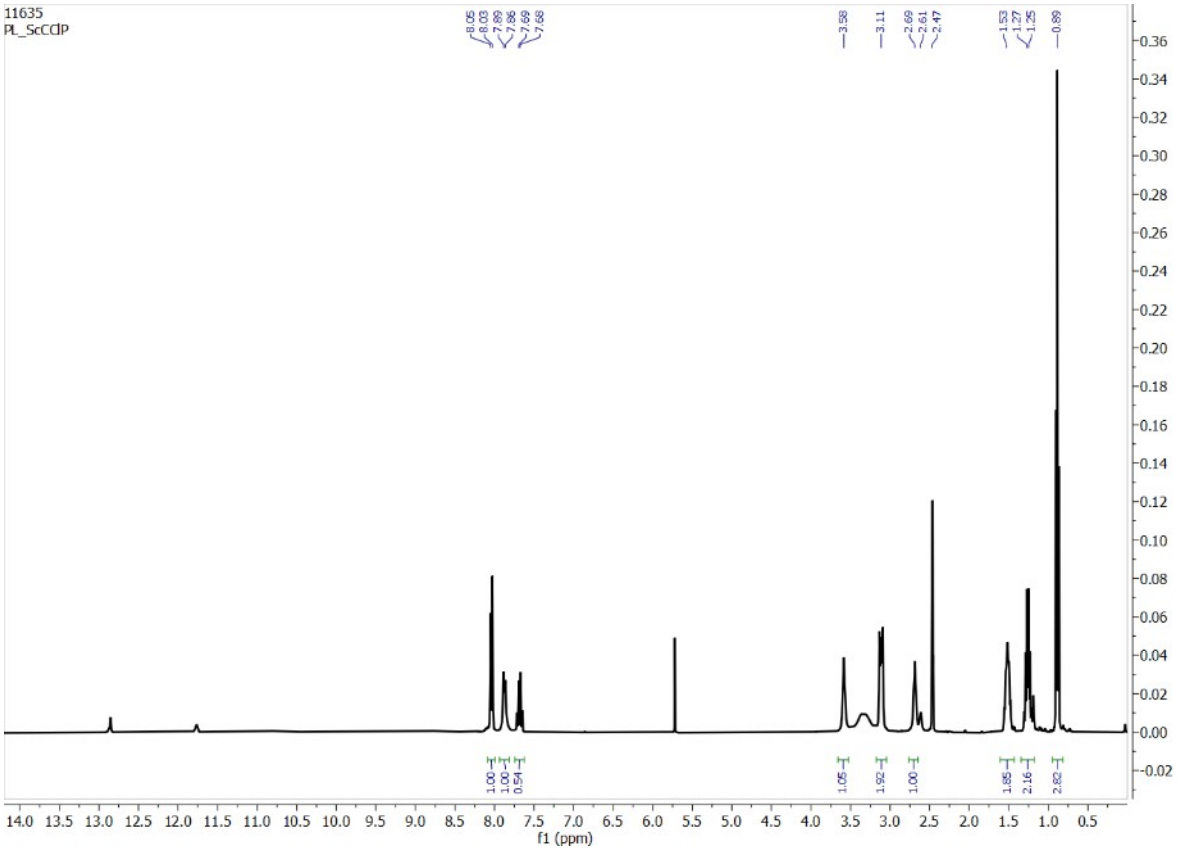

Fig. S88. ^{1}H-NMR spectrum of phosphate complex obtained from LLE in the presence of SeO_4^{2-} and CO_3^{2-} and Cl^-, two sets of aromatic -CH signals observed for a mixture of [(n-$Bu_4N)_2$(2**L**$_4$·HPO_4)] and [(n-$Bu_4N)_3$(2**L**$_4$·PO_4)] with 80:20 ratio.

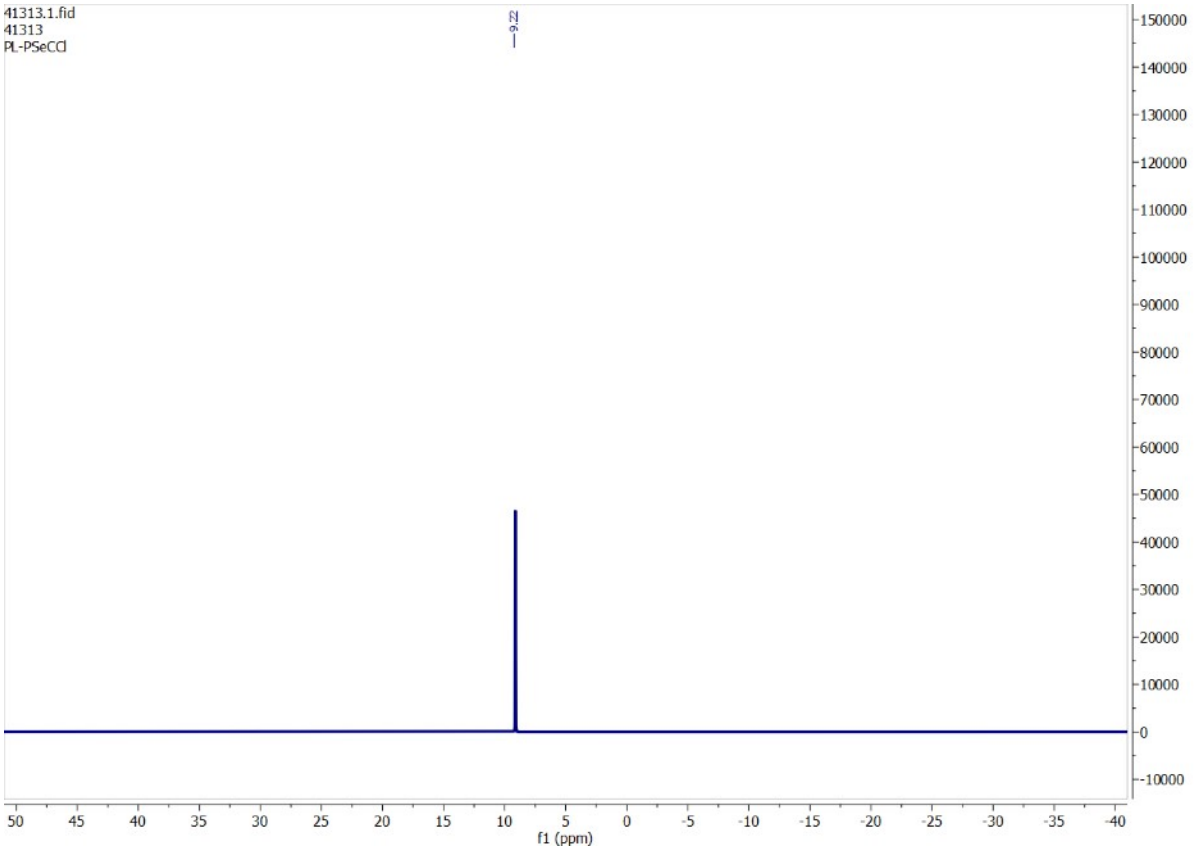

Fig. S89. ^{31}P-NMR spectrum of phosphate complex obtained from LLE in the presence of selenate, carbonate and chloride as competing anions.

14. Sulfate extraction under environmentally relevant conditions

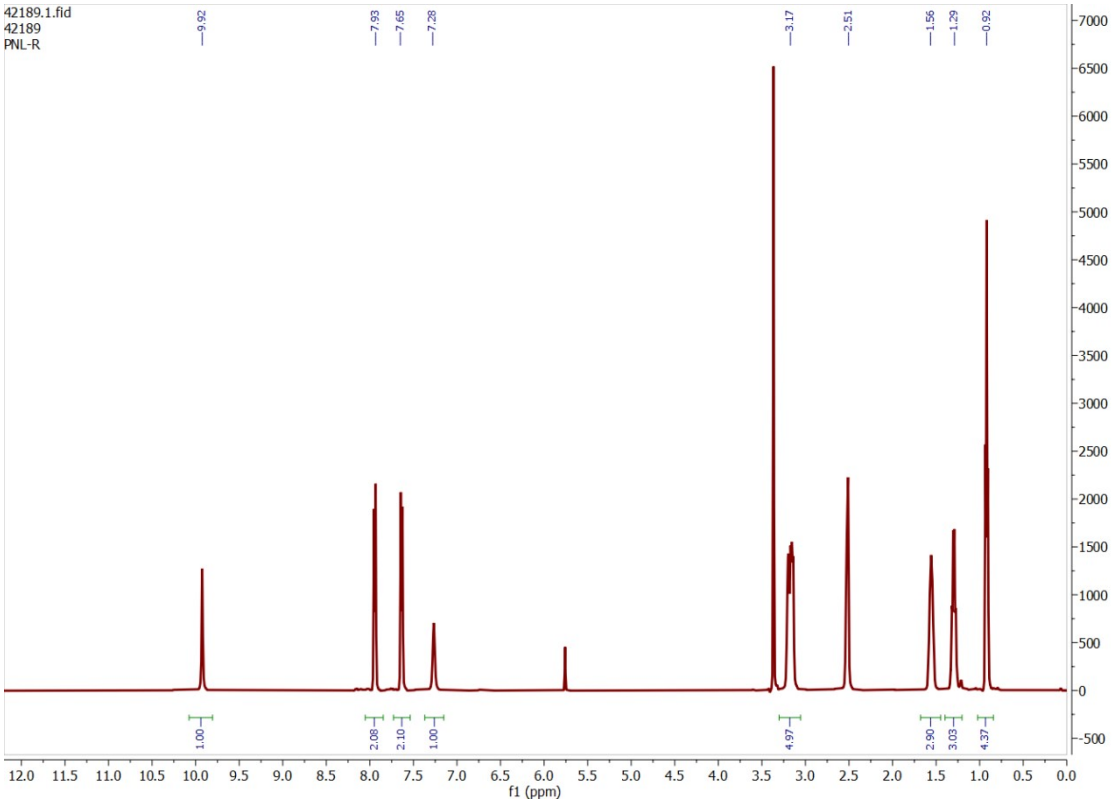

Fig. S90. ^{1}H-NMR spectrum of [(n-$Bu_4N)_2$(2**L$_2$**·SO_4)] obtained from LLE using aqueous solution mimicking the anion distribution in upper Ganga River basin.

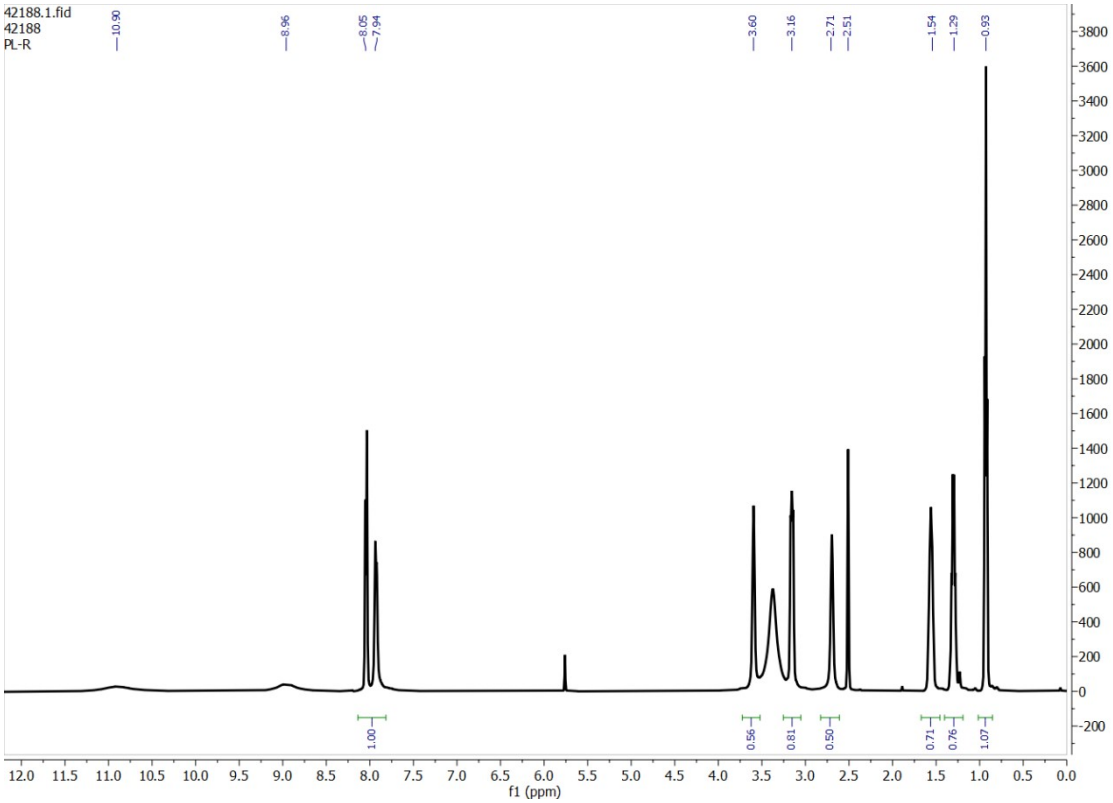

Fig. S91. ^{1}H-NMR spectrum of [(n-$Bu_4N)_2$(2**L$_4$**·SO_4)] obtained from LLE using aqueous solution mimicking the anion distribution in upper Ganga River basin

15. Control experiments: ^{1}H-NMR and ^{31}P-NMR spectra

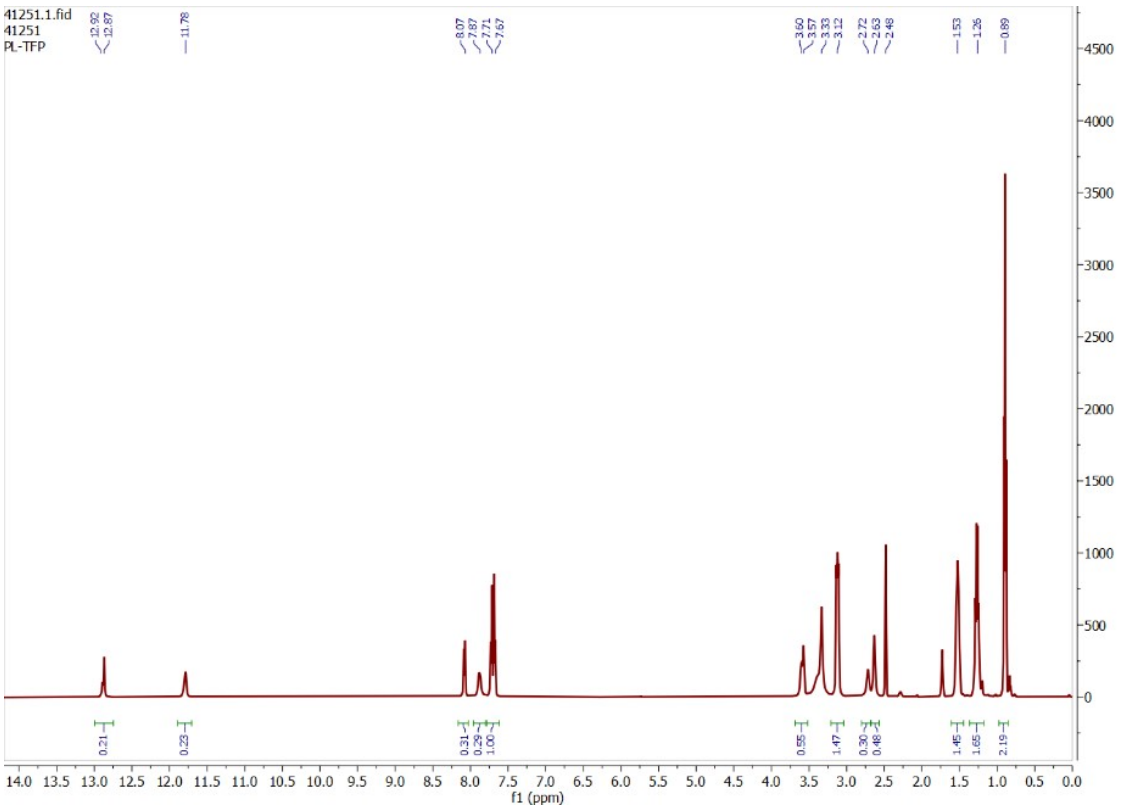

Fig. S92. ^{1}H-NMR spectrum of phosphate complex obtained from LLE in the presence of tetrabutylammonium fluoride as an anion-exchanger in the organic phase for phosphate extraction by **L_4** from aqueous phase (Ratio of $[(n\text{-}Bu_4N)_2(2\mathbf{L_4}\cdot HPO_4)]$ and $[(n\text{-}Bu_4N)_3(2\mathbf{L_4}\cdot PO_4)]$ = 40:60).

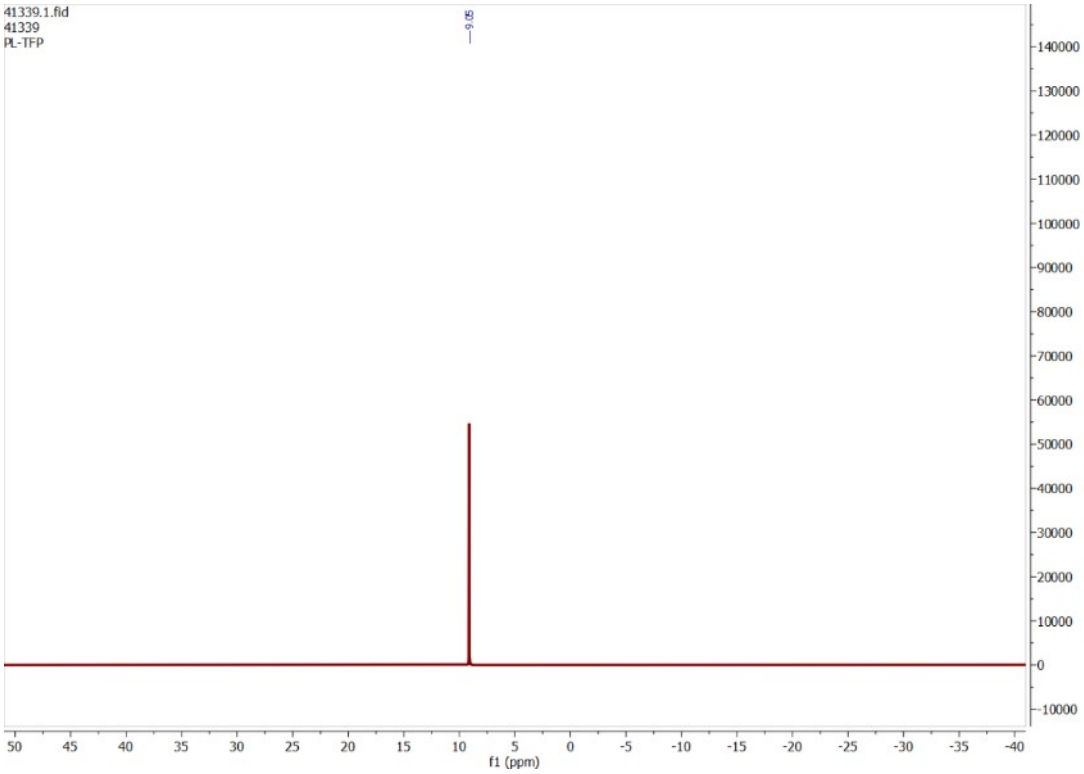

Fig. S93. ^{31}P-NMR spectrum of phosphate complex obtained from LLE in the presence of tetrabutylammonium fluoride as an anion-exchanger in the organic phase for phosphate extraction by **L_4** from aqueous phase.

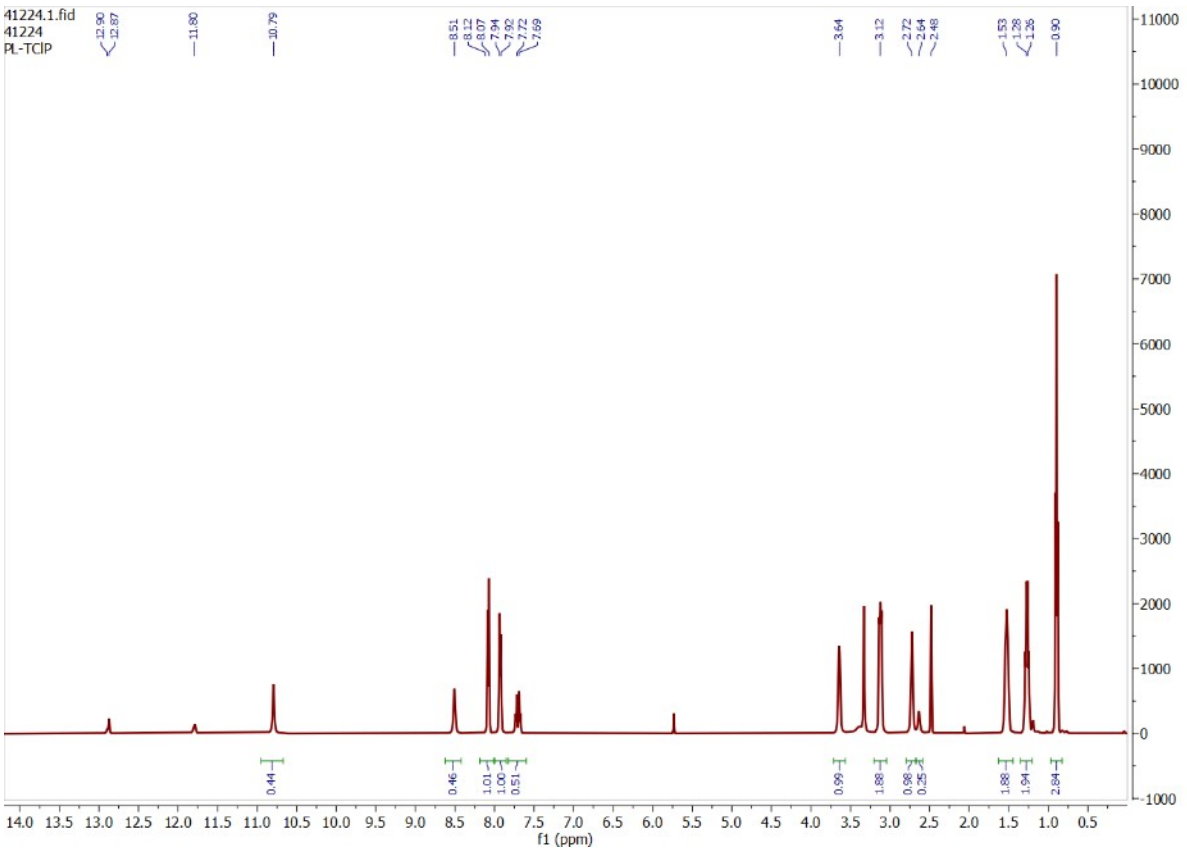

Fig. S94. ^{1}H-NMR spectrum of phosphate complex obtained from LLE in the presence of tetrabutylammonium chloride as an anion-exchanger in the organic phase for phosphate extraction by **L_4** from aqueous phase (Ratio of [(n-$Bu_4N)_2$(2**L_4**·HPO_4)] and [(n-$Bu_4N)_3$(2**L_4**·PO_4)]: 80:20).

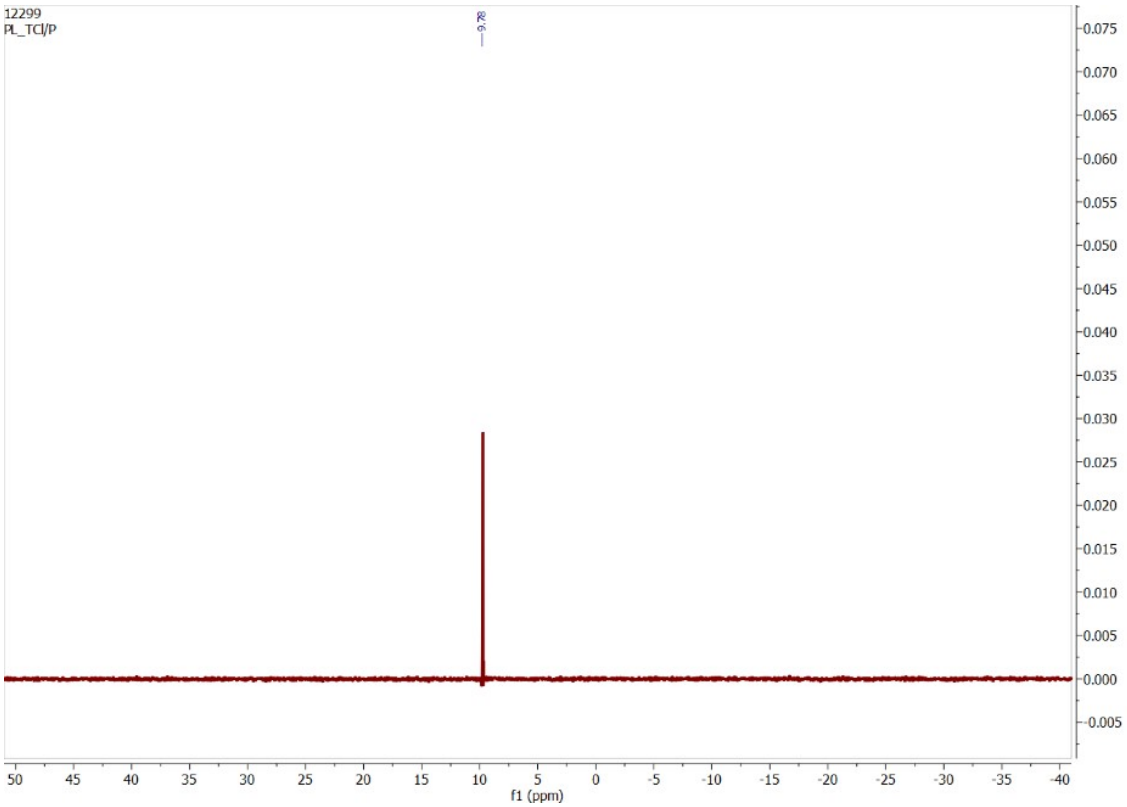

Fig. S95. ^{31}P-NMR spectrum of phosphate complex obtained from LLE in the presence of tetrabutylammonium chloride as an anion-exchanger in the organic phase for phosphate extraction by **L_4** from aqueous phase.

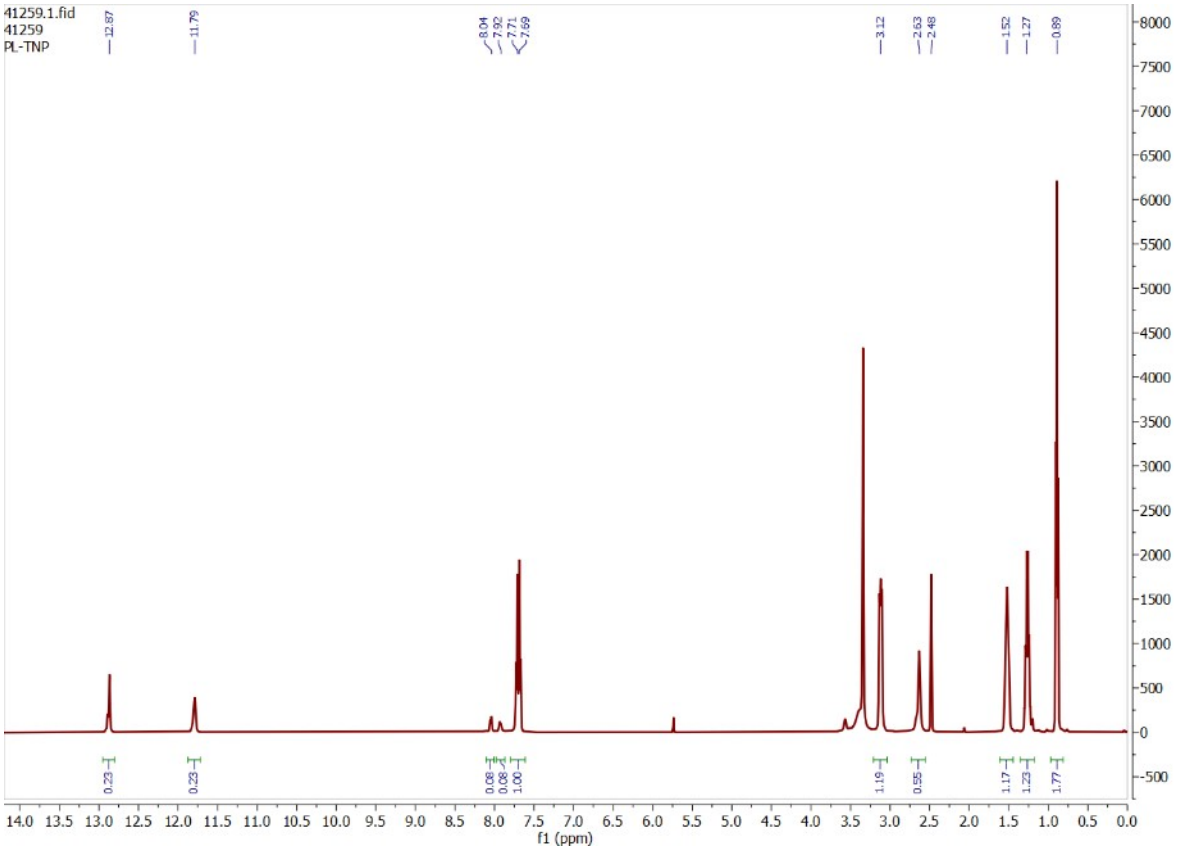

Fig. S96. ^{1}H-NMR spectrum of phosphate complex obtained from LLE in the presence of tetrabutylammonium nitrate as an anion-exchanger in the organic phase for phosphate extraction by **L_4** from aqueous phase (Ratio of $[(n\text{-}Bu_4N)_2(2\mathbf{L_4}\cdot HPO_4)]$ and $[(n\text{-}Bu_4N)_3(2\mathbf{L_4}\cdot PO_4)]$: 15:85).

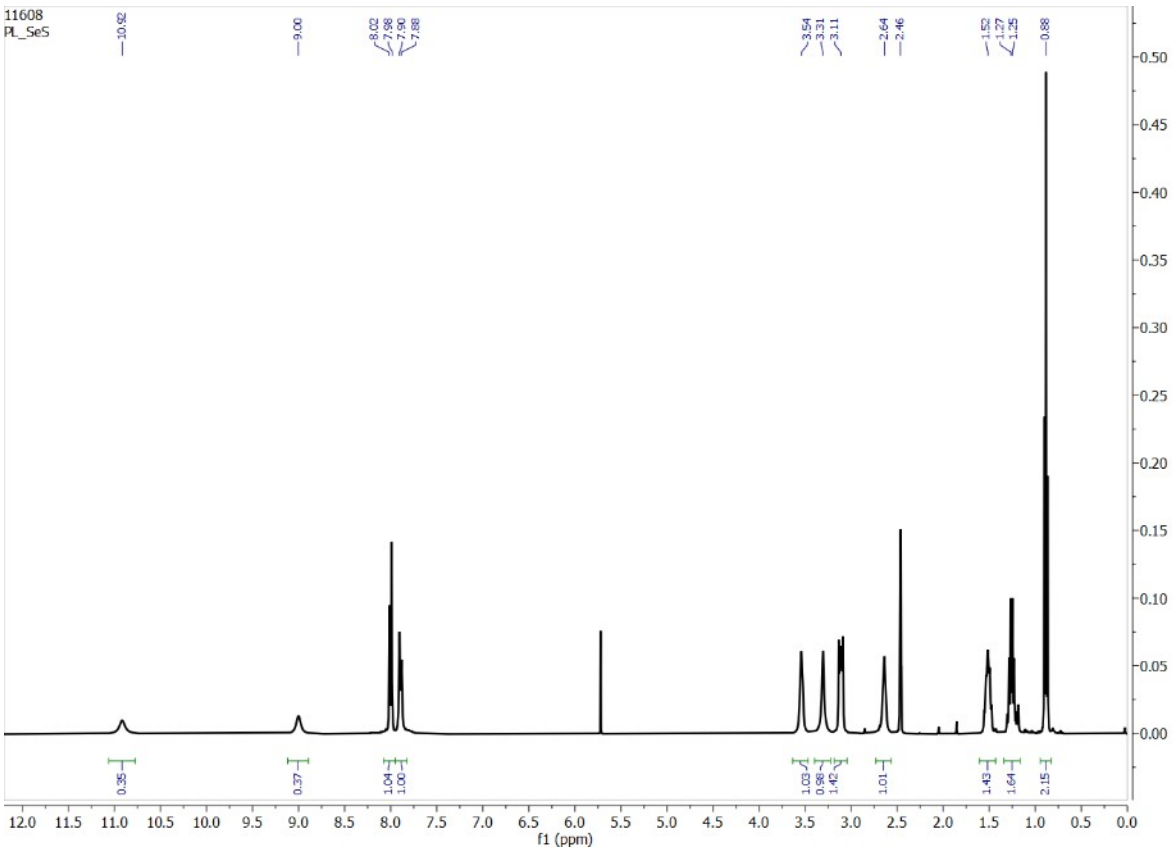

Fig. S97. ^{1}H-NMR spectrum of [(n-$Bu_4N)_2$(2**L$_4$**·SO_4)] obtained from LLE in the presence of selenate as a competing anion.

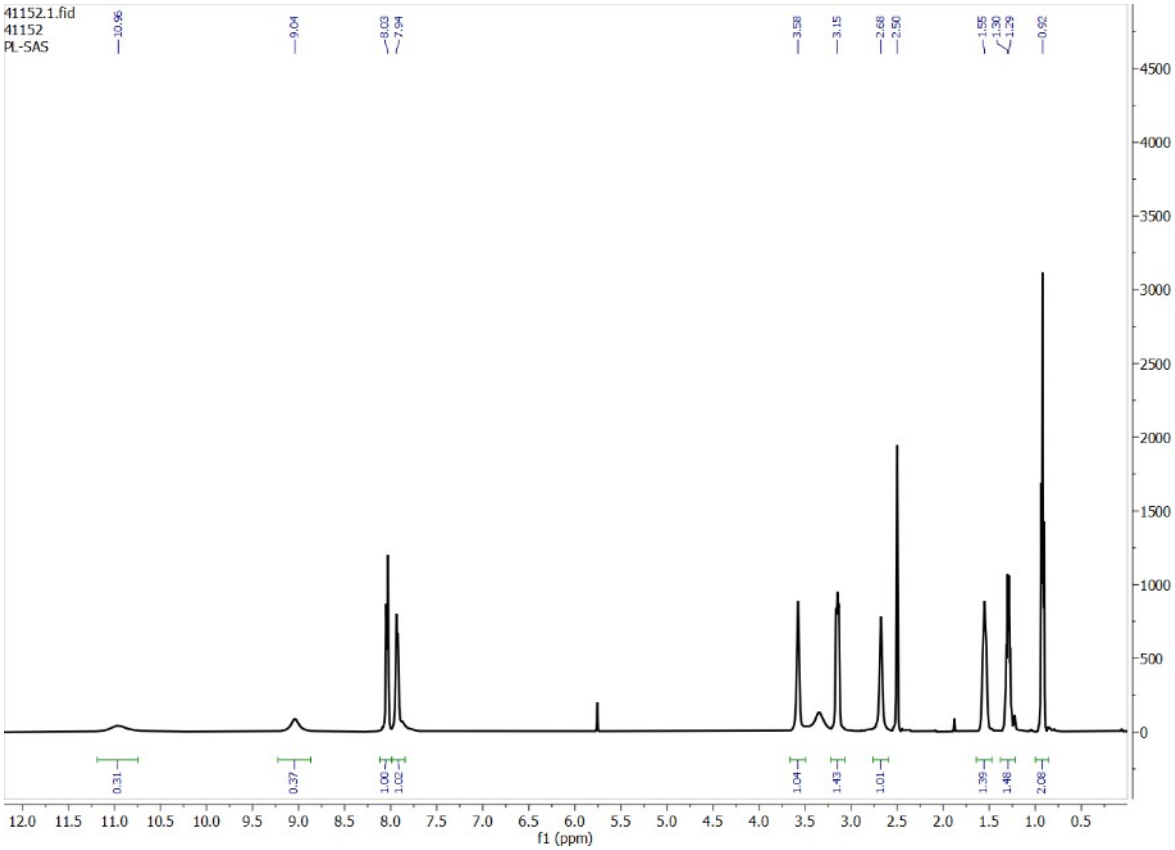

Fig. S98. ^{1}H-NMR spectrum of [(n-$Bu_4N)_2$(2**L$_4$**·SO_4)] obtained from LLE in the presence of hydrogenarsenate as a competing anion.

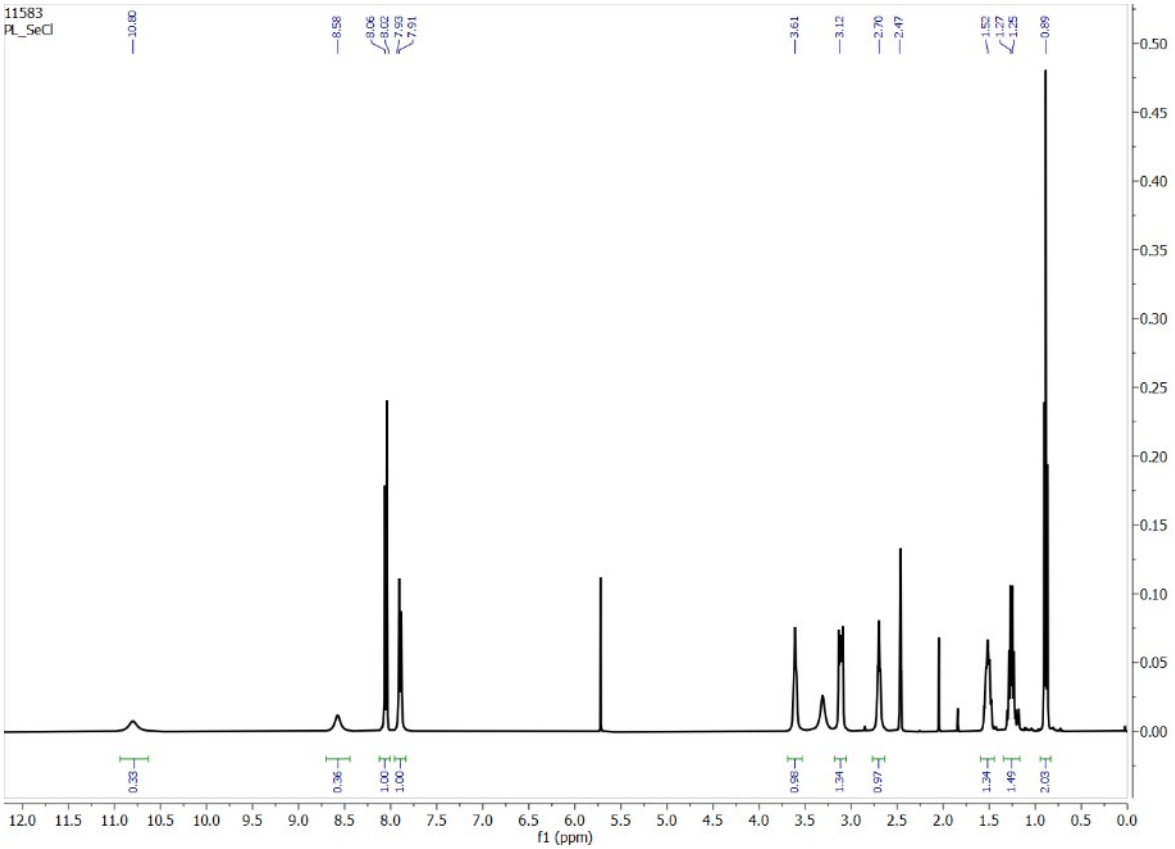

Fig. S99. ^{1}H-NMR spectrum of [(n-Bu_4N)(**L_4**·Cl)] obtained from LLE in the presence of selenate as a competing anion.

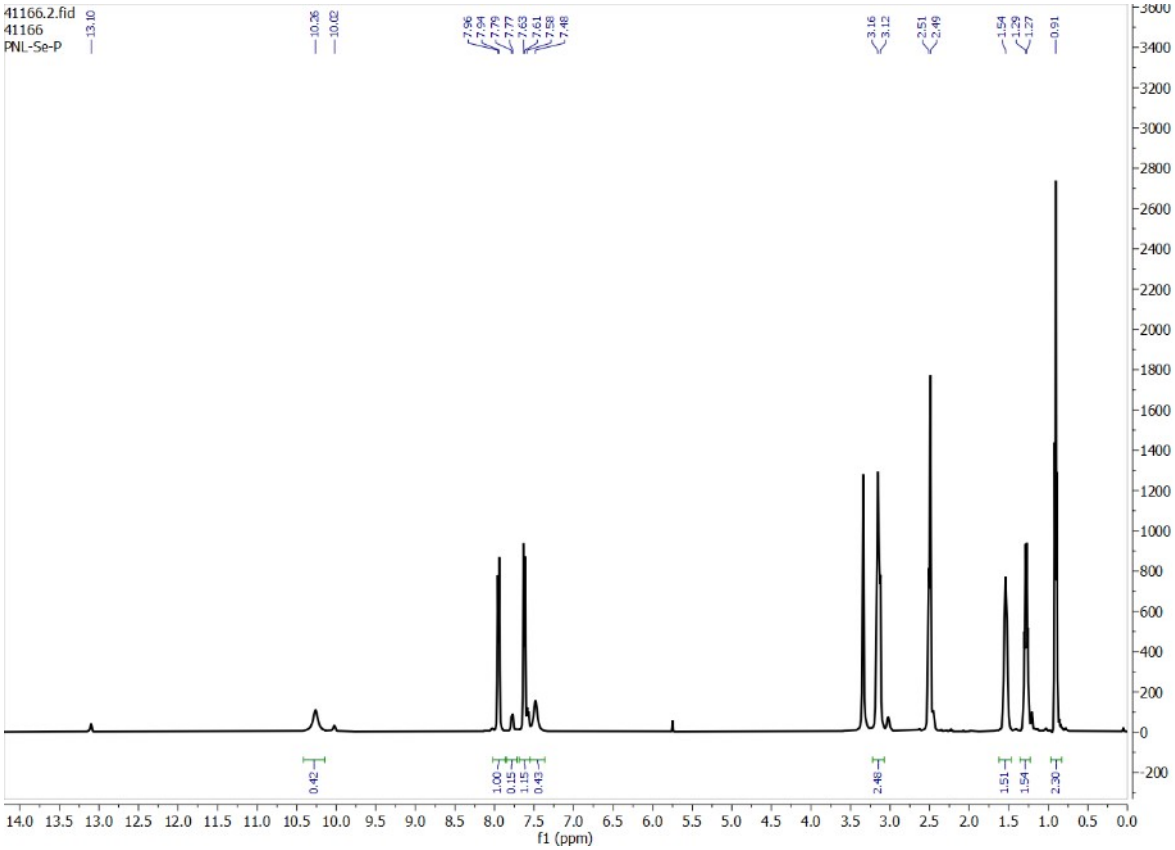

Fig. S100. ^{1}H-NMR spectrum of [(n-Bu_4N)$_2$(2**L_2**·HPO_4)] obtained from LLE in the presence of selenate as a competing anion.

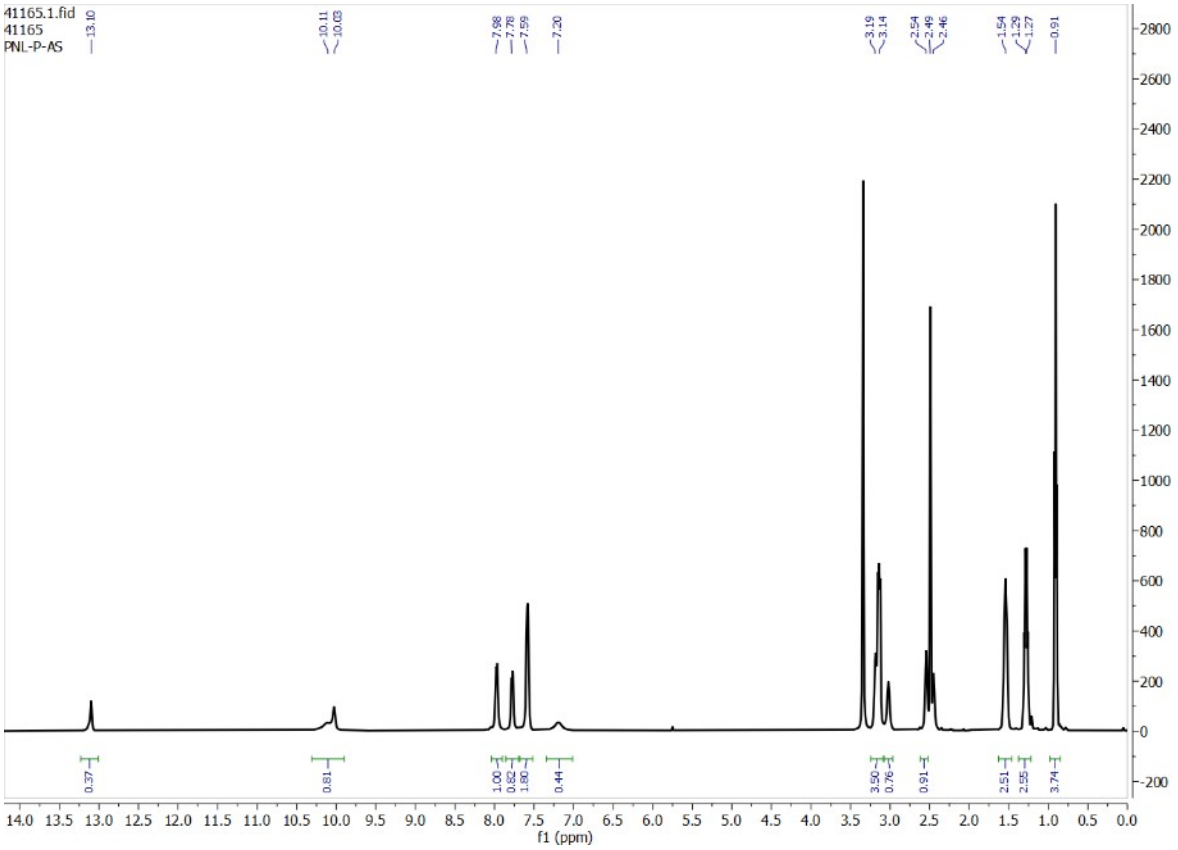

Fig. S101. ^{1}H-NMR spectrum of [(n-Bu_4N)$_2$(2**L$_2$**·HPO_4)] obtained from LLE in the presence of arsenate as a competing anion.

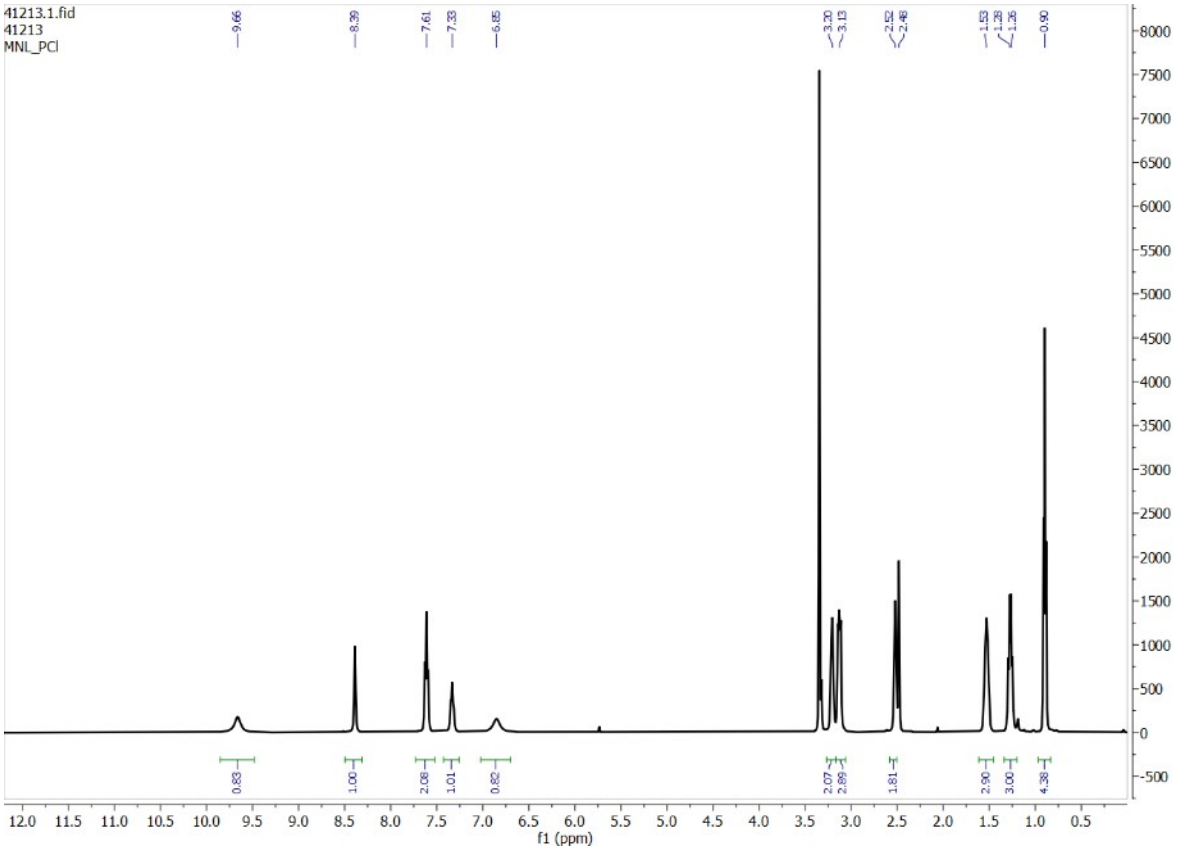

Fig. S102. ^{1}H-NMR spectrum of [(n-Bu_4N)(**L$_1$**·Cl)] obtained from LLE in the presence of hydrogenphosphate as a competing anion.

16. Powder X-ray diffraction analysis

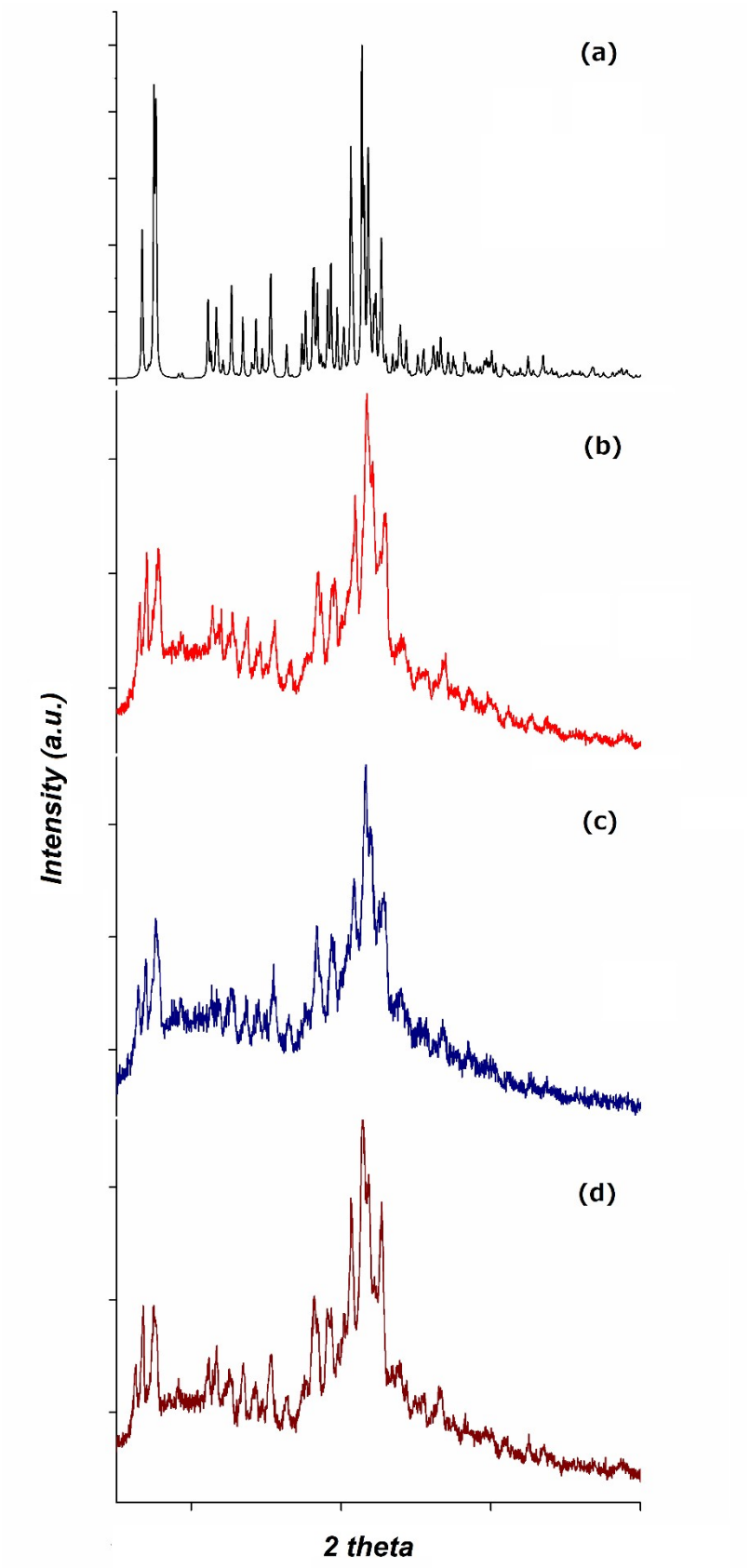

Fig. S103. (a) Simulated PXRD of the crystal structure of [(n-$Bu_4N)_2$(2$\mathbf{L_3}$·SO_4)], and experimental PXRD of [(n-$Bu_4N)_2$(2$\mathbf{L_3}$·SO_4)] complex obtained from LLE in the presence of (b) hydrogenphosphate, (b) hydrogenphosphate and carbonate, (c) hydrogenphosphate, carbonate and fluoride, as competing anions.

Single-crystal XRD data collection: Single-crystal XRD data were collected at 293(2) K with an Agilent SuperNova diffractometer with micro-focus X-ray on Cu-K_α radiation (λ = 1.5418 Å). CrysalisPro software was used to collect, index, scale and apply analytical absorption correction based on Gaussian method[3].

Structure Analysis and Refinement. The structure was solved by direct methods *(SHELXS-2018/2)*[4], refinement was done by full-matrix least squares on F^2 using the *SHELXL-2018/3* program suite[5] and the graphical user interface (GUI) *ShelXle*[6] was used. All non-hydrogen positions were refined with anisotropic temperature factors.

Hydrogen atoms were placed geometrically for aromatic C-H hydrogen of the tris-urea receptor and refined using a riding model (AFIX 43) with $U_{iso}(H) = 1.2U_{eq}(C)$.

Urea N−H hydrogen atoms were positioned geometrically (N−H = 0.86 Å) and refined using a riding model (AFIX 43) with $U_{iso}(H) = 1.2U_{eq}(N)$.

Secondary hydrogen atoms of tris-urea receptors carbon atoms and tetrabutylammonium cation were also positioned geometrically (C-H=0.94 Å) and refined using a riding model (AFIX 23) with $U_{iso}(H) = 1.2U_{eq}(C)$.

Hydrogen atoms of the methyl groups of tetrabutylammonium cation were positioned geometrically (C-H=0.96 Å) and refined using a riding model (AFIX 137) with $U_{iso}(H) = 1.5U_{eq}(C)$.

4-fluorophenyl ring of the labelled “A” arm of the tris-urea receptor displays disorder, so that in order the C-C distances to be similar, this ring was fitted to a regular hexagon with AFIX 66. Moreover, atomic displacement parameters of the carbon atoms were restricted to be similar by the use of SIMU restraints.

Terminal methyl group and neighbor carbon atom of the labelled “E” tetrabutylammonium ligand arm were refined using RIGU restraints to model the anisotropic atomic displacement parameters. These atoms appear also disordered in two positions which were modelled using PART commands and DFIX and DANG restraints for the C-C and C-H distances involved.

Table S1. Selected hydrogen bond parameters of the sulfate complex, [(n-$Bu_4N)_2$(2**L**$_3$·SO_4)].

D—H···*A*	H···*A* (Å)	*D*···*A* (Å)	*D*—H···*A* (º)
N1*A*—H1*A*···O2	2.55	3.227 (5)	136
N1*A*—H1*A*···O3	2.42	3.243 (5)	161
N1*A*—H1*A*···O4^{i}	2.15	2.957 (5)	157
N1*B*—H1*B*···O1	2.45	3.197 (5)	145
N1*B*—H1*B*···O4^{i}	2.07	2.924 (5)	170
N1*C*—H1*C*···S1	3.02	3.862 (3)	167
N1*C*—H1*C*···O2	2.22	3.034 (5)	158
N1*C*—H1*C*···O4^{i}	2.19	3.017 (6)	161
N2*A*—H2*A*···O1^{i}	2.35	3.155 (4)	156
N2*A*—H2*A*···O2	2.16	2.965 (4)	156
N2*B*—H2*B*···S1	2.94	3.765 (2)	162
N2*B*—H2*B*···O2^{i}	2.39	3.107 (5)	141
N2*B*—H2*B*···O3	2.05	2.898 (4)	169

N2*B*—H2*B*···O4^{i}	2.59	3.353 (6)	148
N2*C*—H2*C*···O1	2.22	2.997 (5)	151
N2*C*—H2*C*···O3^{i}	2.25	3.071 (5)	160

References

1. (a) S. K. Dey, R. Chutia and G. Das, *Inorg. Chem*., 2012, **51**, 1727−1738, (b) N. Busschaert, M. Wenzel, M. E. Light, P. Iglesias-Hernández, R. Pérez-Tomás, and P. A. Gale, *J. Am. Chem. Soc*., 2011, **133**, 14136−14148.

2. S. K. Dey and G. Das, *Dalton Trans*., 2012, **41**, 8960–8972.

3. O. D. Rigaku, *CrysAlis PRO*, 1.171.41.122a, Oxford, U.K., 2021.

4. G. M. Sheldrick, SHELXT−Integrated space-group and crystal-structure determination. *Acta Crystallogr. Sect. A,* 2015**, 71**, 3-8.

5. G. M. Sheldrick, SHELXL version 2018/3; University of Göttingen, Germany, 2018.

6. C. B. Hubschle, C. B. Sheldrick, B. Dittrich, ShelXle: A Qt graphical user interface for SHELXL. *J. Appl. Crystallogr,* 2011**, 44**, 1281-1284.